0 0 0 0 4 3 0 2 2 3 0

LBL-3713
c.1

BAINITIC TRANSFORMATION IN STEELS

RECEIVED
LAWRENCE
BERKELEY LABORATORY

AUG 1 1975

LIBRARY AND
DOCUMENTS SECTION

Der-Hung Huang
(Ph. D. thesis)

May 1975

Prepared for the U. S. Energy Research and
Development Administration under Contract W-7405-ENG-48

For Reference

Not to be taken from this room

LAWRENCE BERKELEY LABORATORY • UNIVERSITY OF CALIFORNIA • BERKELEY

LBL-3713
c.1

DISCLAIMER

This document was prepared as an account of work sponsored by the United States Government. While this document is believed to contain correct information, neither the United States Government nor any agency thereof, nor the Regents of the University of California, nor any of their employees, makes any warranty, express or implied, or assumes any legal responsibility for the accuracy, completeness, or usefulness of any information, apparatus, product, or process disclosed, or represents that its use would not infringe privately owned rights. Reference herein to any specific commercial product, process, or service by its trade name, trademark, manufacturer, or otherwise, does not necessarily constitute or imply its endorsement, recommendation, or favoring by the United States Government or any agency thereof, or the Regents of the University of California. The views and opinions of authors expressed herein do not necessarily state or reflect those of the United States Government or any agency thereof or the Regents of the University of California.

0 0 0 0 4 3 0 2 2 3 1

TABLE OF CONTENTS

ABSTRACT v

PREFACE vii

GENERAL INTRODUCTION 1

PART I. METALLOGRAPHY OF BAINITIC TRANSFORMATION IN STEELS 3

ABSTRACT 3

I. INTRODUCTION 4

II. EXPERIMENTAL PROCEDURE 7

A. Materials and Heat Treatment 7

B. Electron Microscopy 9

III. RESULTS AND DISCUSSION 11

A. Isothermal Transformation at 275°C 11

B. Isothermal Transformation at 315°C 19

C. Isothermal Transformation at 400°C 22

D. Isothermal Transformation at 480°C 24

IV. SUMMARY AND CONCLUSIONS 26

APPENDIX 28

REFERENCES 34

FIGURE CAPTIONS 36

FIGURES 41

PART II. TRANSMISSION ELECTRON MICROSCOPE STUDY OF THE BAINITE TRANSFORMATION IN Fe/12Ni/4Co/0.4 C ALLOY 63

ABSTRACT 63

I. INTRODUCTION 64

II. EXPERIMENTAL PROCEDURE 67

A. Materials and Heat Treatment.....67

B. Electron Microscopy.....67

III. RESULTS AND ANALYSIS.....69

A. Morphology and Substructure of Lower Bainite.....69

B. Crystallography of Bainitic Carbides.....76

C. Internal Twinning.....78

D. Summary of Principal Results.....80

IV. DISCUSSION.....81

A. Precipitation of Cementite in Lower Bainite.....81

B. Mechanism of Bainite Transformation.....83

V. CONCLUSIONS.....89

REFERENCES.....90

FIGURE CAPTIONS.....93

FIGURES.....97

GENERAL SUMMARY AND CONCLUSIONS.....118

ACKNOWLEDGMENTS.....120

0 0 0 0 4 3 0 2 2 3 2

BAINITIC TRANSFORMATION IN STEELS

Der-Hung Huang

Inorganic Materials Research Division, Lawrence Berkeley Laboratory
and Department of Materials Science and Engineering, College of Engineering;
University of California, Berkeley, California

ABSTRACT

The formation of carbide in lower bainite was studied in a series of carbon steels by thin foil transmission electron microscopy and electron diffraction techniques. Epsilon carbide was identified in the isothermally transformed bainite structure of a silicon steel. The crystallographic relationship between epsilon carbide and bainitic ferrite was found to follow the Jack orientation relationship, viz., $(0001)_\varepsilon || (011)_\alpha, (10\bar{1}1)_\varepsilon || (101)_\alpha$. The cementite observed in lower bainite was in the shape of small platelets and demonstrated the Isaichev orientation relationship with the bainitic ferrite, viz., $(010)_c || (1\bar{1}1)_\alpha$, $(103)_c || (011)_\alpha$. In the silicon containing steels, a thin layer of retained austenite was detected to form initially in contact with the bainitic ferrite when transformed in the bainite range at 315°C (the Ms temperature of the corresponding steel is 250°C). The retained austenite delineated the ferrite grain and subsequently decomposed into cementite and ferrite upon isothermal holding resulting in the characteristic bainitic microstructure of silicon containing steels. Based on these observations together with other crystallographical features, it is concluded that the bainitic carbide precipitated directly from austenite (γ) instead of from ferrite (α) at the γ/α interface.

The isothermal decomposition of a Fe/12Ni/4Co/.4C alloy (Ms=142°C) into lower temperature range of lower bainite was also studied by thin foil transmission electron microscopy. In addition to the characteristic short

bainitic carbide, long carbide stringers arranged in rows parallel to the longitudinal axis of the bainite plates were also observed. These carbides were identified as cementite.

The trace normal of the bainitic carbide falls in the region of (112) and (335) ferrite plane. The cementite/ferrite orientation relationship deviates slightly from the Bagaryatskii orientation relationship.

Evidence showing the existence of internal twinning in lower bainite is also presented. The fact that the observed twins, whether accommodation or transformation, persist after isothermal holding suggests the unidirectional precipitation of carbides cannot be attributed to carbide nucleation on the transformation twins.

The transformation mechanisms are discussed in terms of the observed evidence.

0 0 0 0 4 3 0 2 2 3 3

PREFACE

This thesis is divided into two parts. In Part I, the bainite transformation and the associated carbide precipitation in silicon containing steels are investigated. The salient metallographic features of the bainite have been characterized using direct transmission electron microscopy observations from which a model of bainite formation is proposed.

In Part II, special attention has been given to lower bainite formed in an Fe/Ni/Co/C alloy transformed at 200°C which is believed to be the lowest temperature range ever studied. The morphology of this low temperature bainite together with its unique internal structure are discussed. Several transformation mechanisms of bainite are also reviewed.

GENERAL INTRODUCTION

When steels are quenched to low temperature so rapidly that diffusion of carbon is not allowed, supersaturated ferrite will form from austenite by a diffusionless shear mechanism which results in the structure known as martensite.

Quenching into an intermediate temperature range does not provide sufficient driving force for the martensitic reaction. However, a complex series of transformation products form from austenite as a result of decomposition at subcritical temperatures, ranging from coarse pearlite at higher temperature through fine pearlite, to upper bainite then to lower bainite at the lowest temperatures.

The term bainite, so named in honor of E. C. Bain, refers to the microstructural constituent formed in steels when austenite decomposes at temperatures above that of martensite formation but below that of pearlite through either isothermal transformation or continuous cooling. The microscopic structure of bainite consists of nonlamellar aggregates of ferrite and carbide and it has been emphasized recently that this microstructural description be accepted as the definition of bainite. (See e.g. Aaronson, 1969)*. The morphology of bainite changes gradually with reaction temperature, so no pronounced structural changes are observed over any small temperature range. Although the microstructure may assume a variety of forms, two major variants of bainite morphology, namely upper and lower bainite, are observed in steels in different ranges of temperature. Other kinds of bainite are also known to exist, for example, granular bainite and inverse bainite, etc. In many steels there has been shown

*H. I. Aaronson, The Mechanism of Phase Transformation in Crystalline Solids, The Institute of Metals, Monograph and Report No. 33, 1969, P. 270.

to be a distinct microstructural difference between upper and lower bainite.* In upper bainite, which occurs mainly at high temperature, the carbides frequently form elongated particles between the bainite ferrite grains, while in lower bainite, the carbides tend to precipitate unidirectionally at an angle of 55 ~ 65° to the major growth direction, or longitudinal axis of the bainitic ferrite grain. However, it does not always seem possible to detect any sharp change in microstructural morphology.

Even more than 40 years after its discovery, the nature of the bainitic transformation remains so controversial that almost the only aspect of it upon which there is general agreement is that still more research is needed. Much debate is still going on as to the essential characteristics of a bainitic transformation; there are several schools of thought on what metallographic and mechanistic features characterize a bainitic phase change. The problem is mainly one of definition and exists simply because a word that was used originally to designate a new transformation product in carbon steels has been often used to imply a mechanism of transformation.

Since the mechanism of bainite transformation is not well understood and as one of the major areas of doubt is concerned with the mode of carbide precipitation, the present study was performed to attempt to clarify these questions.

* Electron Microstructure of Bainite in Steel, Second Progress Reported by Subcommittee XI of Committee E-4, ASTM Proc., 1952, Vol. 52, P. 543.

PART I.

Metallography of Bainitic Transformation in Steels

ABSTRACT

The formation of carbide in lower bainite was studied in a series of carbon steels by thin foil transmission electron microscopy and electron diffraction techniques. Epsilon carbide was identified in the isothermally transformed bainite structure of a silicon steel. The crystallographic relationship between epsilon carbide and bainitic ferrite was found to follow the Jack orientation relationship, viz., $(0001)_\varepsilon || (011)_\alpha$, $(10\bar{1}1)_\varepsilon || (101)_\alpha$. The cementite observed in lower bainite was in the shape of small platelets and demonstrated the Isaichev orientation relationship with the bainitic ferrits, viz., $(010)_C || (1\bar{1}1)_\alpha$, $(103) || (011)_\alpha$. In the silicon containing steels a thin layer of retained austenite was detected to form initially in contact with the bainitic ferrite when transformed in the bainite range at 315°C (the Ms temperature of the corresponding steel is 250°C). The retained austenite delineated the ferrite grain and subsequently decomposed into cementite and ferrite upon isothermal holding resulting in the characterictic bainitic microstructure of silicon containing steels. Based on these observations together with other crystallographical features, it is concluded that the bainitic carbide precipitated directly from austenite (γ) instead of from ferrite (α) at the γ/α interface.

I. INTRODUCTION

It has long been known[1] that there are two major different morphologies of bainite in steels, namely upper and lower bainite. In upper bainite, the carbides frequently form large elongated particles parallel to the longitudinal axis of the ferrite grain, while in lower bainite, the carbides tend to be oriented at an angle of about 55°-65° to the major axis of the ferrite grain.[1,2] Both the nature of carbides and whether the carbides in bainite precipitated from supersaturated ferrite or from austenite is of fundamental significance to the bainite reaction mechanism. The morphology and crystallographic relationship between bainitic ferrite and cementite have suggested that carbides in upper bainite precipitate directly from carbon enriched austenite trapped between the ferrite grains whereas those in lower bainite precipitate from supersaturated ferrite.[2,3] On the other hand, from an analysis of data in the literature on the average carbon content of retained austenite associated with partial transformation to bainite, it was pointed out recently that the carbon content of the ferritic component of bainite lies between the $\alpha/(\alpha + Fe_3C)$ and the extrapolated $\alpha/(\alpha+\gamma)$ phase boundaries.[4] This indicates there is a lack of support to existence of an appreciable carbon supersaturation in bainitic ferrite (relative to the extrapolated $\alpha/(\alpha+\gamma)$ curve). Furthermore, based on the thermodynamic analysis, it[4] has been argued that carbides in lower bainite form primarily from austenite at an austenite/ferrite boundary. Therefore, the origin of the carbides in lower bainite remains to be elucidated.

The characterization of the nature and the crystallography of the carbide phase are important in order to understand the structural features

of bainite. It is generally accepted that cementite constitutes the carbide phase of upper bainite. Although cementite is likewise frequently observed in lower bainite, the exact carbide precipitation process is still uncertain. It has been reported that ε carbide is the first carbide formed in low temperature bainite which is subsequently replaced by cementite on further transformation.[5,6] These reports were either based on conclusions drawn indirectly from physical measurements[5] or on direct electron microscope observation.[6] The evidence is, however, to the author's viewpoint, insufficient. The iron carbides may assume different forms in steel, e.g., epsilon carbide, Hägg carbide and cementite depending on the heat treatment and the composition of the material. Consequently the characterization of carbide must be approached with great care. Unfortunately, it has not always been possible to unambiguously determine the nature of the carbides present because of competing factors and their complex structures.

In view of the lack of exact evidence for identification of epsilon carbide in lower bainite in the literature, it is the purpose of the current investigation to provide such information, and to study the relevant crystallographic relationships.

Most of the literature on bainite transformation concern the kinetic aspects. Except for the work of Shackleton and Kelly[7] and Srinivasan and Wayman[8], there are not much data reported on the crystallography of the transformation. A knowledge of the crystallographic features of bainite is essential for a complete understanding of the transformation mechanism. It has been generally accepted that ferrite in lower bainite forms martensitically and the transformation is completed by a subsequent tempering

process similar to that of auto-tempering in martensitic steels. This idea was first suggested by Ko and Cottrell[9] after the observation of a martensitic type surface relief effect during the formation of bainite. Besides, the typical Bagaryatskii ferrite/cementite orientation relationship,[10] viz., $(100)_c||(110)_\alpha$, $(010)_c||(\bar{1}11)_\alpha$, $(001)_c||(1\bar{1}2)_\alpha$, occurred in martensite was also found to exist between ferrite and cementite in lower bainite[7]. This further supported the theory that bainite initially formed martensitically. However, many crystallographic and morphological features in lower bainite, e.g., bainite habit plane,[11] the unidirectional carbide, to name a few, are not explained satisfactorily to any extent by the martensitic mechanism. It is thus the aim of the present study to use thin foil transmission electron microscopy and diffraction to re-examine the morphological and crystallographic features of cementite and ferrite in lower bainite, in the hope that some more light will be shed on the mechanism of bainite formation.

II. EXPERIMENTAL PROCEDURE

A. Materials and Heat Treatment

The chemical composition of the alloys under investigation are given in Table 1 along with their M_s temperatures. M_s temperatures were determined by dilatometric measurements. The steels will be referred to by their designations as given in Table 1. Note the nominal composition is indicated by the alloy designation: the first digit and letter represent nominal wt.% of the major alloying element, the last two digits represent wt.% of carbon. Alloy 2S40 was kindly donated by Dr. H. I. Aaronson. It was vacuum melted and cast as a twenty-five pound ingot. After hot rolling, homogenization at 1300°C was done for several days. The details of heat treatment and the corresponding TTT diagram have been described in reference 12.

The particular composition of the alloy 2S54 selected provided an opportunity to compare the results with those of Oblak and Hehemann[6] on the morphology and crystallography of these transformations. Alloy 2S54 was vacuum induction melted in this laboratory using high purity material and poured in a fast chilled copper mold as a 4-lb. ingot.

All materials were sandblasted to remove any surface oxide. They were subsequently homogenized at 1100°C for three days and furnace cooled. A simple low-cost but successful technique was employed to prevent decarburization during homogenization. The as-received or as-cast materials were wrapped in stainless steel envelopes then sealed inside an Inconel tube filled with cast iron chips. The cast iron chips created a neutral atmosphere inside the Inconel tube during homogenization anneal and thus reduced

Table I. Chemical Composition of the Alloys (in wt%)

with their Ms Temperatures

Designation	Manufacturer's Original Heat Number	Composition	Ms Temperature
2S54	Si Steel	Fe-0.54C-1.87Si-0.79Mn-0.30Cr	250°C(482°F)
2S40	1	Fe-0.40C-1.73Si	370°C(698°F)

the degree of decarburization of the heat-treated material. Alloys 2S54 and 2S40 were then hot rolled to strips of 0.040 inch thickness, intermediate surface grinding was also employed to remove the scales.

Coupons of 1 in. by 1-1/2 in. were cut from these stripes, austenitized at 900°C for 1-1/2 hr in a dynamic argon atmosphere, and then quenched directly into a neutral salt bath. Isothermal transformation was then done at a predetermined temperature above M_s for a certain time. Carbon analyses before and after heat treatment showed no significant decarburization. It should be mentioned here that all the isothermal transformation temperatures employed throughout this research were above the M_s temperature of the material investigated.

B. Electron Microscopy

The heat treated 0.040 in. thick specimen were first mechanically ground slightly (flood cooling was employed) and then chemically thinned in a solution of 1:1 phosphoric acid and hydrogen peroxide (30%) to about 0.005 in. They were electropolished first by the window technique to a thickness of 0.002 to 0.003 in. using the following solution which gave rapid thinning.

10 ml perchloric acid

100 ml acetic acid

The final electropolishing was accomplished either by the conventional window method or by a double jet polishing apparatus using the following electrolyte.

75 gm CrO_3

400 ml Acetic Acid

21 ml H_2O

The temperature of the electrolyte was held at 10°C during polishing using an ice water bath. The applied voltage was about 25DC volts although the exact voltage varied from specimen to specimen. Thin foils were examined in a Siemens Elmiskop IA electron microscope at 100kV using a double tilt stage.

Selected area diffraction patterns of epsilon carbide were indexed with the aid of tables of d-spacings and angles between crystallographic planes calculated from a general computer program which has been compiled for non cubic crystal systems. The input data were a = 2.735 Å and C = 4.339 Å which yields a c/a ratio of 1.586. A listing of the program is included in the appendix.

Stereographic projection and trace analysis was extensively employed to study the crystallographic features of bainite.

III. RESULTS AND DISCUSSION

A. Isothermal Transformation at 275°C

Thin foils suitable for transmission electron microscopy were made from isothermally transformed lower bainite of steel 2S54. In many cases the precipitates were too small to give a satisfactory diffraction pattern to be uniquely identified. Nevertheless, the presence of epsilon carbide in lower bainite was detected by employing careful selected area diffraction and dark field imaging techniques.

Figure 1(a) shows the structure of lower bainite of the steel 2S54 after being isothermally transformed at 275°C for 17 hr. A high density of carbide precipitates is distributed uniformally throughout the bainitic ferrite matrix. These carbides form as thin platelets or laths varying in size from 60 to 200 Å wide and 700 to 4000 Å long. The corresponding selected area diffraction pattern is shown in Fig. 1(b) together with its indexing. From this and many other photographs which give a variety of orientation of the ferrite and carbide with respect to the incident electron beam, it has been possible to determine the orientation relationship between the two phases. In Fig. 1, the matrix has the $[011]_\alpha$ zone orientation and the carbide is analyzed as epsilon carbide with $[0001]_\varepsilon || [011]_\alpha$. It is clearly seen that the volume fraction of carbide is very large and the carbide/ferrite interface is rather ragged suggesting that the interface is partial or non-coherent and contains structural dislocations. In addition to the identification of epsilon carbide in lower bainite, the orientation relationships between epsilon carbide and bainitic ferrite may be obtained directly by plotting the orientations

determined from the diffraction pattern, Fig. 1(b), on a stereographic projection as in Fig. 2. It is clearly seen that $(0001)_\varepsilon$ plane is parallel with $(011)_\alpha$, $(10\bar{1}1)$ is only 1° from $(101)_\alpha$. This is practically the same as the Jack orientation relationship[13] which may be stated:

$$(0001)_\varepsilon \parallel (011)_\alpha$$

$$(10\bar{1}1)_\varepsilon \parallel (101)_\alpha$$

The one degree discrepancy between our result and that of Jack's could arise from inaccuracies introduced during measurements.

Characteristic wavy epsilon carbide in better contrast is seen in one of the bainite grains in Fig. 3 which is another area of the same treated specimen as that in Fig. 1. The waviness of the carbide could be interpreted as simultaneous transformation, i.e., the epsilon carbide is deformed along with the ferrite when austenite decomposed. As indexed in the insert, the matrix gives a $[100]_\alpha$ diffraction pattern and the epsilon carbide is slightly tilted from the $[11\bar{2}0]_\varepsilon$ zone. The angular discrepancy may be partly accounted for by the fact that spots in the diffraction pattern are not symmetrical and the actual foil orientation is about 5 degrees from the $[11\bar{2}0]_\varepsilon$ zone. This is reasonably consistent with the orientation relationship described in Fig. 2 where it is seen that $(11\bar{2}0)_\varepsilon$ is at 5 degrees from $(100)_\alpha$.

In order to provide further evidence to support the current work, the tempered martensitic structure of this steel was also studied and presented for comparison. This was done by water quenching a specimen of the same steel to martensite followed by tempering at 275°C for 17 hr. The microstructure is entirely different from its bainite counterpart.

A typical area of this specimen is shown in Fig. 4 demonstrating dense internal twinning, which is a characteristic of high carbon martensite.[14] Analysis of the selected area diffraction pattern indicates that the orientation of the matrix and twin are $[\bar{1}\bar{3}1]$ and $[10\bar{1}]$ respectively. The twin plane is $(\bar{1}21)$. Both the bright field image and the selected area diffraction pattern demonstrated little evidence of carbide precipitation. The result is not surprising owing to the fact that silicon is famous for contributing tempering resistance when used as an alloying element in steel.[15] It is evident that lower bainite and tempered martensite are easily distinguishable in this alloy and only those structures pertaining to lower bainite are studied in this research.

Summarizing the above results, we can say that epsilon carbide is unambiguously identified in lower bainite. The orientation relationship between the epsilon carbide and the bainitic ferrite is:

$$(0001)_\varepsilon \,||\, (011)_\alpha$$

$$(10\bar{1}1)_\varepsilon \,||\, (101)_\alpha$$

which is same as the Jack orientation relationship.[13]

a. <u>Formation of epsilon carbide</u>

The observed crystallographic orientation relationship between epsilon carbide and ferrite can be accounted for by nucleation of epsilon carbide in either austenite or supersaturated ferrite. They will be discussed as follows:

(i) <u>Epsilon carbide formed in ferrite</u>. In bainite, if epsilon

carbide forms directly from supersaturated ferrite, there will be little difference between bainite and martensite in the morphology of the precipitation process. The crystallographic analysis shows the the orientation relationship between epsilon carbide and ferrite is that suggested by Jack,[13] viz.,

$$(0001)_\varepsilon \;||\; (011)_\alpha$$

$$(10\bar{1}1)_\varepsilon \;||\; (101)_\alpha$$

There are two things worth noting in this lattice relationship. First, the parallel planes in bainitic ferrite and epsilon carbide are those of the lowest mismatch, viz., the $(10\bar{1}0)_\varepsilon$ and the $(2\bar{1}1)_\alpha$ planes. The calculated lattice misfit between ferrite and epsilon is listed in Table II. It can be seen that the misfit between $(10\bar{1}0)_\varepsilon$ and $(2\bar{1}1)_\alpha$ planes is 1.2 percent. Second, there is no low index epsilon plane which is exactly parallel with the $\{100\}_\alpha$ planes. A nucleus of epsilon carbide in this orientation can be formed by small movements of iron atoms from their position in the matrix. This may be seen from Fig. 5, which shows the position of iron atoms in ferrite projected onto a $(011)_\alpha$ plane.[16] The filled circles represent atoms at a distance of 1/2 [011] above this plane while the open circles represent the atomic positions in this plane. An outline of the basal plane is also delineated according to the orientation relationship determined. It is seen that once the carbide has grown to several unit cells in size, the atom movements are no longer small and further growth must then occur by long range diffusion of atoms.

Table II. Calculated Lattice Misfit Between Ferrite and ε Carbide

	Ferrite				%	ε Carbide			
	Plane	Interplanar Spacing(Å)	Number of Planes	Length(Å)	Expansion or Contraction	Corresponding Length(Å)	Number of Planes	Interplanar Spacing(Å)	Plane
	(011)	2.0268	2	4.0536	+6.8	4.3390	1	4.3390	(0001)
Jack	$(2\bar{1}1)$	1.1702	2	2.3404	+1.2	2.3686	1	2.3686	$(10\bar{1}0)$
	(101)	2.0268	1	2.0268	+2.5	2.0790	1	2.0790	$(10\bar{1}1)$
P-S	(100)	2.8664	1	2.8664	-4.7	2.7350	2	1.3675	$(11\bar{2}0)$
	$(0\bar{1}1)$	2.0268	1	2.0268	+15.6	2.3686	1	2.3686	$(1\bar{1}00)$

XBL 753-792

0 0 0 0 4 3 0 2 2 3 9

A more symmetrical orientation relationship for a hexagonal phase in a bcc matrix has been proposed by Doi and Nishiyama[17] and further reported by Pitsch and Schrader.[18] This may be stated as follows:

$$(0001)_{hcp} \parallel (011)_{bcc}$$

$$(11\bar{2}0)_{hcp} \parallel (100)_{bcc}$$

The orientation differs from the Jack orientation relationship by a rotation of 5 degrees in the hcp basal plane. This relationship has been verified for precipitation of Mo_2C in martensite. The projection of (011) ferrite lattice is delineated in Fig. 6. In this case $(11\bar{2}0)_{Mo_2C}$ and $(100)_{\alpha}$ have the smallest lattice mismatch, 4.6 percent, as calculated in Table III. The choice of the Jack orientation relationship in the case of epsilon precipitation most probably resulted from the necessity of minimizing the surface energy of the carbides as it forms at low temperature.

The formation of epsilon carbide in silicon steel is a phenomenon which has not been observed in other steels both in this laboratory and by previous investigations. Silicon is known to have a unique effect when used as an alloy element, for example, the stabilization of austenite, retarding the formation of cementite, etc. Although it has been suggested that the reason is due to the effect of silicon on kinetics the exact mechanism(s) has not been resolved.[19]

(ii) <u>Epsilon carbide formed in austenite</u>. It is also possible that epsilon carbide formed on the γ side of the γ/α interface and gave rise

Table III. Calculated Lattice Misfit Between Ferrite and Mo_2C

Ferrite				%	Mo_2C			
Plane	Interplanar Spacing(Å)	Number of Planes	Length(Å)	Expansion or Contraction	Corresponding Length(Å)	Number of Planes	Interplanar Spacing(Å)	Plane
(011)	2.0268	2	4.0536	+15.3	4.724	1	4.724	(0001)
(100)	2.8664	1	2.8664	+ 4.6	3.002	2	1.501	$(11\bar{2}0)$
$(0\bar{1}1)$	2.0268	1	2.0268	+24.8	2.600	1	2.600	$(1\bar{1}00)$
$(2\bar{1}1)$	1.1702	2	2.3404	+10.5	2.600	1	2.600	$(10\bar{1}0)$
(101)	2.0268	1	2.0268	+11.7	2.278	1	2.278	$(10\bar{1}1)$

XBL 753-793

0 0 1 5 4 3 0 2 2 4 0

to the Jack relationship. Because of the close lattice matching between fcc austenite and epsilon carbide one could expect that the orientation relationship of the epsilon carbide in austenite to be the familiar one viz.,

$$(111)_\gamma \parallel (0001)_\varepsilon$$

$$(1\bar{1}0)_\gamma \parallel (1\bar{2}10)_\varepsilon$$

But unfortunately it was not possible to retain sufficient austenite to verify this assumption. However, it is known that the K-S relationship[20] is obeyed between austenite and bainitic ferrite formed at low temperature,[21] i.e.,

$$(111)_\gamma \parallel (011)_\alpha$$

$$(1\bar{1}0)_\gamma \parallel (\bar{1}\bar{1}1)_\alpha$$

This leads to the ferrite/epsilon-carbide relationship of the Jack type[13] observed in the present research.

$$(0001)_\varepsilon \parallel (011)_\alpha$$

$$(1\bar{2}10)_\varepsilon \parallel (\bar{1}\bar{1}1)_\alpha$$

In a recent investigation,[22] a similar orientation relationship was observed when Ni_3Ti precipitated from a Fe/28Ni/2Ti alloy during ausaging, suggesting that the precipitate must have already formed in austenite during annealing. Upon the transformation to martensite on subsequent cooling, the obtained orientation relationship reflects a relationship between the precipitates and the matrix before transformation, i.e., the austenite phase. The same lattice correspondence was also observed after isothermal decomposition of a molybdenum austenitic alloy where fibers of Mo_2C nucleated on the γ side of the γ/α interface.[23]

As will be shown and discussed in the latter sections, the bainitic cementite in silicon steel precipitated directly from austenite. It appears that the precipitation of epsilon carbide most likely followed the same process, i.e., from austenite.

B. Isothermal Transformation at 315°C

As the isothermal transformation temperature was raised to 315°C, a structure which is unique to silicon containing steel developed. Figure 7 shows the structure of bainite isothermally transformed at 315°C(600°F) for 24 hr. It does not exhibit morphologies normally associated with classical bainite. Second phase particles of various shapes and sizes are seen roughly along the long direction of the bainite grain. The selected area diffraction pattern together with its schematic representation are shown in Figs. 7(b) and (c). The analysis shows that the bainitic ferrite is in [111] orientation and austenite in [011], i.e., following the famous Kurdjumov-Sachs orientation relationship.[20] A third constituent is identified as cementite in $[01\bar{2}]$ zone. It should be mentioned

that the lattice correspondence described above appeared very frequently during the course of the examination of this heat treated specimen. The dark field image micrograph of the $(1\bar{1}1)$ austenite spot, Fig. 7(d), reverses the contrast for the retained austenite which positively shows that the wide stringers mainly at the lath boundary are retained austenite. Figure 7(e) is the dark field image using a $(0\bar{2}\bar{1})$ cementite reflection. A thin layer of cementite, as indicated by the arrow, is in contact with the retained austenite. The formation of bainitic carbide is seen to bear a definite relation with the untransformed austenite. Another similar area is shown in Fig. 8(a). The diffraction pattern and the analysis are as those for Fig. 7. Dark field micrograph, Fig. 8(d), using $(\bar{1}1\bar{1})$ austenite reflection clearly shows the distribution of retained austenite. Many of them follow along the lath boundary and then bend into the matrix as indicated by arrows. In another area, Fig. 9(a), similar microstructure is seen which shows extensively decorated lath boundaries. The entrapped retained austenite has been decomposed to a further extent than those shown in Figs. 7 and 8. This can only be revealed by dark field imaging. Figure 9(d) is the dark field micrograph of a $(0\bar{2}\bar{1})$ cementite reflection which reverses the contrast of the cementite along the lath boundaries. Retained austenite, indicated by the arrow, is seen in Fig. 9(e) where both the $(0\bar{2}\bar{1})$ cementite spot and the $(1\bar{1}1)$ austenite spot are imaged.

The "wavy" or "S-shaped" retained austenite and carbide are in a more defined structure in the early stage of decomposition as shown in Fig. 10 which has been isothermally transformed for 17 minutes.

The retained austenite will eventually decompose into carbide and ferrite after prolonged holding. Similar decomposition of retained austenite

has been observed in the tempering of martensite.[24] Figure 11(a) shows the structure of bainite after transformation at 315°C for 168 hr. There is no distinct difference from the transformation product formed after a shorter time. The corresponding selected area diffraction pattern, Fig. 11(b), is slightly different from the ones observed before. Analysis of the diffraction pattern Fig. 11(c) shows that the carbide is cementite in $[1\bar{2}\bar{2}]$ zone and the ferrite matrix in [100] and [111] orientations. The cementite is delineated clearly in the dark field image of the (201) cementite reflection, Fig. 11(d). It should be mentioned here that the carbide pattern can also be indexed as epsilon carbide in $[\bar{1}101]$ orientation. The corresponding plane normal to $[\bar{1}101]$ is $(\bar{3}305)$ following the derivation of Okamoto and Thomas.[25] The Jack orientation relationship is closely followed between the carbide and ferrite in [001] orientation. However, it seems most unlikely that epsilon carbide is present in this case, since the carbide phase has been identified as cementite in specimens with shorter isothermal holding time at the same reaction temperature (Figs. 7, 8, and 9). Therefore we rule out the possibility of indexing it as epsilon carbide. Again, this carbide pattern, Fig. 11(b), bears a certain similarity to the diffraction pattern of austenite in (110) orientation as seen in the previous figures. Compounded by the fact that $(110)_\gamma$ is parallel to $(111)_\alpha$ in the Kurdjumov-Sachs relationship, it is liable to be erroneously indexed as austenite. However, it should be noticed that the planar angle between reflections A and B in Fig. 11(b) is 78°, whereas an angle of 70.53° is extended between the $\{111\}$ planes in austenite. <u>Thus it cannot be indexed as austenite</u>.

From the morphology observed above, we can say that at 315°C, the bainite in silicon steel is formed by the procedure shown schematically in Fig. 12. After the bainitic ferrite has nucleated in the austenite, a layer of carbon enriched austenite exists around it. Due to the rapid diffusion of carbon in austenite away from the tip of the ferrite needle, another ferrite unit is formed on the top of the retained austenite following the same procedure. This process then gives rise to the "bamboo shaped" structure. Carbides are precipitated gradually from the enriched austenite during isothermal holding. After prolonged transformation, the retained austenite decomposes completely and results in a structure consisting of ferrite and cementite.

In the absence of silicon the decomposition of retained austenite is rather fast and the existence of retained austenite may not be noticed.

C. Isothermal Transformation at 400°C

At this higher transformation temperature, in silicon containing steels, the ferrite regions are in general coarser than those found in the lower temperature formed bainite. This is seen very clearly in Fig. 13, which shows the bright field and dark field structure of the bainite of steel 2S40 isothermally transformed at 400°C for 7 hr. It is typical of a lower bainite and consists of ferrite plates which were filled with the cementite platelets precipitated on a specific ferrite plane. Cementite particles of varying sizes and shapes are seen in Fig. 14(a). Dark field images of the cementite reflections reversed the contrast of the carbides in the lower and top grains separately, Fig. 14(b) and (c). Morphologically, the carbides in the top grain have the appearance of the carbide in high

temperature formed bainite while carbides in the bottom grain appear to be very similar to those formed at lower temperatures.

The shape of the cementite particles, although appearing to be lath-like in many cases, was confirmed to be platelets, by observing the bainite in the direction nearly perpendicular to the cementite habit plane as shown in Fig. 15(a). In the selected area diffraction pattern, Fig. 15(b), the matrix and the cementite were indexed as $[\bar{1}\bar{1}0]_\alpha$ and $[10\bar{1}]_c$ orientations respectively. The stereographic analysis of the diffraction pattern, Fig. 15(c), show that the orientation is close to that of Bagaryatskii:[10]

$$(100)_c \,||\, (\bar{1}01)_\alpha$$
$$(010)_c \,||\, (1\bar{1}1)_\alpha$$
$$(001)_c \,||\, (121)_\alpha$$

By close examination of the stereogram, it is seen that the cementite/ferrite orientation relationship deviates slightly from that of Bagaryatskii. Much better agreement can be obtained by the Isaichev orientation relationship,[26] i.e.,

$$(010)_c \,||\, (1\bar{1}1)_\alpha$$
$$(103)_c \,||\, (011)_\alpha$$

It is seen that in the Isaichev orientation relationship, the ferrite lattice should be rotated around the $[1\bar{1}1]$ pole about 4° with respect to the Bagaryatskii relationship. This small difference between the two lattice relationships is of significance in the argument whether cementite nucleates in austenite or in ferrite. As reported in the research done on the Fe/12Ni/4Co/0.4C alloy in Part II of this thesis, the detected Isaichev lattice relationship between bainitic ferrite and cementite coupled with

the Kurdjumov-Sachs relationship between austenite and bainitic ferrite allows one to conclude that the bainitic cementite precipitated from austenite at the austenite/ferrite interface. Another area showing carbide to be in the shape of platelets instead of rods is demonstrated in Fig. 16(a). The internal fringes of the carbide can be seen in the dark field micrograph.

In addition to the typical lower bainitic carbide, longer cementite particles directed along, rather than at an angle to, the boundaries of the ferrite regions are also detected as pointed out by arrows in Figs. 17(a) and (b).

In view of the fact that both upper and lower bainite were observed at this transformation temperature the transition between these two structures must occur in the vicinity of 400°C.

D. Isothermal Transformation at 480°C

At this transformation temperature the structures produced showed little similarity to those resulting from transformation at 315°C or 400°C. In general, the structure resembles an acicular ferrite bounded by carbide particles (or with a few carbide particles dispersed throughout the ferrite). Such a structure is illustrated in Fig. 18. The foil is in [112] orientation. This structure has been termed the "accicular or plate-like ferrite" by Jolivet and Portevin,[27] "X-constituent" by Davenport,[28] "pro-bainitic ferrite" by Hultgren[29] and "carbide-free bainite" or "clear bainite" by Ko.[30] This is different from the proeutectoid ferrite formed by incoherent growth in hypoeutectoid steel. Under the light optical microscope, these structures appear to be of Widmanstatten ferrite. Sometimes the accicular ferrite is bounded by a stabilized-austenite envelope of varying thickness instead of bounded by carbide clusters. This type of

structure can be clearly observed at the high temperatures of the bainitic transformation, provided the products of the proeutectoid transformation do not interfere with the growth of bainite.

It appears that these structures must be attributed, at least partly, to the heterogeneity of austenite at high temperature. This heterogeneity increases further during the incubation period. As a result elongated ferrite plates or lenses form in the carbon-depleted regions, as was the case for upper bainite. On the other hand, the enriched zones which separate these ferrite plates decompose into ferrite and cementite. In some cases, when these zones are fairly restricted, austenite areas may remain and become stabilized.

IV. SUMMARY AND CONCLUSIONS

Structurally, bainite is an aggregate of ferrite and carbide, although the microstructure may assume a variety of forms. The morphology changes gradually with the reaction temperature, so no pronounced structural change is observed over any small temperature range. As is true of martensitic structures, the appearance of bainite is dictated primarily by the temperature of the formation. However, completely different microstructures can be obtained in steels with different composition even transformed at the same transformation temperature.

Epsilon carbide has been unambiguously identified in the bainitic structure of a Fe/1.87Si/0.54C steel when isothermally transformed at 275°C. The orientation relationship between epsilon carbide and bainitic ferrite was found to follow that of the Jack relationship,[13] viz., $(0001)_\varepsilon || (011)_\alpha$, $(10\bar{1}1)_\varepsilon || (101)_\alpha$. When transformed at 315°C, a layer of retained austenite formed along the boundary of the ferrite component of bainite bearing Kurdjumov-Sachs relationship.[19] Upon further isothermal holding, the retained austenite decomposed into cementite and ferrite. Thus, it is ascertained that bainitic carbide precipitated directly from austenite instead of from ferrite. The transformation is paced by the diffusion of carbon in austenite away from the tip of the ferrite needle. It appears that the degree of carbon enrichment in retained austenite varies with transformation temperature. At low transformation temperature, the carbon enrichment in retained austenite is high which results the precipitation of epsilon carbide. While at high reaction temperature, cementite forms in retained austenite because carbon enrichment is lower due to

higher carbon mobility. The kinetics of precipitation also determines the nature of the carbides.

At 400°C, the transformation product of a Fe/1.73Si/0.4C steel reveals that cementite in platelet shape is formed on a specific crystallographic plane in the bainitic ferrite plates. The Isaichev orientation relationship[26] was observed between cementite and ferrite instead of that of Bagaryatskii.[10] The cementite has been analyzed to form on the austenite side of the ferrite/austenite interface. Microstructural observations have indicated that the "transition" from lower to upper bainite took place at about 400°C in this steel. Carbides in bainite formed in the temperature range of 275°C to 400°C were concluded to precipitate from austenite at the austenite/ferrite interface and thus in direct contact with the austenite from which they formed.

At 480°C, accicular ferrite or carbide free bainite were observed.

The observation of epsilon carbide and cementite in bainite with different morphology when transformed at different temperature indicates that the carbide precipitation in bainite reaction depends on the transformation temperature as well as the composition of the steel. Furthermore, the cementite morphology adopted is first determined by the substructure of ferrite and then dictated by the diffusivity of carbon.

APPENDIX

```
                PROGRAM HEXANGL(INPUT,OUTPUT,TAPE1=INPUT,TAPE3=OUTPUT)
000002          DIMENSION M(750),D(750),REC(750),DIG(750),ITEM(5)
000002     1113 FORMAT(1H1,19X,4A10,A4,7H SYSTEM//)
000002     6231 FORMAT(1H1,19X,9H  H  K  L,11X,1HD,15X,3H1/D//)
000002       37 FORMAT(1H1,19X,19H  H  K  L   H  K  L,13X,3HHKL,11X,4HHK-L,11X,4HH
                1-KL,10X,5HH-K-L/1H ,/)
000002       11 FORMAT(2H1,55X,7HTABLE 2/)
000002        1 FORMAT(1H0,39X,7HTABLE 1)
000002        2 FORMAT(20X,48HLATTICE SPACINGS AND RECIPROCAL LATTICE SPACINGS)
000002        3 FORMAT(1H0,19X,3X,1HA,11X,1HB,11X,1HC)
000002        5 FORMAT(20X,     2(F7.3,5X),F7.3/)
000002        6 FORMAT(20X,     9H  H  K  L,11X,1HD,15X,3H1/D/)
000002        7 FORMAT(20X,      3I3,6X,F9.4,8X,F9.4)
000002       14 FORMAT(20X,     2(F7.3,5X),F7.3/)
000002       15 FORMAT(20X,     3I3)
000002     1000 CONTINUE
000002          READ(1,1112)ITEM,ISYST,A,B,C,MH,MK,ML
000026     1112 FORMAT(4A10,A4,I2,1X,3F8.0,3I3)
000026          IF(ISYST.EQ.99) STOP
000032          WRITE(3,1113)ITEM
000040          WRITE(3,1)
000044          WRITE(3,2)
000050          WRITE(3,3)
000054          WRITE(3,5)A,B,C
000066          WRITE(3,6)
          C     KSW = 1  HEXAG
          C     KSW=2    ORTHO,TETRA
000072          IF(ISYST)222,141,222
000073      141 KSW=1
000074          GO TO 19
000075      222 KSW=2
000101       19 STAR=.75*((A*A)/(C*C))
000103          A2=A*A
000104          B2=B*B
000105          C2=C*C
          C    TEST TO SEE IF COMBINATIONS READ IN
000106          IF(MH)356,357,357
000110      356 READ(1,92) (M(KK),KK=1,MK)
000117       92 FORMAT(8I10)
000117          DO 91 KK=1,MK
000125       91 DIG(KK)=M(KK)
000127          NUM=MK
000130          N=MK
000132          DO 190 KK=1,MK
000134          IH = IABS(M(KK)/10000)
000140          H=IH
000141          K=IABS((M(KK) -(IH*10000))/100)
000146          XK=K
000147          L = IABS(M(KK) - (IH*10000) - (K*100))
000154          XL = L
000156          GO TO (197,198),KSW
000164      197 D(KK)= SQRT((3.*A2*C2)/(4.*C2*(H*H+H*XK+XK*XK)+3.*A2*XL*XL))
000202          GO TO 190
000202      198 D(KK)=(A*B*C)/ SQRT(B2*C2*H*H+A2*C2*XK*XK+A2*B2*XL*XL)
000221      190 CONTINUE
000224          GO TO 358
000224      357 MMH=MH+1
000226          MMK=MK+1
```

```
000227          MML=ML+1
000231          N=(MMH*MMK*MML)-1
000235          KK=0
000236          DO 90 IH=1,MMH
000237          DO 90  K=1,MMK
000240          DO 90  L=1,MML
000241          H=IH-1
000243          XK=K-1
000245          XL=L-1
000247          IF (H+XK+XL) 10,90,10
000251       10 KK=KK+1
000253          IF(KK.EQ.751) GO TO 358
000254          M(KK)=10000.*H+100.*XK+XL
000262          GO TO (97,98),KSW
000270       97 D(KK)= SQRT((3.*A2*C2)/(4.*C2*(H*H+H*XK+XK*XK)+3.*A2*XL*XL))
000305          GO TO 90
000306       98 D(KK)=(A*B*C)/( SQRT(B2*C2*H*H+A2*C2*XK*XK+A2*B2*XL*XL))
000325       90 CONTINUE
          C    ARRANGE IN ORDER   -  LARGEST TO SMALLEST
000335      358 MM=N-1
000337           NN=N
000340          DO 70 I=1,MM
000341          NN=N-1
000343          DO 70 KK=1,NN
000344          IF (D(KK+1)-D(KK)) 70,70,60
000350       60 BUB=D(KK+1)
000351          D(KK+1)=D(KK)
000353          D(KK)=BUB
000353          SUB=M(KK+1)
000355          M(KK+1)=M(KK)
000356          M(KK)=SUB
000360       70 CONTINUE
000365          L13 = 13
          C     PRINT OUT
000366           DO 120 KK=1,N
000371          REC(KK)=(1./D(KK))
000373          REC(KK)=REC(KK)+.00005
000374          D(KK)=D(KK)+.00005
000376          IH = IABS(M(KK)/(10000))
000402          K = IABS((M(KK)-(IH*10000))/100)
000407          L = IABS(M(KK) - (IH*10000) - (K*100))
000415          GO TO (8000,8001),KSW
000423     8000 JNO = IH + K + K
000425          JJNO = JNO/3
000430          IF(JNO - 3*JJNO)8002,8003,8002
000432     8003 JNOO = L/2
000433          IF(L-2*JNOO)120,8002,120
000436     8002 IF(L13-57)8005,8006,8005
000440     8006 WRITE(3,6231)
000444          L13=2
000445     8005 WRITE(3,7)IH,K,L,D(KK),REC(KK)
000463          L13=L13 + 1
000465          GO TO 120
000465     8001 IF(L13-57)8007,8008,8007
000467     8008 WRITE(3,6231)
000473          L13=2
000474     8007 WRITE(3,7) IH,K,L,D(KK),REC(KK)
000512          L13=L13+1
```

```
000514      120 CONTINUE
          C     PART 2 OF PROGRAM
000517       18 WRITE(3,11)
000523          WRITE(3,12)
000527       12 FORMAT(20X,29X,21HANGLES BETWEEN PLANES/)
000527          WRITE(3,13)
000533       13 FORMAT(20X,3X,1HA,11X,1HB,11X,1HC)
000533          WRITE(3,14) A,B,C
000545          WRITE(3,17)
000551       17 FORMAT(20X,19H  H  K  L   H  K  L,13X,3HHKL,11X,4HHK-L,11X,4HH-KL
                110X,5HH-K-L)
000551          LLL = 7
000552          IF(MH)368,367,367
          C     TEST TO SEE IF COMBINATIONS READ IN
000554      367 IF(MH-MK) 112,112,111
000557      111 MEL=MH
000561          GO TO 113
000561      112 MEL=MK
000563      113 IF(MEL-ML) 116,116,114
000566      114 LIM=MEL
000570          GO TO 117
000570      116 LIM=ML
000572      117 II=0
000573          DO 700 JH=1,MMH
000575          XH=JH-1
000577          DO 700  K=1,MMK
000600          XK=K-1
000602          DO 700  L=1,MML
000603          XL=L-1
000605          IF(XH+XK+XL)707,700,707
000610      707 IF(XH-1.)333,600,333
000612      333 IF(XK-1.)444,600,444
000614      444 IF(XL-1.)445,600,445
000616      445 DO 400 J=2,LIM
000620          IRULE = XH+XK+XK
000622          IIRULE = IRULE/3
000625          IF(IRULE -3*IIRULE)7020,7021,7020
000630     7021 IF(XL - 2.)7020,600,7020
000632     7020 CONTINUE
000632          DIV=J
000633          YH=XH/DIV
000635          IH=YH
000636          ZH=IH
000637          IF(YH-ZH) 400,200,400
000641      200 YK=XK/DIV
000643          IK=YK
000644          ZK=IK
000645          IF(YK-ZK)400,300,400
000647      300 YL=XL/DIV
000651          IL=YL
000652          ZL=IL
000653          IF(YL-ZL) 400,700,400
000655      400 CONTINUE
000660      600 II=II+1
000662          DIG(II)=10000.*XH+100.*XK+XL
000667      700 CONTINUE
000677          NUM=II
000700      368 DO 801 JJ = 1, NUM
```

```
        C       TO GET EACH CHANGE IN K1,K1,L1 ON A NEW PAGE
000703    1101  JH1=DIG(JJ)/10000.
000705          XH1=JH1
000707          K1=(DIG(JJ)-(XH1*10000.))/100.
000712          XK1=K1
000714          L1=DIG(JJ)-(XH1*10000.)-(XK1*100.)
000720          XL1=L1
000722          GO TO (27,28),KSW
000730      27  PART=XH1*XH1+XK1*XK1+XH1*XK1+STAR*XL1*XL1
000736          GO TO 29
000736      28  PART2=(XH1*XH1)/A2+(XK1*XK1)/B2+(XL1*XL1)/C2
000745      29  GO TO (7000,7004),KSW
000753    7000  JNO = JH1+K1+K1
000755          JJNO = JNO/3
000760          IF(JNO-3*JJNO)7004,7003,7004
000762    7003  JNOO = L1/2
000763          IF(L1-2*JNOO)7005,7004,7005
000766    7004  IF(LLL-57)7007,7006,7007
000770    7006  WRITE(3,37)
000774          LLL=2
000775    7007  KH8=XH1
000776          KK8=XK1
001000          KL8=XL1
001002          WRITE(3,15) KH8,KK8,KL8
001013          LLL = LLL+1
001015          GO TO 7008
001015    7005  LL = NUM
001017          GO TO 801
001017    7008  CONTINUE
001017          DO 801 LL = JJ,NUM
001022          JH2=DIG(LL)/10000.
001024          XH2=JH2
001025          K2=(DIG(LL)-(XH2*10000.))/100.
001030          XK2=K2
001032          L2=DIG(LL)-(XH2*10000.)-(XK2*100.)
001036          XL2=L2
001040          GO TO (2000,3000),KSW
        C       HEXAGONAL SYSTEM
001046    2000  ATEST=XH1*XH2+XK1*XK2+.5*(XH1*XK2+XH2*XK1)+STAR*XL1*XL2
001057          IF(ATEST)506,505,506
001060     506  ALPHA=ATEST/ SQRT(PART*(XH2*XH2+XK2*XK2+XH2*XK2+STAR*XL2*XL2))
001071          XALPHA =  ATAN( SQRT(1.000- ALPHA*ALPHA)/ALPHA)
001100          XALPHA=XALPHA*57.2958
001102          IF(XALPHA) 874,872,874
001103     872  IF(ALPHA) 873,874,874
001105     873  XALPHA=180.
001107     874  XALPHA=XALPHA+.0005
001111          IF(XALPHA)611,612,612
001112     611  XALPHA=XALPHA+180.
001114          GO TO 612
001115     505  XALPHA=90.
001117     612  BTEST=XH1*XH2+XK1*XK2+.5*(XH1*XK2+XH2*XK1)+STAR*XL1*(-XL2)
001132          IF(BTEST)606,605,606
001133     606  BETA=BTEST/ SQRT(PART*(XH2*XH2+XK2*XK2+XH2*XK2+STAR*XL2*XL2))
001144          XBETA =  ATAN( SQRT(1.000-BETA*BETA)/BETA)
001153          XBETA=XBETA*57.2958
001155          IF(XBETA)884,882,884
001156     882  IF(BETA)883,884,884
```

```
001160      883 XBETA = 180.
001162      884 XBETA = XBETA+.0005
001164          IF(XBETA) 613,614,614
001165      613 XBETA=XBETA+180.
001167          GO TO 614
001170      605 XBETA=90.
001172      614 GTEST=XH1*XH2+XK1*(-XK2)+.5*(XH1*(-XK2)+XH2*XK1)+STAR*XL1*XL2
001205          IF(GTEST)706,705,706
001206      706 GAMMA=GTEST/ SQRT(PART*(XH2*XH2+XK2*XK2+XH2*(-XK2)+STAR*XL2*XL2))
001220          XGAMMA= ATAN( SQRT(1.000-GAMMA*GAMMA)/GAMMA)
001227          XGAMMA=XGAMMA*57.2958
001231          IF(XGAMMA)894,892,894
001232      892 IF(GAMMA) 893,894,894
001234      893 XGAMMA=180.
001236      894 XGAMMA=XGAMMA+.0005
001240          IF(XGAMMA)615,616,616
001241      615 XGAMMA=XGAMMA+180.
001243          GO TO 616
001244      705 XGAMMA=90.
001246      616 DTEST=XH1*XH2+XK1*(-XK2)+.5*(XH1*(-XK2)+XH2*XK1)+STAR*XL1*(-XL2)
001262          IF(DTEST)806,805,806
001263      806 DELTA=DTEST/ SQRT(PART*(XH2*XH2+XK2*XK2+XH2*(-XK2)+STAR*XL2*XL2))
001275          XDELTA= ATAN( SQRT(1.000-DELTA*DELTA)/DELTA)
001304          XDELTA=XDELTA*57.2958
001306          IF(XDELTA)864,862,864
001307      862 IF(DELTA) 863,864,864
001311      863 XDELTA=180.
001313      864 XDELTA=XDELTA+.0005
001315          IF(XDELTA)617,800,800
001316      617 XDELTA=XDELTA+180.
001320          GO TO 800
001321      805 XDELTA=90.
001323          GO TO 800
          C      ORTHORHOMBIC  AND  TETRAGONAL  SYSTEM
001323     3000 AXTEST = (XH1*XH2)/A2+(XK1*XK2)/B2+(XL1*XL2)/C2
001333          IF(AXTEST)906,905,906
001334      906 ALPHA=AXTEST/SQRT(PART2*((XH2*XH2)/A2+(XK2*XK2)/B2+(XL2*XL2)/C2))
001346          XALPHA= ATAN( SQRT(1.000-ALPHA*ALPHA)/ALPHA)
001355          XALPHA = XALPHA*57.2958
001357          IF(XALPHA)814,812,814
001360      812 IF(ALPHA)813,814,814
001362      813 XALPHA = 180.
001364      814 XALPHA =XALPHA+.0005
001366          IF(XALPHA)911,912,912
001367      911 XALPHA=XALPHA+180.
001371          GO TO 912
001372      905 XALPHA =90.
001374      912 BXTEST = (XH1*XH2)/A2+(XK1*XK2)/B2-(XL1*XL2)/C2
001404          IF(BXTEST)1006,1005,1006
001405     1006 BETA=BXTEST/ SQRT(PART2*((XH2*XH2)/A2+(XK2*XK2)/B2+(XL2*XL2)/C2))
001417          XBETA= ATAN( SQRT(1.000-BETA*BETA)/BETA)
001426          XBETA=XBETA*57.2958
001430          IF(XBETA)824,822,824
001431      822 IF(BETA)823,824,824
001433      823 XBETA=180.
001435      824 XBETA=XBETA+.0005
001437          IF(XBETA)1013,1014,1014
001440     1013 XBETA=XBETA+180.
```

```
001442          GO TO 1014
001443     1005 XBETA =90.
001445     1014 GXTEST=(XH1*XH2)/A2-(XK1*XK2)/B2+(XL1*XL2)/C2
001455          IF(GXTEST)1106,1105,1106
001456     1106 GAMMA=GXTEST/ SQRT(PART2*((XH2*XH2)/A2+(XK2*XK2)/B2+(XL2*XL2)/C2))
001470          XGAMMA= ATAN( SQRT(1.000-GAMMA*GAMMA)/GAMMA)
001477          XGAMMA=XGAMMA*57.2958
001501          IF(XGAMMA)834,832,834
001502      832 IF(GAMMA)833,834,834
001504      833 XGAMMA=180.
001506      834 XGAMMA=XGAMMA+.0005
001510          IF(XGAMMA)1115,1116,1116
001511     1115 XGAMMA=XGAMMA+180.
001513          GO TO 1116
001514     1105 XGAMMA=90.
001516     1116 DXTEST=(XH1*XH2)/A2-(XK1*XK2)/B2-(XL1*XL2)/C2
001526          IF(DXTEST)1206,1205,1206
001527     1206 DELTA=DXTEST/ SQRT(PART2*((XH2*XH2)/A2+(XK2*XK2)/B2+(XL2*XL2)/C2))
001541          XDELTA= ATAN( SQRT(1.000-DELTA*DELTA)/DELTA)
001550          XDELTA=XDELTA*57.2958
001552          IF(XDELTA)844,842,844
001553      842 IF(DELTA)843,844,844
001555      843 XDELTA=180.
001557      844 XDELTA=XDELTA+.0005
001561          IF(XDELTA)1217,800,800
001562     1217 XDELTA=XDELTA+180.
001564          GO TO 800
001565     1205 XDELTA=90.
001567      800 GO TO(9000,9004),KSW
001575     9000 JNO=JH2+K2+K2
001577          JJNO=JNO/3
001602          IF(JNO-3*JJNO)9004,9003,9004
001604     9003 JNOO=L2/2
001605          IF(L2-2*JNOO)801,9004,801
001610     9004 IF(LLL-57)9007,9006,9007
001612     9006 WRITE(3,37)
001616          WRITE(3,15)KH8,KK8,KL8
001630          LLL=2
001631     9007 KH3=XH2
001632          KK3=XK2
001634          KL3=XL2
001636          WRITE(3,16)KH3,KK3,KL3,XALPHA,XBETA,XGAMMA,XDELTA
001657          LLL=LLL+1
001661      801 CONTINUE
001666       16 FORMAT(20X,10X,3I3,1X,4F15.2)
001666          GO TO 1000
001666          END
```

REFERENCES

1. Electron Microstructure of Bainite in Steel. Second Progress Report by Subcommittee XI of Committee E-4, ASTM Proc., 1952, vol. 52, p. 543.

2. D. N. Shackleton and P. M. Kelly, The Iron and Steel Institute, Special Report No. 93, 1965, p. 126.

3. K. J. Irvine and F. B. Pickering, The Iron and Steel Institute, Special Report No. 93, 1965, p. 110.

4. R. F. Hehemann, K. R. Kinsman and H. I. Aaronson, Met. Trans., 1972, vol. 3, p. 1077.

5. S. J. Matas and R. F. Hehemann, Trans. AIME., 1961, vol. 221, p. 179.

6. J. M. Oblak and R. F. Hehemann, Transformation and Hardenability in Steels, p. 15, Climax Molybdenum Company, Ann Arbor, 1967.

7. D. N. Shackleton and P. M. Kelly, ACTA Met., 1967, vol. 15, p. 979.

8. G. R. Srinivasan and C. M. Wayman, ACTA Met., 1968, vol. 16, p. 621.

9. T. Ko and S. A. Cottrell, JISI, 1952, vol. 172, p. 307.

10. Yu. A. Bagaryatskii, Doklady, Akademiia Nauk SSSR, 1950, vol. 73, p. 1161.

11. J. S. Bowles and N. F. Kennon, J. Aust. Inst. Metals, 1960, vol. 5, p. 106.

12. H. I. Aaronson and H. A. Domian, Trans. AIME, 1966, vol. 236, p. 781.

13. K. H. Jack, JISI, 1951, vol. 169, p. 26.

14. P. M. Kelly and J. Nutting, Proc. Royal Soc., 1960, vol. A259, p. 45.

15. W. S. Owen, Trans ASM, 1954, vol. 46, p. 812.

16. S. Murphy and J. A. Whiteman, Met. Trans., 1970, vol. 1, p. 843.

17. M. Doi and Z. Nishiyama, Nippon Kinzoku Gakkai-Si, 1953, vol. 17, p. 487.

18. W. Pitsch and A. Schrader, Arch. Eissen., 1958, vol. 29, p. 715.

19. W. C. Leslie, R. L. Pickett, C. P. Stoble and G. Konovol, Trans. ASM, 1961, vol. 53, p. 715.

0 0 0 0 4 3 0 2 2 4 9

20. G. Kurdjumov and G. Sachs, Z. Physik, 1930, vol. 64, p. 325.

21. G. V. Smith and R. F. Mehl, Trans. AIME, 1942, vol. 150, p. 211.

22. I-Lin Cheng and G. Thomas, Met. Trans., 1972, vol. 3, p. 503.

23. F. G. Berry, A. T. Davenport and R. W. K. Honeycombe, Inst. of Metals, Monograph No. 33, 1969, p. 288.

24. J. A. McMahon and G. Thomas, Presented at the Third International Conference on the Strength of Metals and Alloys, Cambridge, England, 1973, LBL-1490.

25. P. R. Okomoto and G. Thomas, Phys. Stat. Sol., 1968, vol. 95, p. 81.

26. I. V. Isaichev, Zhur, Tekhn, Fiziki, 1947, vol. 17, p. 835.

27. H. Jolivet and A. Porterin, Compt. Rend., 1939, vol. 209, p. 379.

28. E. S. Davenport, Trans. ASM, 1939, vol. 27, p. 837.

29. A. Hultgren, Trans. ASM, 1947, vol. 39, p. 915.

30. T. Ko, JISI, 1953, vol. 175, p. 16.

FIGURE CAPTIONS

Fig. 1 (a)Structure of bainite which was obtained in isothermally transformed steel 2S54 (Fe/1 87Si/0.54C + 0.79Mn/0.3Cr) at 275°C for 17 hr. (b)is the corresponding selected area diffraction pattern showing a $[0001]_{\varepsilon}$ zone parallel with a $[011]_{\alpha}$ zone.

Fig. 2 Stereographic projection, based on the orientations determined in Fig. 1, representing the orientation relationship between epsilon carbide and bainitic ferrite.

Fig. 3 Another area of the bainite formed in steel 2S54 at 275°C characteristic wavy epsilon carbide with size of 60 to 200Å in width and 700 to 4000Å in length are seen in a bainitic ferrite grain. The insert shows the selected area diffraction pattern where the foil orientation is $[100]$ and the epsilon carbide is in approximate $[11\bar{2}0]$ orientation.

Fig. 4 Structure of martensite of steel 2S54 tempered at 275°C for 17 hr. (a) shows typical internally twinned martensite plate where no carbide was detected. It is distinctly different from the bainitic structure. (b) selected area diffraction pattern and indexed representation showing orientation of the matrix and twin are $[\bar{1}\bar{3}1]$ and $[10\bar{1}]$ respectively. Twin plane is $(\bar{1}21)$.

Fig. 5 $(011)_{\alpha}$ projection of iron atoms in ferrite lattice, the hexagon indicates the epsilon carbide, exhibiting Jack orientation relationship with the matrix. The open circles represent atoms in this plane of the diagram, filled circles represent atoms in the plane at a distance of 1/2 $[011]$ above or below this plane.

Fig. 6 $(011)_\alpha$ projection of iron atoms in ferrite lattice, the hexagon indicates the Mo_2C, exhibiting Pitsch - Schrader orientation relationship with the matrix.

Fig. 7 Structure of bainite in steel 2S54 after isothermal transformation at 315°C (600°F) for 24 hr. (a) Bright field micrograph showing retained austenite and cementite embedded in dislocated bainitic ferrite grain. (b) The corresponding selected area diffraction pattern and its schematic representation, (c), showing the ferrite, austenite and cementite in $\left[111\right]_\alpha$, $\left[011\right]_\gamma$ and $\left[01\bar{2}\right]_{Fe_3C}$ zone respectively. Kurdjmov-Sachs orientation relationship is followed between bainitic ferrite and austenite. (d) The retained austenite reverses contrast in the dark field image using $(1\bar{1}1)$ reflection. (e) A very thin layer of cementite (pointed by arrow) in contact with austenite is seen clearly in the dark field image of a $(0\bar{2}\bar{1})$ cementite reflection.

Fig. 8 Another region of bainite in steel 2S54 obtained by isothermal transformation at 315°C for 24 hr (a) bright field micrograph showing "S-shaped" retained austenite forms along the lath boundary and then bends into the ferrite lath. (b) and (c) are the selected area diffraction pattern and its indexing, is the same as in Fig. 7. The unique shape of retained austenite is pointed out by arrows in the dark field image of a $(\bar{1}1\bar{1})_\gamma$ spot.

Fig. 9 Another area of bainite in steel 2S54 after isothermal transformation at 315°C for 24 hr (a) bright field image which shows extensive lath boundary decoration of cementite suggesting retained austenite has been decomposed to a further extent. (b) and (c) are the selected

area diffraction pattern and the schematic representation same as in Fig. 7. (d) dark field image of a $(0\bar{2}\bar{1})$ cementite reflection showing carbide forms along the lath boundary. (e) Both the carbide and retained austenite (indicated by arrow) reverse contrast in the dark field image using $(0\bar{2}\bar{1})$ cementite and $(1\bar{1}1)$ austenite reflections.

Fig. 10 Structure of bainite in steel 2S54 after isothermal transformation at 315°C for a shorter time, 17 minutes, showing unique "S-shaped" retained austenite and cementite.

Fig. 11 Bainite in steel 2S54 obtained by isothermal transformation at 315°C for 168 hr (a) Bright field micrograph showing ferrite lath with cementite. (b) the corresponding selected are diffraction pattern, (c) the schematic representation demonstrating ferrite in $[\bar{1}00]$ and $[111]$ orientation and the cementite in $[1\bar{2}\bar{2}]$ zone, no retained austenite is detected. (d) dark field image of a (201) cementite reflection showing reversal of contrast for the carbides. (e) The carbide can also be indexed as epsilon carbide in $[\bar{1}011]$ zone. The corresponding plane normal to $[\bar{1}101]$ is $(\bar{3}305)$. See text for details.

Fig. 12 Schematic drawing of bainite forming in silicon containing steel showing the nucleation of ferrite lath and a thin layer of carbon enriched austenite is retained in contact with the ferrite lath. The austenite subsequently decomposes into cementite and ferrite. In the absence of silicon the decomposition of retained austenite is very fast and the formation of retained austenite may be by-passed without being noticed.

Fig. 13 Structure of typical lower bainite in steel 2S40 (Fe/1,73Si/0.4C) after isothermal transformation at 400°C for 7 hrs.(a) cementite particles precipitated on a certain crystallographic plane in dislocated bainitic ferrite. These carbides reverse contrast in the dark field as in (b).

Fig. 14 Bainite in steel 2S40 formed at 400°C after transforming for 7 hrs. (a) Carbides of varying sizes are seen probably due to sectioning effect in two different bainite grains. (b) and (c) Dark field micrographs using cementite reflections reverse contrast of carbide in the top and bottom grains respectively.

Fig. 15 (a) Structure of bainite in steel 2S40 obtained by isothermal transformation at 400°C for 7 hrs. showing cementite platelet have precipitated (b) The corresponding selected area diffraction pattern, demonstrating the ferrite matrix in $\left[\bar{1}\bar{1}0\right]$ zone and cementite in $\left[10\bar{1}\right]$ zone. (c) Stereographic projection corresponding to Fig. 15 (b) representing the lattice relationship between cementite and bainitic ferrite; Isaichev orientation relationship, viz., $(010)_c || (1\bar{1}1)_\alpha$, $(103)_c || (011)_\alpha$.

Fig. 16 Transmission electron micrograph of structure of bainite in all alloy 2S40 after transformation at 400°C for 7 hrs.(a) indicating the shape of cementite is platelet instead of rod. The contrast of the cementite is reversed in the dark field image, (b).

Fig. 17 Electron micrograph of structure of bainite in alloy 2S40 obtained by isothermal transformation at 400°C for 7 hr. (a) showing long striations of cementite (dilineated by arrows) which is characteristic of upper bainite is seen in addition to the typical short

lower bainitic carbide. (b) another area of bainite where carbides as marked by arrow, starts to precipitate at the lath boundary suggesting the transition of carbide morphology from transgranular to intergranular is taking place.

Fig. 18 Structure of transformation product in 2S40 alloy after isothermal holding at 480°C for 2 hr. (a) showing accicular ferrite bounded by a few carbide particles which has been termed as "carbide-free" bainite. (b) selected area diffraction pattern in [112] orientation.

0 0 0 0 4 3 0 2 2 5 2

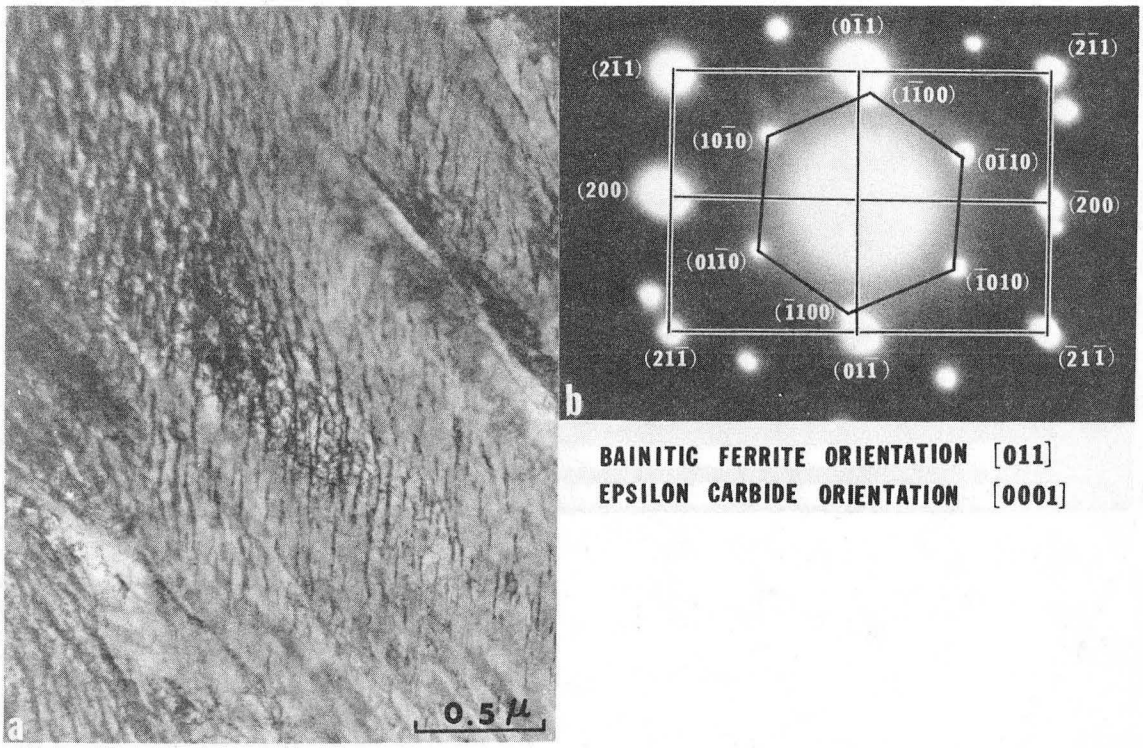

BAINITIC FERRITE ORIENTATION [011]
EPSILON CARBIDE ORIENTATION [0001]

XBB 735-3158

Fig. 1

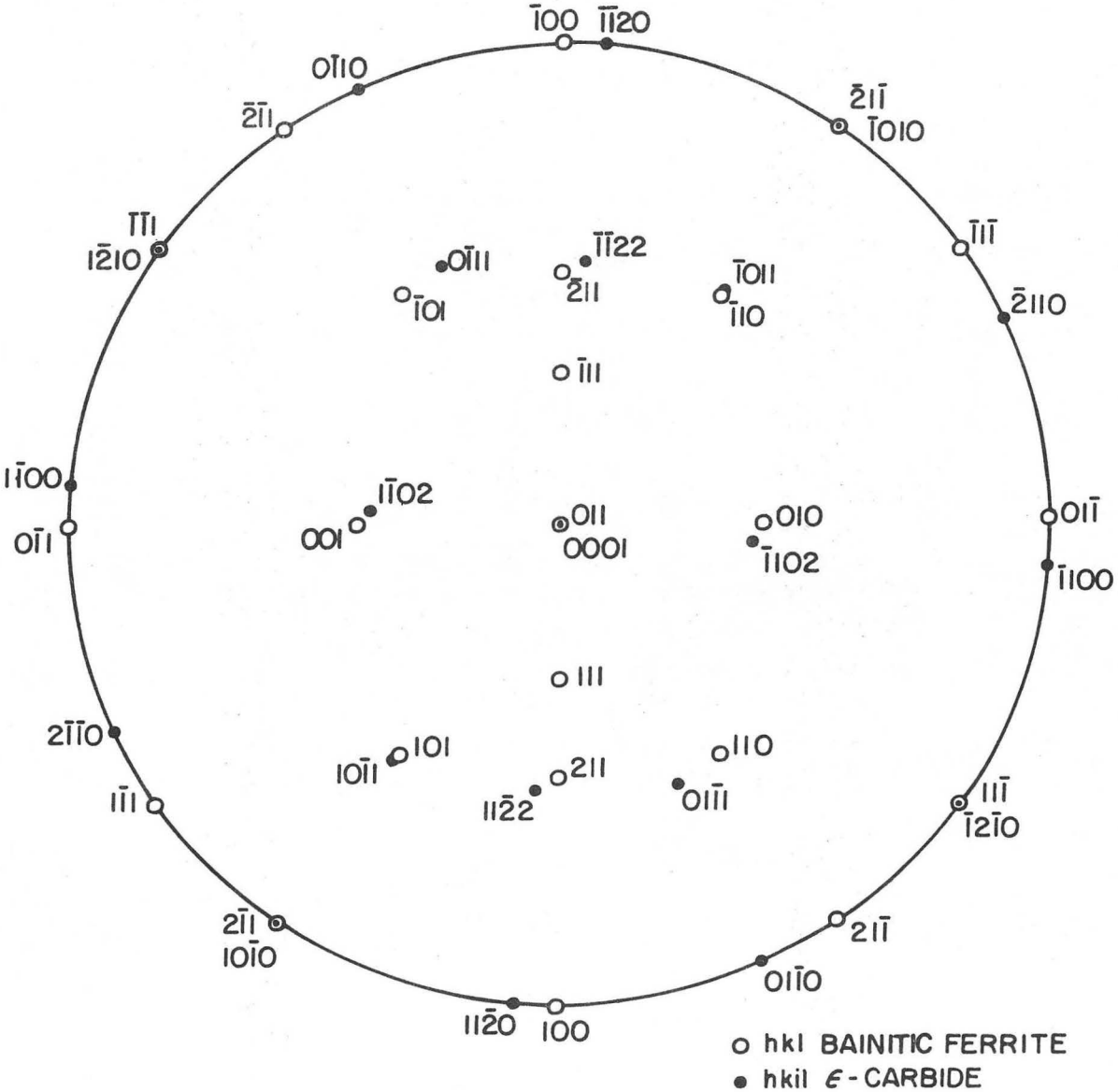

STEREOGRAPHIC PROJECTION REPRESENTING ORIENTATION RELATIONSHIP BETWEEN ϵ CARBIDE AND BAINITIC FERRITE

(0001) ϵ-CARBIDE // (011) FERRITE
($10\bar{1}0$) ϵ-CARBIDE // ($2\bar{1}1$) FERRITE
($10\bar{1}1$) ϵ-CARBIDE // (101) FERRITE

XBL-735-6152

Fig. 2

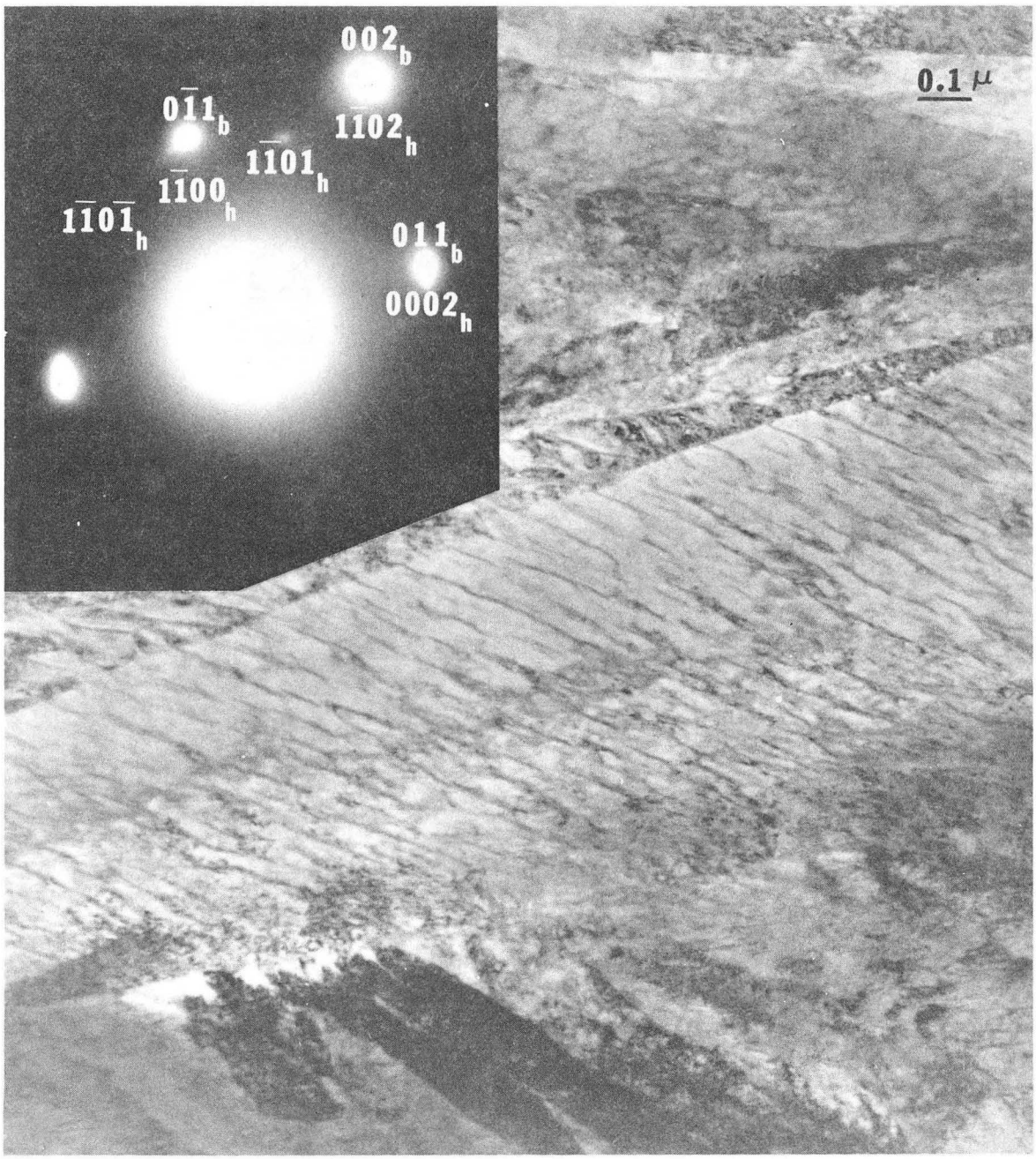

XBB 7212-6112

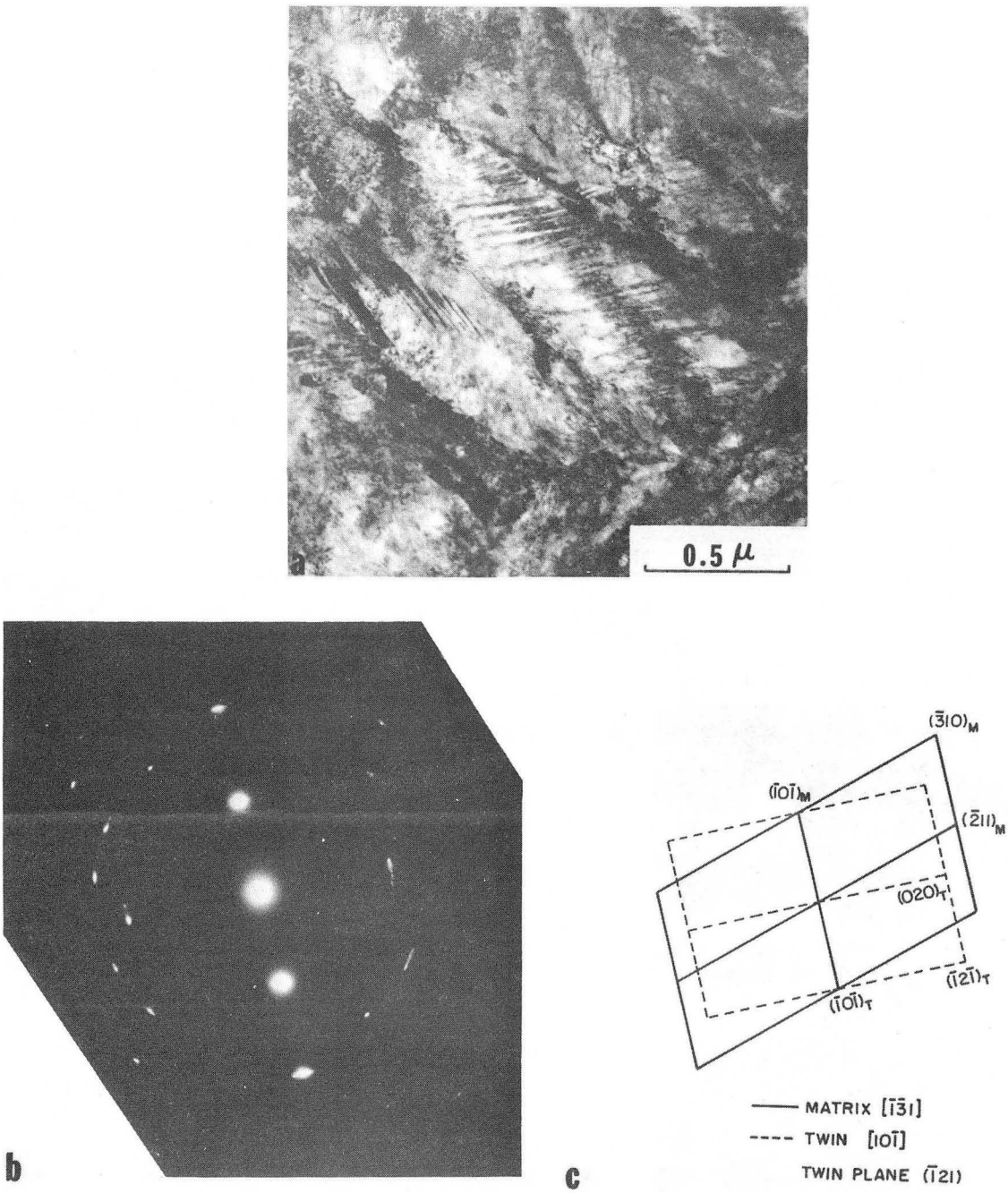

XBB 752-1323

Fig. 4

0 0 0 0 4 3 0 2 2 5 4

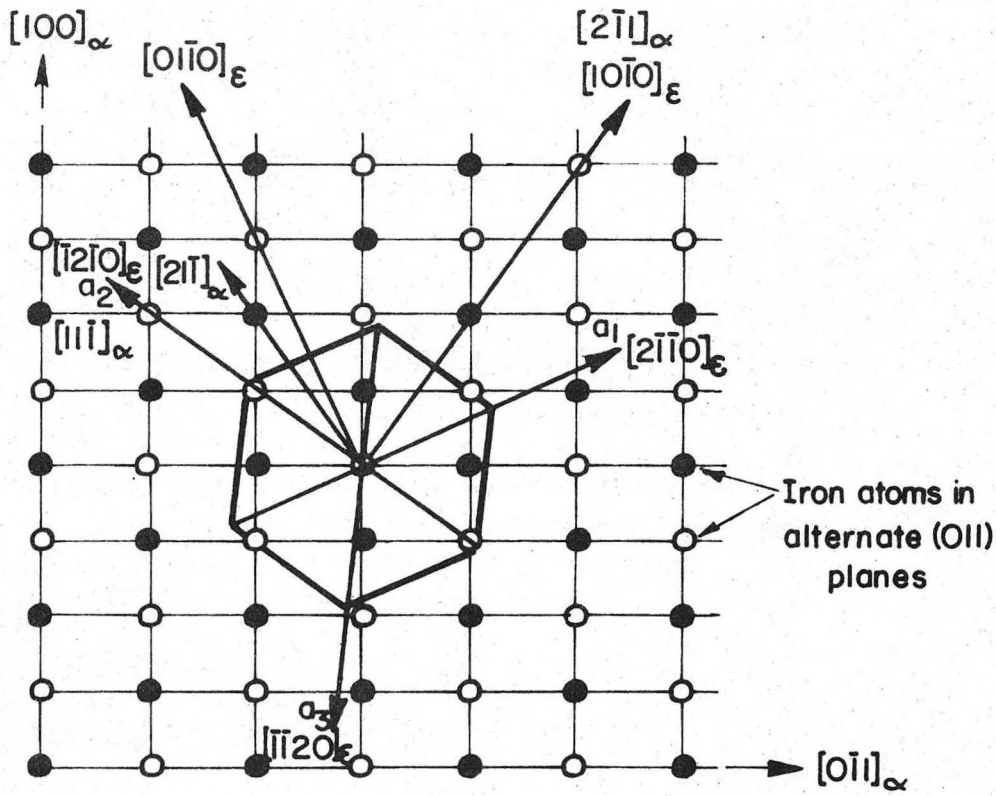

$(011)_\alpha$ projection of iron atoms in ferrite lattice, the hexagon indicates the ε carbide, exhibiting Jack orientation relationship with the matrix.

XBL 7312-7144

Fig. 5

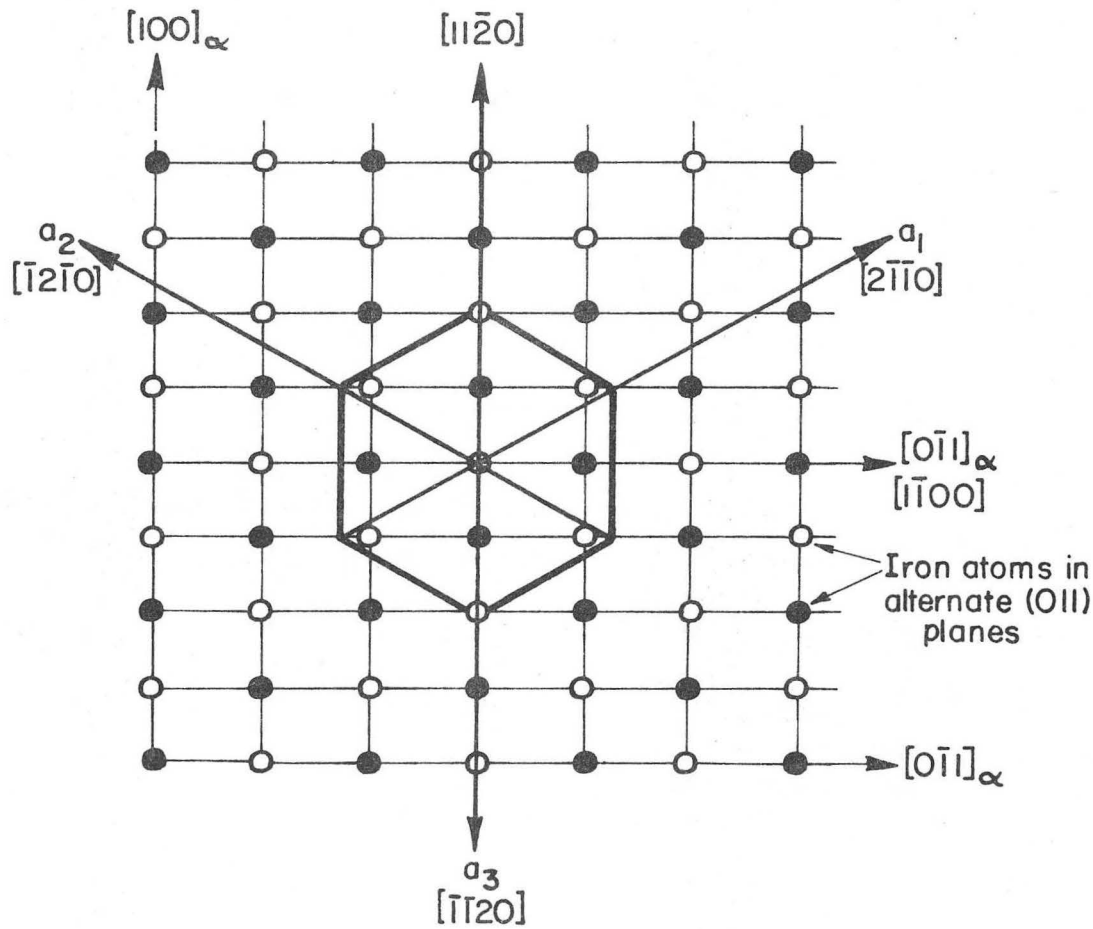

$(011)_\alpha$ projection of iron atoms in ferrite lattice, the hexagon indicates the Mo_2C, exhibiting Pitsch-Schrader orientation relationship with the matrix.

XBL741-5406

Fig. 6

0 0 0 0 4 3 0 2 2 5 5

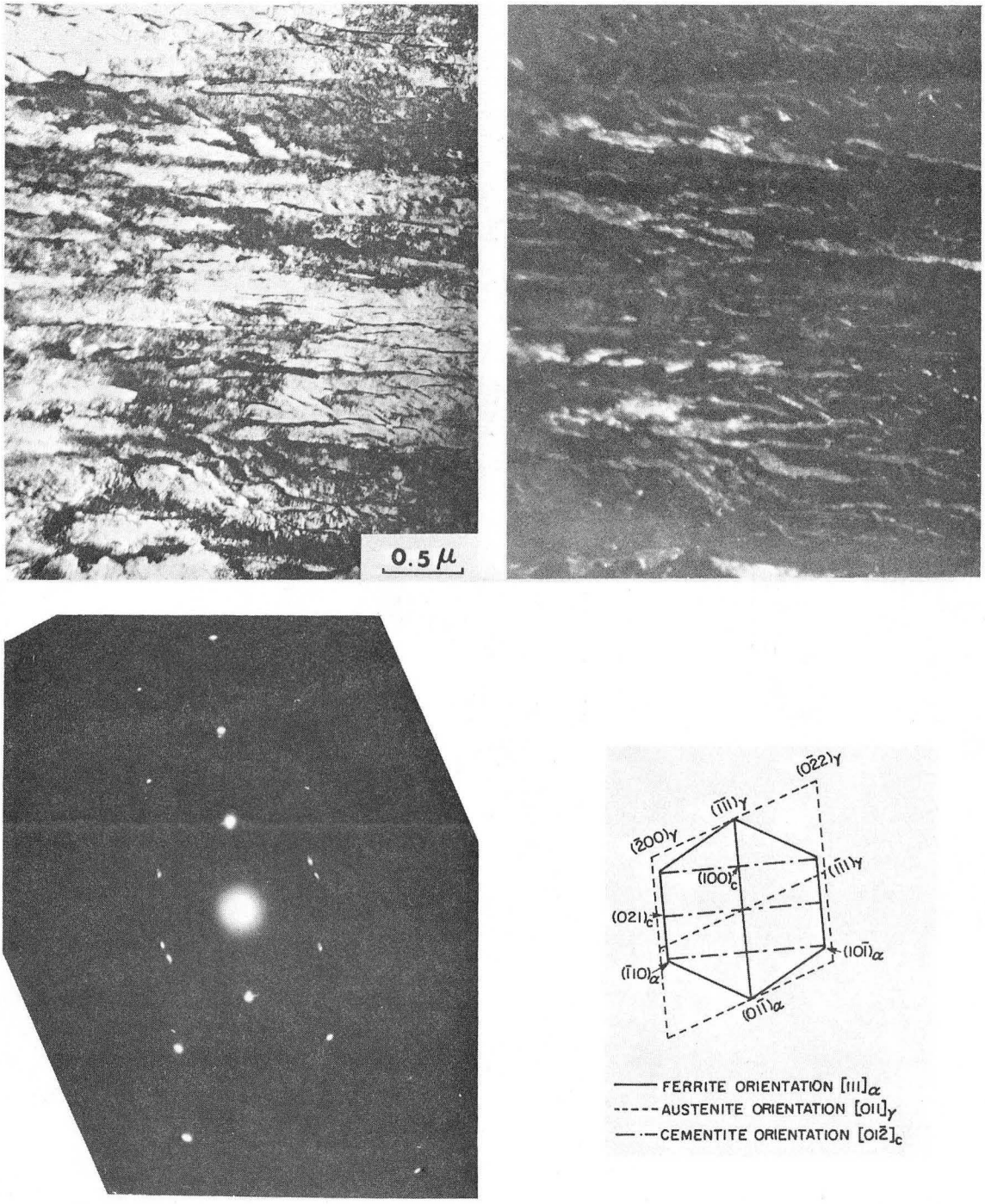

XBB 749-5957

(a) (d)

Fig. 7

(b) (c)

XBB 749-5958

Fig. 7 (e)

0 0 0 0 4 3 0 2 2 5 6

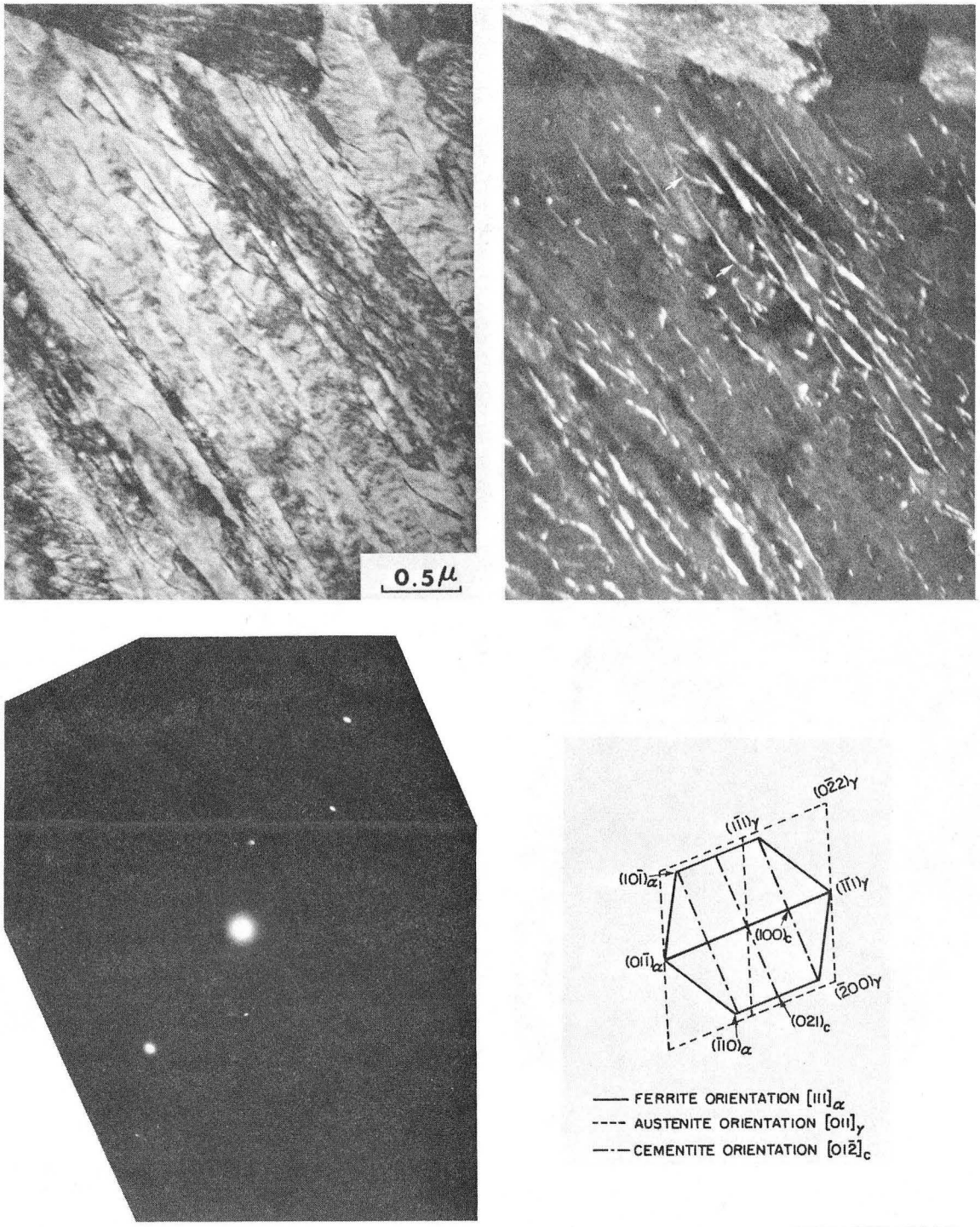

XBB 749-5962

(a) (d)

Fig. 8 (b) (c)

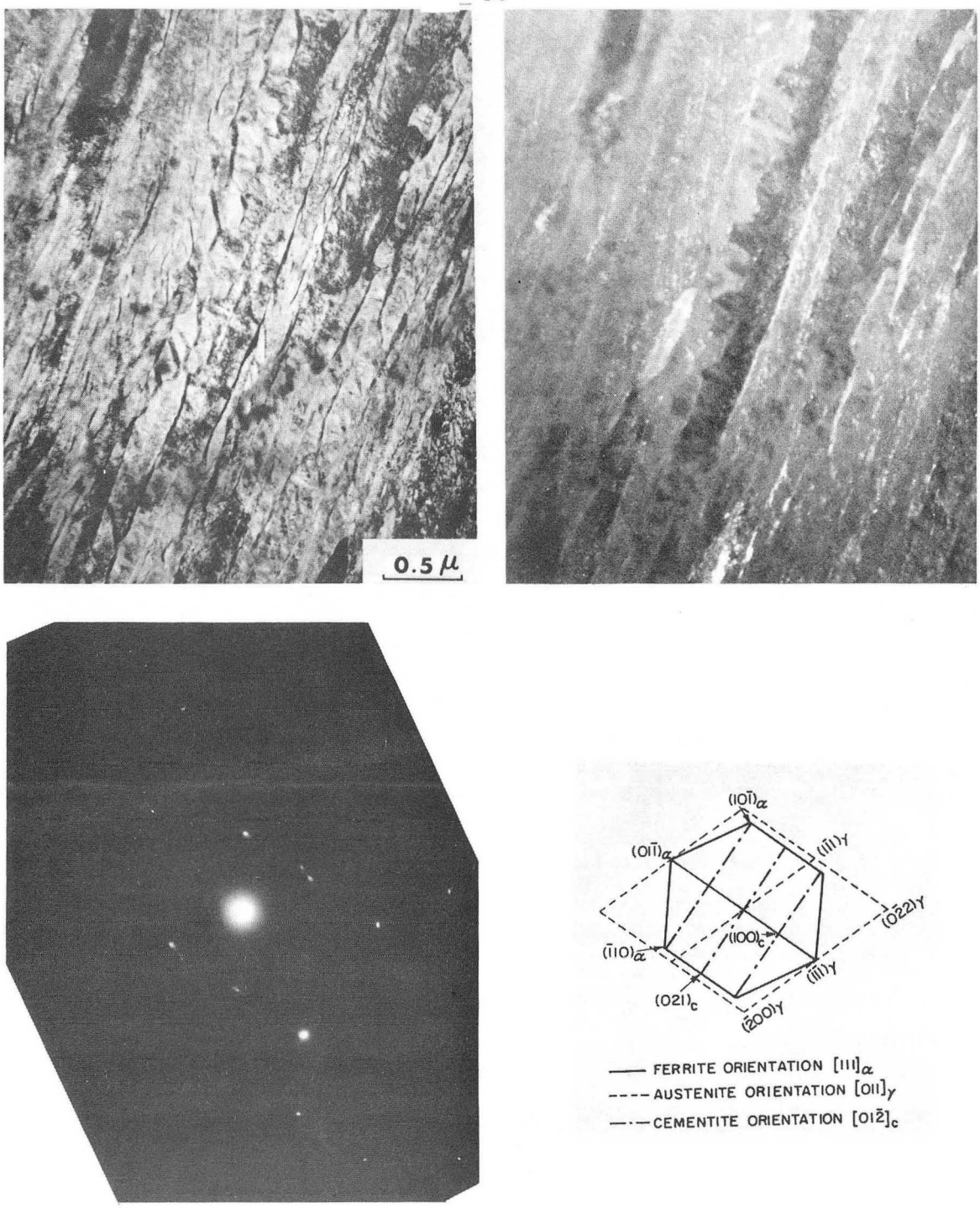

XBB 749-5959

(a) (d)

Fig. 9 (b) (c)

0 0 0 0 4 3 0 2 2 5 7

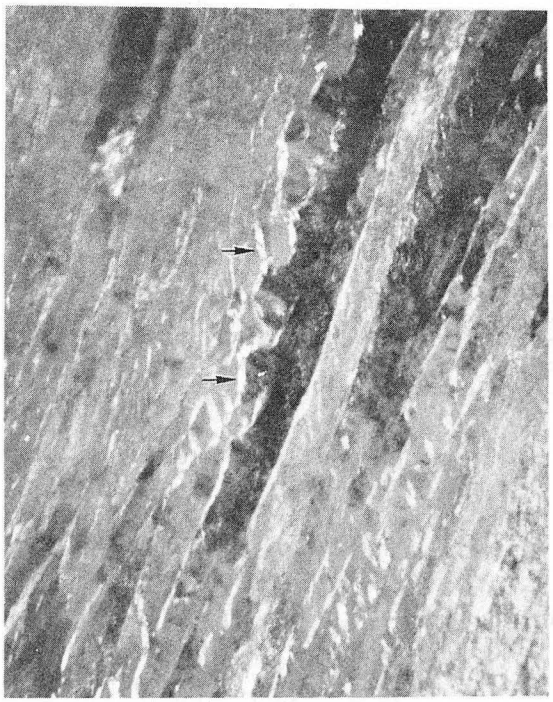

XBB 749-5960

Fig. 9 (e)

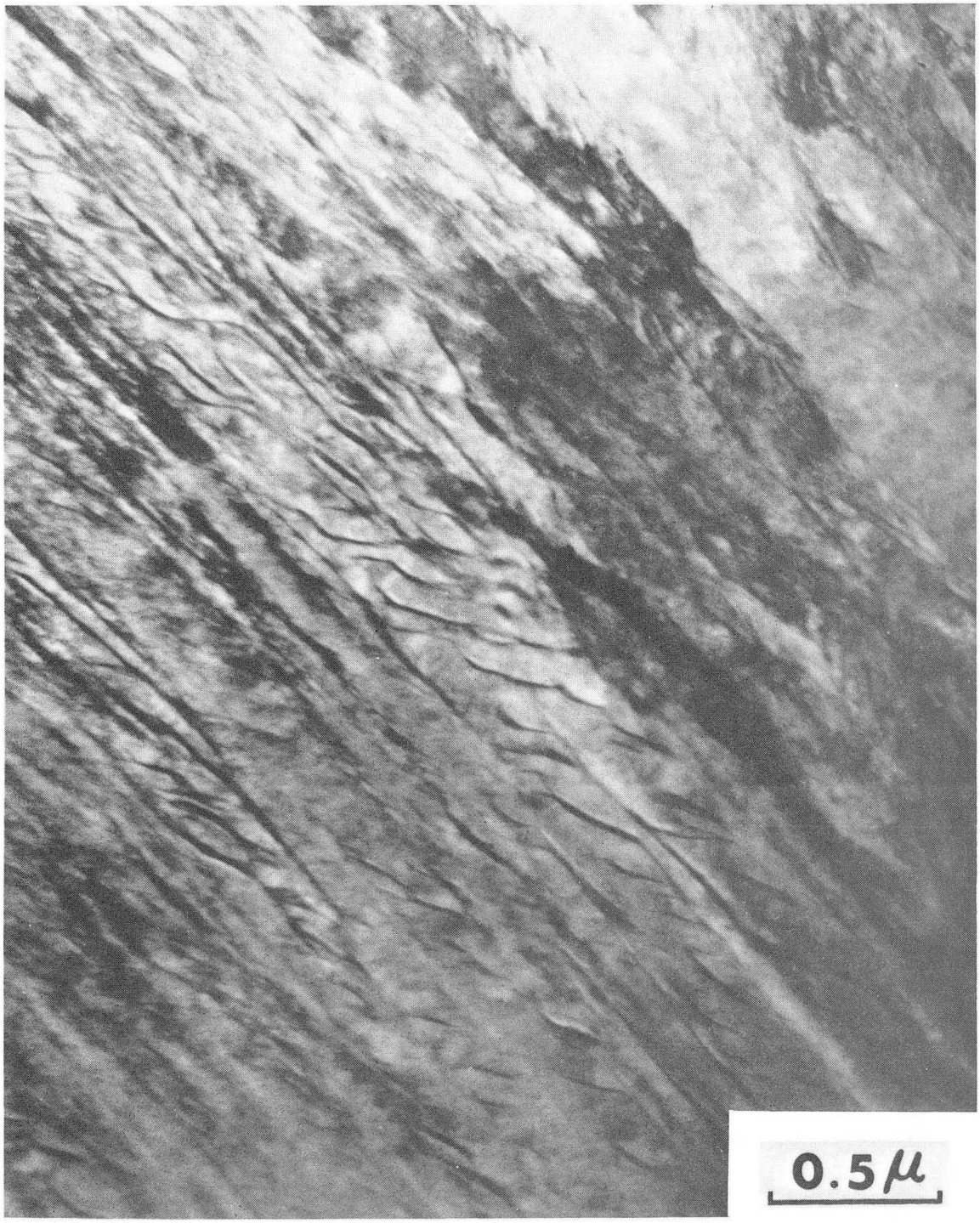

XBB 749-5964

Fig. 10

0 0 0 0 4 3 0 2 2 5 8

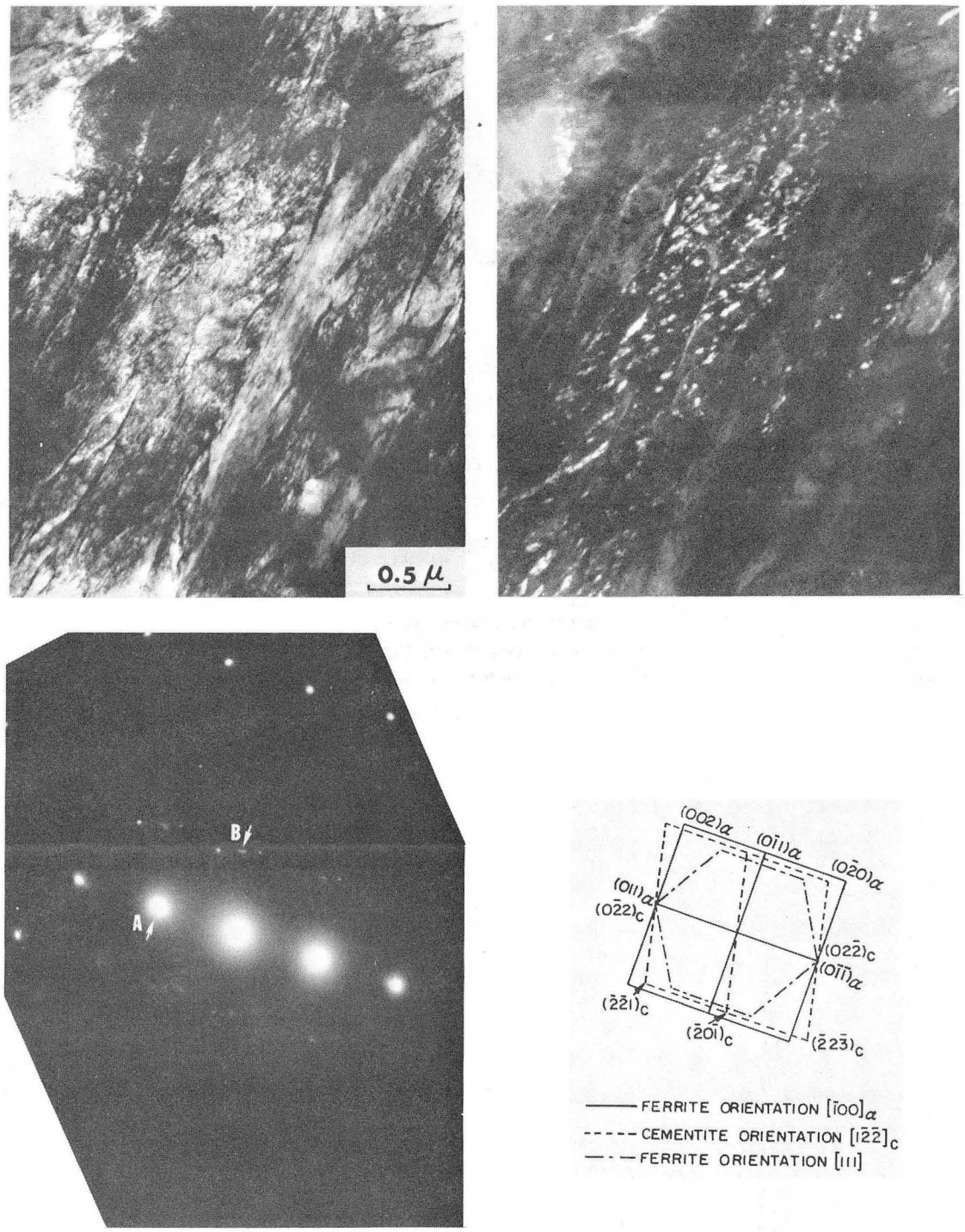

XBB 749-6296

(a) (d)

Fig. 11 (b) (c)

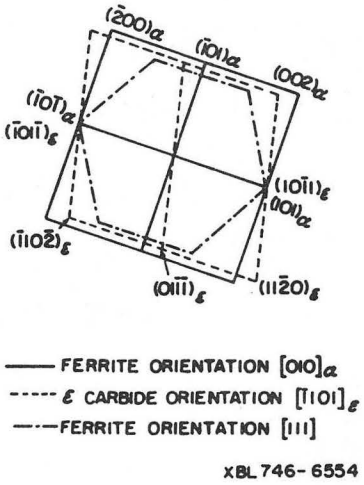
$(\bar{2}00)_\alpha$
$(\bar{1}01)_\alpha$
$(002)_\alpha$
$(\bar{1}0\bar{1})_\alpha$
$(\bar{1}01\bar{1})_\varepsilon$
$(10\bar{1}1)_\varepsilon$
$(101)_\alpha$
$(\bar{1}10\bar{2})_\varepsilon$
$(01\bar{1}\bar{1})_\varepsilon$
$(11\bar{2}0)_\varepsilon$
FERRITE ORIENTATION $[010]_\alpha$
ε CARBIDE ORIENTATION $[\bar{1}101]_\varepsilon$
FERRITE ORIENTATION [111]
XBL 746-6554

Fig. 11 (e)

0 0 0 0 4 3 0 2 2 5 9

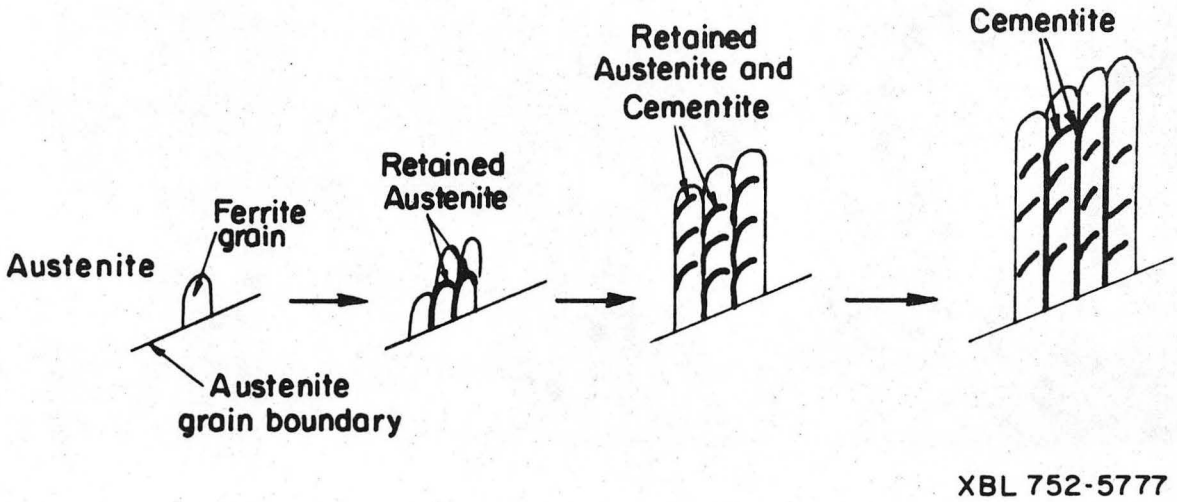

Fig. 12

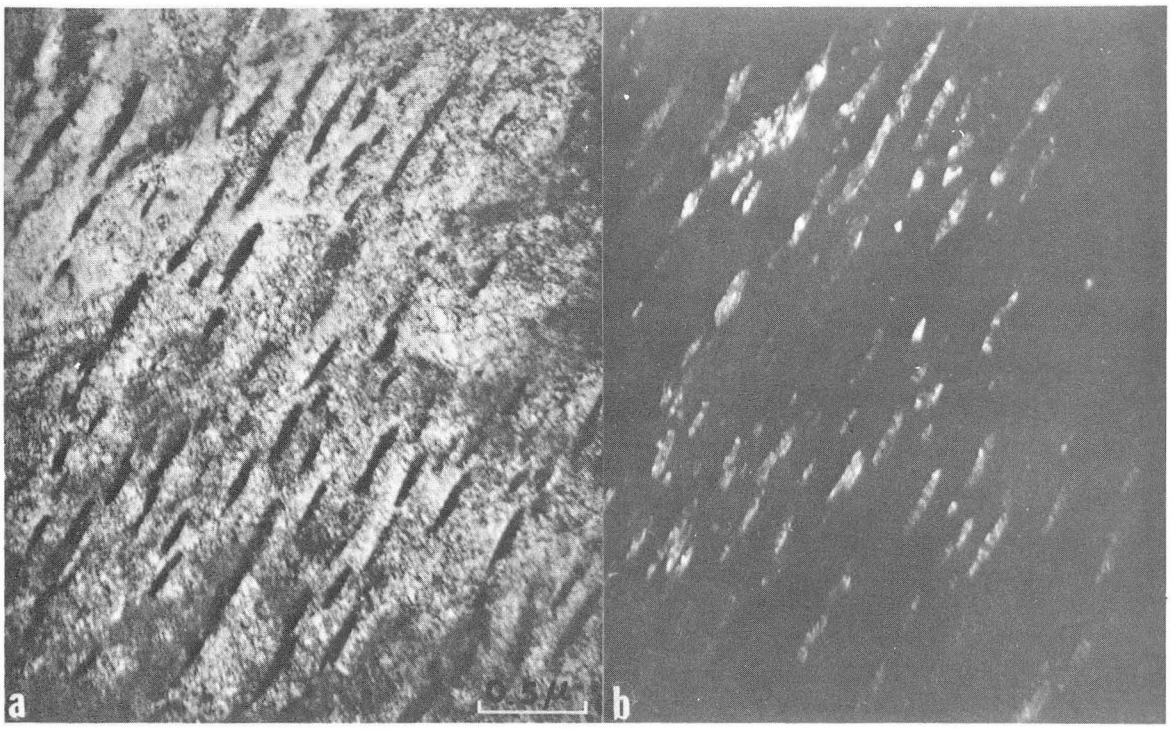

XBB 735-3152

Fig. 13

0 0 0 0 4 3 0 2 2 6 0

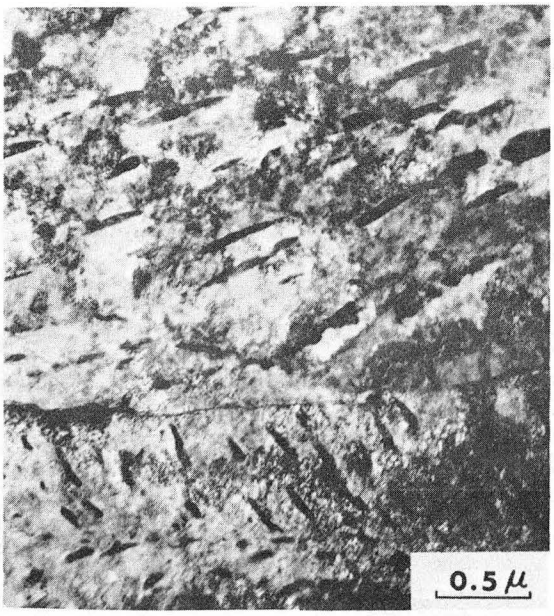

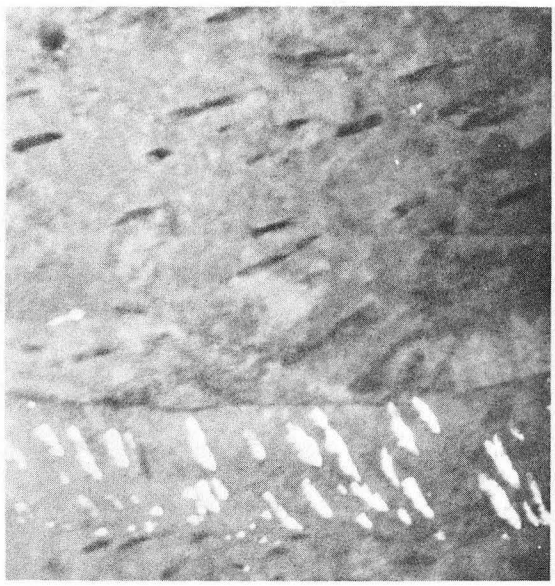

XBB 749-5965

(a)

Fig. 14 (b) (c)

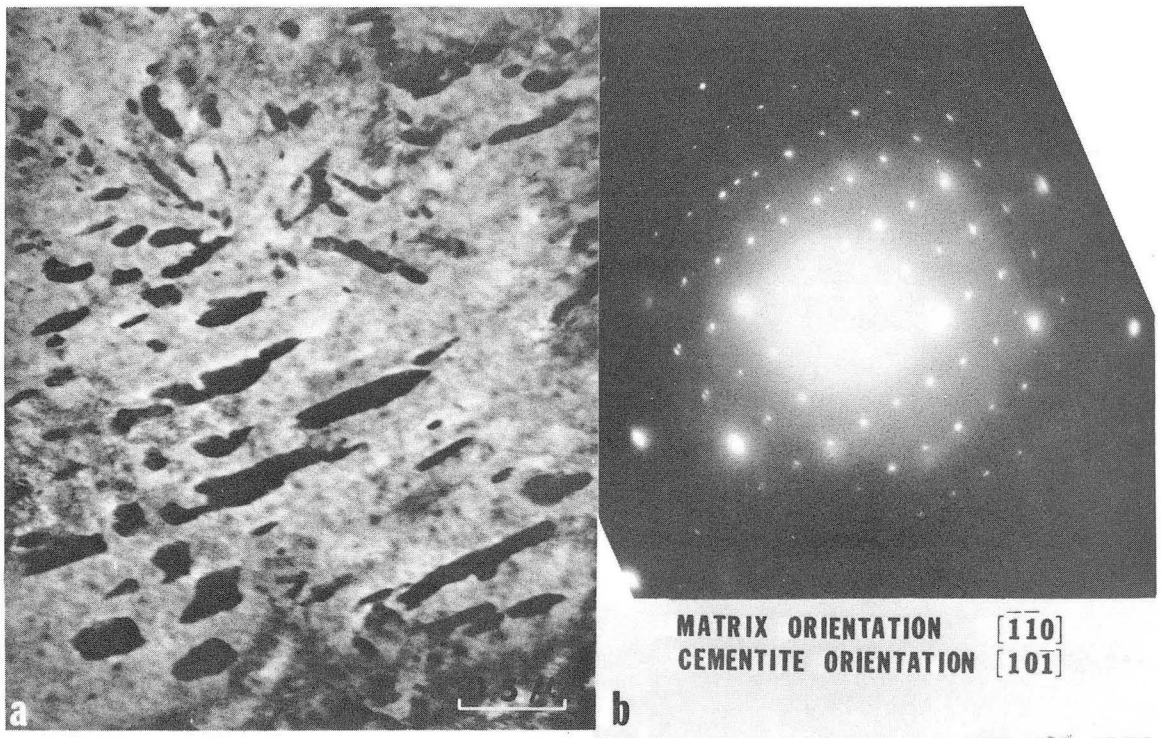

XBB 735-3159

Fig. 15

0 0 0 0 4 3 0 2 2 6 1

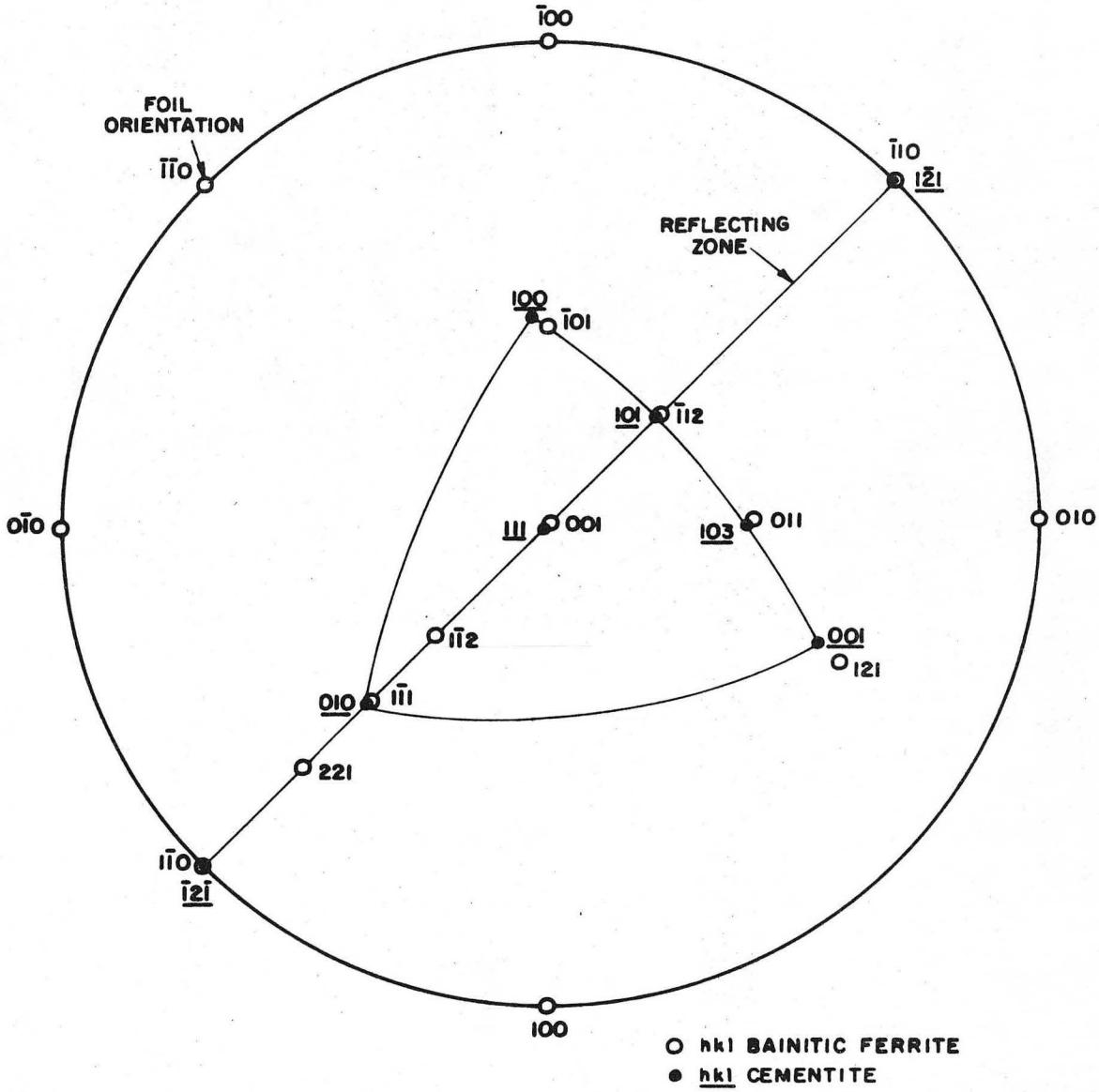

STEREOGRAPHIC PROJECTION REPRESENTING ORIENTATION RELATIONSHIP BETWEEN CEMENTITE AND BAINITIC FERRITE

XBL 735-6187

Fig. 15 (c)

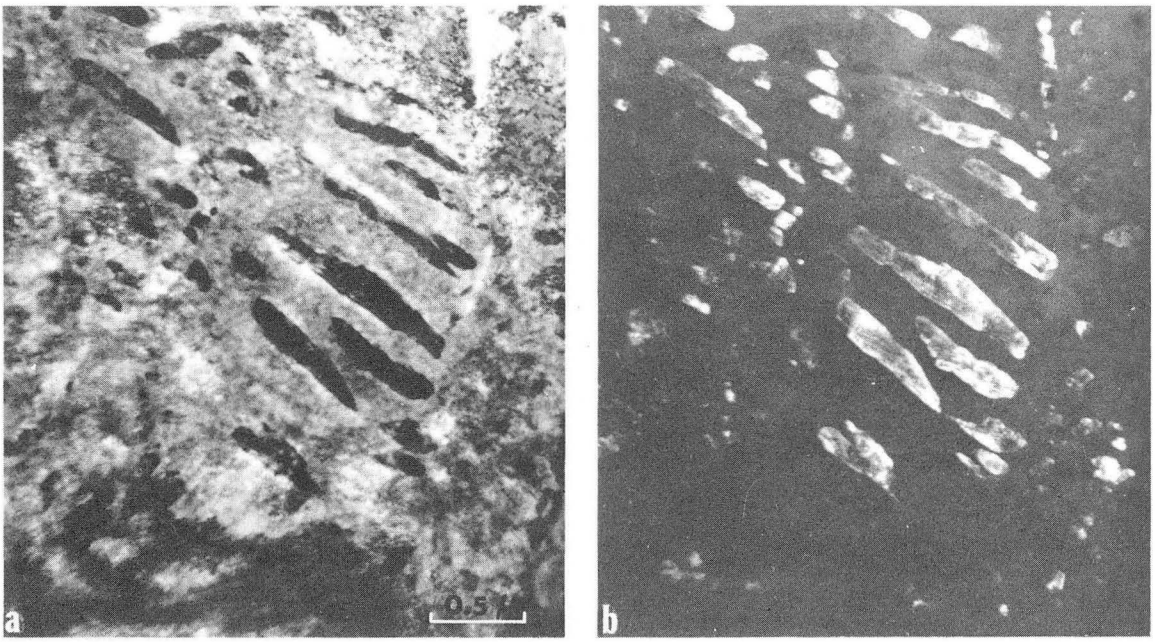

XBB 741-328

Fig. 16

0 0 0 0 4 3 0 2 2 6 2

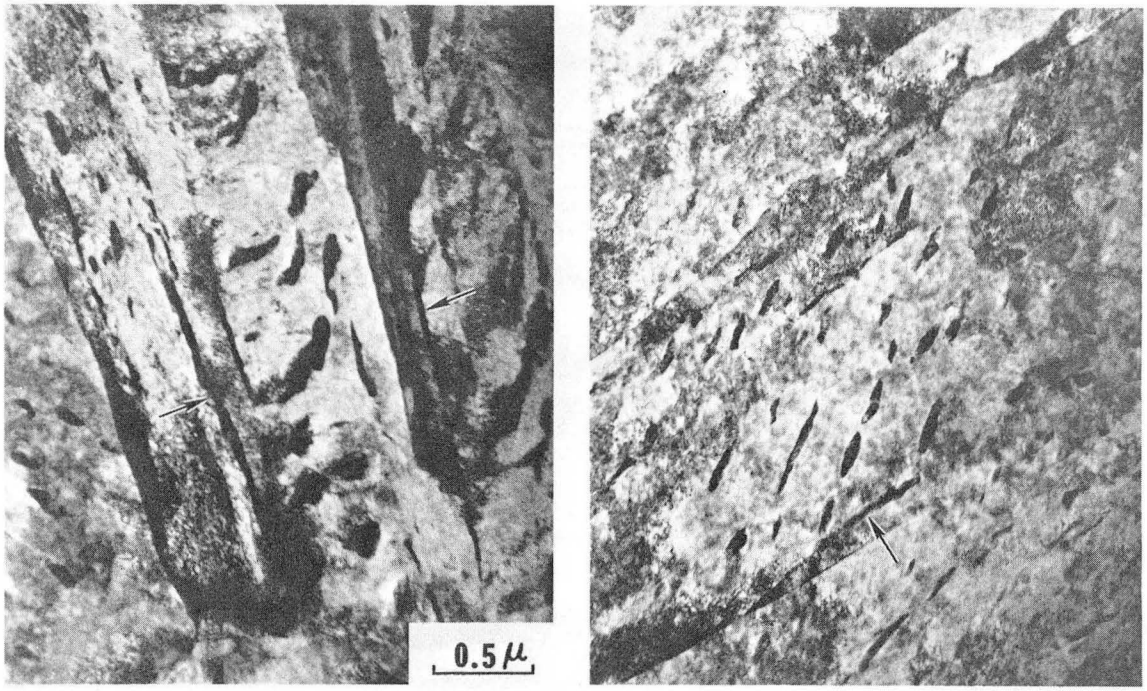

XBB 754-2668

Fig. 17 (a) (b)

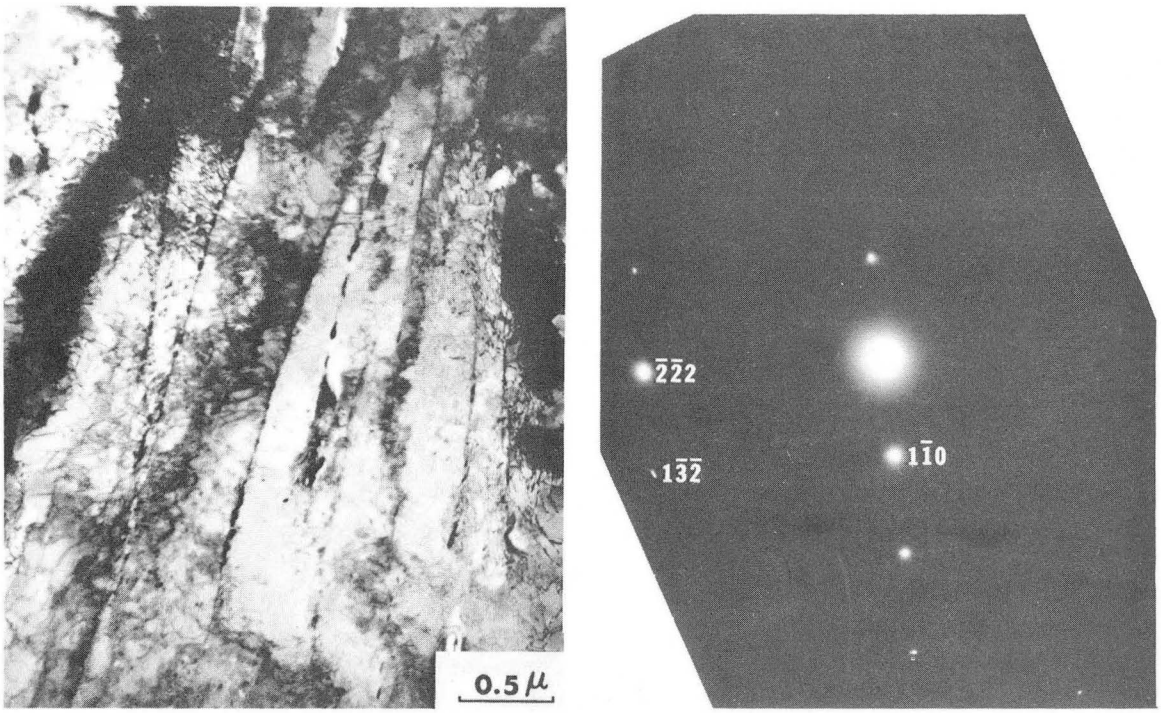

XBB 749-5966

Fig. 18 (a) (b)

0 0 0 0 4 3 0 2 2 6 3

PART II.

Transmission Electron Microscope Study of the Bainite Transformation in Fe/12Ni/4Co/0.4 C Alloy

ABSTRACT

The isothermal decomposition of a Fe/12Ni/4Co/.4C alloy (Ms=142°C) into lower temperature range of lower bainite was studied by thin foil electron microscopy. In addition to the characteristic short bainitic carbide, long carbide stringers arranged in rows parallel to the longitudinal axis of the bainite plates were also observed. These carbides were identified as cementite.

The trace normal of the bainitic carbide falls in the region of (112) and (335) ferrite plane. The cementite/ferrite orientation relationship deviates slightly from the Bagaryatskii orientation relationship.

Evidence showing the existence of internal twinning in lower bainite is also presented. The fact that the observed twins, whether accommodation or transformation, persist after isothermal holding suggests that unidirectional precipitation of carbides cannot be attributed to carbide nucleation on the transformation twins.

The transformation mechanisms are discussed in terms of the observed evidence.

I. INTRODUCTION

There is a complex series of transformation products formed in austenite as a result of decomposition at subcritical temperature ranging from proeutectoid ferrite, pearlite to bainite. At most stages, carbide precipitation accompanies ferrite formation because of the lower solubility of carbon in ferrite than in austenite. All the structures are aggregates of ferrite and carbide, but their microstructure varies with the transformation on temperature and the composition of the steel. The various transformation products have been a subject of metallurgical research for a long time. Since the classical study of Davenport and Bain[1] extensive work has been carried out on bainitic structures, but this has only served to reveal their complex nature. Perhaps the bainite reaction is still one of the least well understood of the major phase transformations in alloys, and especially in steels.

The bainite transformation is complicated in view of the fact that it probably involves two basic classes of transformation in iron alloys -- the diffusion controlled and the martensitic type. The fact that bainite bears a certain resemblance to martensite in its morphology and crystallography yet bainite involves a change in composition from austenite and involves diffusion has given rise to numerous and often conflicting theories. They may be divided broadly into three categories: theory of nucleation and growth,[2] theory of shear[1] and theory involving both nucleation and growth, and shear.[3] The habit plane of bainitic ferrite has been determined by a number of workers[2,4,5] and this evidence, together with the observed orientation relationships, supports the proposal

that bainitic ferrite forms by a displacive mechanism.[6] But it has not been successful in proving that the shear involved is the same as the lattice invariant shear involved in the austenite-martensite transformation. Recent thin foil studies of bainite using transmission electron microscopy have led to some determination of the orientation relationship between ferrite and cementite in bainite.[11,12] Some points concerning the transformation have been elucidated. Based on the crystallographic evidence together with the kinetic investigations[13,14] the conclusion that cementite precipitates from austenite in upper bainite has been generally accepted. The reaction mechanism of lower bainite is, however, still in dispute. The controversies center on the origin of the bainitic carbide. The critical question is: does cementite precipitate directly from austenite or does it go through a state of supersaturation and precipitate after $\gamma \rightarrow \alpha$ has occurred? Attempts have been made in the current research to understand this point.

A knowledge of the details of the internal structure of lower bainite is essential for a complete understanding of the bainite transformation. For example, a conclusion usually inferred that if the bainite forms martensitically then it should also be internally twinned. The unidirectional carbides could then be assumed to occur as a result of cementite precipitation along these twins during isothermal holding.[15] However, no evidence for internal twinning in lower bainite has so far been detected. It was thus argued that similar to the dislocated martensite formed at relatively high temperature the transformation strains in bainitic ferrite have been accommodated by slip instead of twinning(i.e. the inhomogeneous shear). However, the unidirectional morphology of cementite

cannot be satisfactorily explained in this case.

It is known that a twinned structure is generally observed in martensite with Ms temperature lower than ~200°C. If bainite truly formed martensitially, there is no reason why the bainitic ferrite formed at low temperature should not have a similar substructure as the twinned martensite. Bearing this in mind an alloy of composition Fe-12wt% Ni-4wt% Co-0.4wt%°C with Ms temperature of 142°C was designed so as to study bainite formed at low termperatures. Special attention has been given to the internal substructure in this low temperature transformation product. The result should provide better insight as to the origin of the distinct carbide morphology of lower bainite. The main aim of the present investigation is thus to use transmission electron microscopy and diffraction techniques to study the morphological and crystallographical features of cementite and ferrite in bainite, in the hope that the observed result would throw some light on the mechanism of bainite transformation.

0 0 0 0 4 3 0 2 2 6 5

II. EXPERIMENTAL PROCEDURE

A. Materials and Heat Treatment

The Alloy chosen for this study has the composition of Fe-12 wt.% Ni-.4 wt.% C with a Ms temperature of 142°C (286°F). It was kindly supplied by Republic Steel Company as 0.080 thick hot-rolled sheets with their designated heat number 523. The alloy was sandblasted to remove any surface oxide. It was subsequently homogenized at 1100°C for three days and furnace cooled. A simple, low-cost but successful technique was employed to prevent decarburization during homogenization. The as-received material was wrapped in a stainless steel envelope then sealed inside an Inconel tube filled with cast iron chips. The cast iron chips created a neutral atmosphere inside the Inconel tube during homogenization anneal and thus reduced to a minimum the degree of decarburization of the heat-treated materials.

Coupons of 1 in. by 1/2 in. were cut from the sheet and austenitized at 900°C for one and a half hour in a dynamic argon atmosphere and then quenched directly into a salt bath and isothermally transformed at a predetermined temperature above Ms for a certain time. Carbon analysis before and after heat treatment showed no significant decarburization. It should be mentioned that the isothermal transformation temperatures employed in this research are always above the Ms temperature of the material investigated.

B. Electron Microscopy

The heat treated 0.070 thick specimens were first mechanically ground slightly (flood cooling was employed) and then chemically thinned in a

solution of 1:1 phosphoric acid and hydrogen peroxide (30%) to about 0.005 inch. They were electropolished initially by the window technique to a thickness of 0.002 to 0.003 inch using the following solution which gave rapid thinning.

10 ml perchloric acid

100 ml acetic acid

The final electropolishing was accomplished either by the conventional window method or by a double jet polishing apparatus using the following electrolyte:

75 gm CrO_3

400 ml acetic acid

21 ml H_2O

The temperature of the electrolyte was kept at 10°C during polishing using an ice water bath. The applied voltage was about 25 dc volts although the exact voltage varied from specimen to specimen. The thin foils were examined in a Siemens Elmiskop IA electron microscopy operated at 100 kV. Stereographic projection and trace analysis were extensively employed to study the cementite/ferrite orientation and other crystallographic features of bainite.

0 0 0 0 4 3 0 2 2 6 6

III. RESULTS AND ANALYSIS

The alloy was isothermally transformed for more than 100 hours at 204°C (400°F). Previous experiments[16] had shown that after 24 hours no bainite was obtained in this alloy, and it is known that the transformation is retarded in the presence of a high alloy content.[17] It should be mentioned here that although the amount of bainite formed increased with isothermal holding time, the bainite transformation did not go to completion even after holding for 900 hours. Some areas of martensite which formed from the untransformed austenite on cooling after isothermal transformation have been detected. Great care has been taken to differentiate between martensite and bainite. Only those results which pertain to bainite are presented here.

A. Morphology and Substructure of Lower Bainite

The structure of lower bainite is known to consist of ferrite laths or plates with carbide particles oriented at 55 ~65° to the long direction of ferrite.[18]

Figure 1(a) shows the typical structure of lower bainite in this alloy where unidirectional cementite particles precipitate in the matrix. Notice the carbides have a wavy or "broken-up" appearance. A similar structure has been reported before.[19,20] A dark field image of the (103) cementite reflection reverses the contrast of the carbide as seen in Fig. 1(b). A different kind of carbide morphology, shown in Fig. 2 is found in other areas. Very long wavy fine carbides arranged in rows parallel to the longitudinal axis of the plate are observed. In addition to these long carbides, short carbide particles can be seen in between them.

Both long and short forms of these carbides were identified as cementite. Both type of carbides reverse contrast by dark field imaging a (040) cementite spot, Fig. 2(b). In a Fe/7.9Cr/1.11C alloy Srinivasan and Wayman[12] observed a similar structure, but in Fe/Ni/C alloys such a structure has not been reported before.

Even after 140 hours only a small amount of bainite was obtained. Figures 3 and 4 show mixed structure of bainite and martensite. The martensite was frequently found to be twinned (not shown here). As shown in Fig. 3(b) the martensite grains are in $[100]_\alpha$ and $[111]_\alpha$ orientation. Austenite grain boundaries have been known to be preferential sites for bainite nucleation.[21] It is clearly seen in Fig. 3(a) that bainite crystals, as pointed by single arrows, appear to have nucleated from prior austenite grain boundary (marked by double-headed arrow) and grown into the grain at the expense of prior austenite during isothermal holding. Dislocated martensite probably formed subsequently from the untransformed austenite after cooling from the isothermal transformation temperature. The impingement of martensite plates on the bainite grains supports the transformation sequence described. In this high-alloy, medium-carbon steel, the structure of martensite formed by the conventional austenitizing and rapid quenching is usually twinned. The observed dislocated martensite morphology in the present case is explained by the effect of the previously occuring bainite formation, which depletes the carbon content of the adjacent austenite and thus raises the corresponding M_s temperature. The inhomogeneous shear during the subsequent martensite transformation is therefore accomplished by slip instead of twinning resulting the

demonstration of a dislocated structure.* Since the initially formed bainite partitions the austenite grain and limits the packet size of the subsequently formed martensite, the technique of partial transformation to lower bainite has been used as a way of heat treatment to improve the fracture toughness of steel through reducing the mean fracture path. Figure 4(c) and (d) show the carbide and matrix reversed their contrast separately when dark field image was taken using a (103) cementite reflection [spot c in Fig. 4(b)] and a ($\bar{1}10$) matrix reflection separately. The bainite/martensite interface are , as denoted by single arrows, fairly straight on both sides as seen in Figs. 3 and 4. This may indicate that bainite started growing from one side by sympathetic nucleation of each subunit as suggested by Oblak and Hehemann.[22]

In order to obtain more bainite the steel was also transformed for a time as long as 900 hours. Although the carbides became coarser, the initial morphology was not destroyed (Fig. 5). These carbides lined up uniformly behind the grain boundary. It has been postulated that in lower bainite the uniformness of the carbide distribution is an outcome of cementite precipitation behind the moving ferrite/austenite interface. This model is also supported by the kinetic results.[8]

Carbides with a morphology different from those mentioned before were also observed, in which the long cementite particles were very wavy or kinked in appearance, rather than the conventional unidirectional pattern. Such a structure is illustrated in Fig. 6(a) and the corresponding

*Reviews of the microstructural characteristics of martensites can be found in G. Thomas, Met. Trans., 2, 2373 (1971), and 2) Iron and Steel International, 46, 451 (1973).

crystallographic data is shown in Fig. 6(b). An angle of 50° is measured between the trace of kink and that of the long portion of the carbide. The trace normals to the two sections of the carbides are found to pass very close to $(112)_\alpha$ and $(1\bar{1}2)_\alpha$ poles respectively. The calculated divergence extended between $(112)_\alpha$ and $(1\bar{1}2)_\alpha$ poles is 48.19° which matches reasonably well with the measured result. Thus it is rational to assume (112) and $(1\bar{1}2)$ to be the trace normals of the carbides.

Aaronson[23] has considered that the ferrite component in austenite developes by a ledge mechanism during isothermal transformation; the ferrite boundaries migrate primarily by the formation and lateral movement of ledges. The kink shaped carbides can be interpreted as marks of the ledge left by the movement of α/γ interface. There are certain similarities between the carbides in Fig. 2 and Fig. 6 where long and short carbides are interrupted in the former but the carbides are continuous in the latter.

From the crystallographic analysis shown in Fig. 6(b), $(112)_\alpha$ and $(1\bar{1}2)_\alpha$ planes seem to be the habit planes for the long portion and the kink part of the cementite respectively. Similar carbide morphology was detected in the bainitic structure of the Si containing alloy 2S54 (Fig. 8 of Part I of this thesis) when transformed at 315°C for 24 hours. It has been explained that such characteristic microstructures develop when carbide precipitated from enriched austenite at the tip of bainitic ferrite.

In some areas, the structures that were developed were quite unlike those normally characteristic of bainite (or tempered products). For example, features of this "bainite" are shown in Fig. 7(a) where long, dark striations arranged in parallel rows following the longitudinal

0 0 0 0 4 3 0 2 2 6 8

directions of the plate. Characteristic bainitic carbides are seen between the striations. The selected area diffraction pattern and its schematic representation are shown in Figs. 7(b) and 7(c). It is seen that the structure contains several orientations of ferrite. The matrix is in $[112]_\alpha$ orientation and the striations have been identified as ferrite islands in $[012]_\alpha$ zone. Figure 7(a) is the dark field micrograph using a $(\bar{2}00)_\alpha$ reflection and reveals that these ferrite islands are all in the same orientation. The contrast of the matrix is reversed when imaging a matrix $(\bar{1}10)_\alpha$ spot as shown in Fig. 7(e). A very thin layer (or rows of small particles) of cementite precipitated along the ferrite island is detected in the dark field image of spot c as indicated in Fig. 7(f). It is found that spot c corresponds to the (310) reflection of cementite. In a slightly tilted position, Fig. 7(g), the short transverse carbides are demonstrated clearly. The current observation indicated that some austenite is trapped during bainite transformation. They subsequently decompose to ferrite and carbide and give rise to this kind of morphology. Again, similar microstructures were observed in the Si bearing steel (Part I of this study).

Another kind of bainite morphology (Fig. 8) was detected which might be easily interpreted erroneously as upper bainite. The selected area diffraction pattern and the schematic representation are shown in Fig. 8(b) and (c) respectively. The dark stringers are identified as retained austenite instead of carbide. The Kurdjumov-Sachs orientation relationship, $[111]_\alpha || [011]_\gamma$ $(01\bar{1})_\alpha || (11\bar{1})_\gamma$ was followed between ferrite and austenite. The distribution of austenite is better revealed in Fig.

8(d) which is a dark field micrograph using the $(111)_\gamma$ reflection. Blocky ferrite of [100] orientation is also indicated in the analysis and shown in Fig. 8(e) by imaging the $(110)_\alpha$ spot. As mentioned before, ferrite in $[100]_\alpha$ and $[111]_\alpha$ orientation coexists in many cases. Ferrite of [111] orientation is seen in Fig. 8(f) which is a dark field image of the $\{110\}_\alpha$, $\{111\}_\gamma$ reflection. A higher magnification of the same area is presented in Fig. 8(g). Here it appears that austenite was confined during transformation and became stabilized by the external stress. By using an X-ray pole figure technique, similar orientation relationship between ferrite and austenite has been observed in bainite formed below 350°C.[2]

It has been generally agreed that ferrite is the nucleating phase in the formation of bainite. All the transformation models agree in one common fact, viz. that the ferrite is supersaturated when transformed from austenite. Now the critical question is what is meant by supersaturated ferrite? If by this we mean that the ferrite has the same composition as the parent austenite, the transformation is diffusionless and once it has started it should continue rapidly without waiting for, or without being controlled by, carbide precipitation from the ferrite. Since this is not the case the ferrite may be saturated but its carbon content should be considerably less than that of the parent austenite. The knowledge of carbon content in bainitic ferrite is very important in terms of understanding the origin of bainitic carbide. If the degree of supersaturation in bainitic ferrite exceeds that of the extrapolated $\alpha/\alpha+\gamma$ curve, carbide precipitation from bainitic ferrite seems inevitable.

0 0 0 0 4 3 0 2 2 6 9

Conversely, if the carbon content of the ferrite lies at or below that of the extrapolate $\alpha/\alpha+\gamma$ phase boundary, a large portion of the carbide must precipitate from austenite. Recently, by using a modified electron microprobe, it[24] has been demonstrated that the carbon content of the bainite was less than the detectability limit (0.03 pct) of the probe in Fe/0.11c/1.95Mo and Fe/0.13c/2.99Cr alloys. It was concluded that the initially formed bainitic ferrite was not supersaturated and the bainitic carbides which formed in these microstructures must have been precipitated from austenite. However, as pointed out by Hehemann,[25] theoretical considerations[26] indicated that the time for complete decarburization of an initially supersaturated ferrite lath is substantially less than 1 second and challenged the validity of the results claimed from the electron microprobe measurements. It seems that it is extremely difficult to decide conclusively the reaction sequence by examining the results from physical or chemical measurements of the carbon content of bainitic ferrite and retained austenite. It is hoped that the morphological and crystallographic data may provide some complementary evidence as to the understanding of the origin of bainitic carbides.

Crystallographic studies of the orientation relationships between the bainitic carbides and between such carbides and austenite have suggested that these carbides precipitate from austenite in upper bainite and from ferrite in lower bainite.[11] These results[11] are consistent with other evidence at high temperature and have generally been accepted. In the lower temperature range, on the other hand, results and analyses to be presented as follows lead to quite a different conclusion as to the

primary source of bainitic carbide precipitation.

B. Crystallography of Bainitic Carbides

Sometimes the selected area electron diffraction patterns of the bainitic carbide showed a single crystal orthorhombic pattern indicating that they have a single orientation with respect to ferrite. When a single crystal pattern of cementite was obtained from the carbide phase, the reflections were consistently indexed, and the cementite/ferrite orientation relationship was determined. Figure 9 shows the transmission electron micrograph and electron diffraction pattern for such a case. The bainite habit plane is nearly parallel to the foil surface and the parallel rows of cementite platelets can be clearly seen.

The electron diffraction pattern and its indexing are presented in Fig. 9(b) and (c), zone axis in this case is $[331]_\alpha$ The stereographic projection corresponding to the diffraction analysis is shown in Fig. 9(e). It is found that the cementite/ferrite orientation relationship is close to that of Bagaryatskii.[27]

$$(100)Fe_3C \parallel (1\bar{1}0)_\alpha$$

$$(010)Fe_3C \parallel (\bar{1}\bar{1}1)_\alpha$$

$$(001)Fe_3C \parallel (112)_\alpha$$

Similar results have been observed by other workers in bainite[11] and tempered martensite.[28] However, it can be seen that the exact Bagaryatskii orientation is not actually satisfied. After numerous investigations to check this out, it was found the discrepancy is real and this cannot be put down to experimental error. Another example of the ferrite/cementite orientation can be found in Fig. 10. The diffraction pattern and its

schematic analysis are given in Fig. 10(b) and (c). The dark field micrograph, Fig. 10(d), using the $(\bar{2}\bar{1}0)Fe_3C$ reflection revealed that all the cementite particles were in the same orientation. This diffraction pattern also gives the orientation relationship which is again close to that of Bagaryatskii[27] (Fig. 10(e)). In this case, however, the $(100)Fe_3C$ is 3° apart from $(\bar{1}10)_\alpha$. This also indicates that the cementite/ferrite orientation relationship slightly deviates from that of the tempering relationship.

In order to determine the habit plane of the carbides, trace analysis was carried out. Figure 11 shows one of many examples. The corresponding stereographic projection is shown in Fig. 11(c). The trace normal to the carbide particles passed close to $(112)_\alpha$ plane. Twelve similar trace normals were plotted in Fig. 12. It is seen that the cementite habit plane lies in the region of $(112)_\alpha$- $(335)_\alpha$ which are 5° apart.

As mentioned before, cementite was related to bainitic ferrite with the Isaichev orientation relationship,[29] and the ferrite/austenite lattice relationship follows that of Kurdjumov-Sachs.[30] The orientation correspondence of the three crystals, i.e. austenite, ferrite and cementite can be summarized in Fig. 13 after proper variants have been chosen. The relationship between the three structure can now be expressed uniquely as follows:

$$(100)c \;||\; (5\bar{4}5)_\gamma \qquad 4.76° \text{ from } (101)_\alpha$$

$$(010)c \;||\; (10\bar{1})_\gamma \;||\; (11\bar{1})_\alpha$$

$$(001)c \;||\; (252)_\gamma \qquad 4.76° \text{ from } (\bar{1}21)_\alpha$$

It should be noted that the above relationship between bainitic carbide

and austenite are those which are involved in the relevant variant of the Pitsch lattice relationship[31,32] which was obtained when cementite formed in austenite. This leads to the conclusion that the bainitic carbide was originally formed in austenite. The kinetic data of Aaronson[25] also supports this analysis.

It is interesting to notice that austenite, bainitic ferrite and cementite are related in a way such that the close-packed plane and direction are parallel in all the three structures, viz.,

$$(111)_\gamma \parallel (011)_\alpha \parallel (103)_c$$

$$(10\bar{1})_\gamma \parallel (11\bar{1})_\alpha \parallel (010)_c$$

C. Internal Twinning

It is known that the matrix of lower bainite consists of dislocated ferrite. The existence of internal twinning in bainite has been speculated for many years, because if bainite is truly formed by a martensitic mechanism, as proposed by some workers then some bainitic ferrites would be expected to contain transformation twins, which is characteristic of low temperature formed martensite. However, no direct evidence of microtwins has so far been presented, but then, most of the structures of lower bainite reported have been obtained by transforming at temperature of 500°F (260°C) or above. These transformation temperatures may be too high for twinning to occur, if we draw the anology to dislocated or twinned martensite. Also extremely careful diffraction and dark field analyses must be carried out. In the current study evidence proving the existence of internal twinning has been found, which will be described as follows. Figure 14(a) shows the structures of lower bainite in this Fe/Ni/Co/C

steel after isothermally transformed at 204°C (400°F) for 15 days. Elongated carbide particles together with some internal twinning in grey contrast (delineated by double arrows) can be seen inside the dislocated matrix. The selected area diffraction pattern, Fig. 14(b), is analyzed and indexed as [115] matrix, [111] twin, and the carbide is identified as cementite in $[01\bar{2}]$ orientation. The twin plane is $(11\bar{2})_\alpha$. Many reflections from these three crystals are superimposed on each other. Dark field images of a series of reflections were taken very carefully. Figure 14(c) shows the dark field image of a (021) cementite spot, the carbide contrast is reversed. The twins are in the background as indicated by double arrows. Both the carbide and the twin reverse the contrast when the $(01\bar{1})$ twin spot and (121) Fe_3C spot was dark imaged as shown in Fig. 14(d). By examining Fig. 14(c) and (d) it should be noticed that some of the cementite are not locating exactly along the twin boundaries. Similar results were obtained by examining the dark field image of reflections of (221) Fe_3C (Fig. 14(e)), $(10\bar{1})$ twin and $(\bar{1}21)$ Fe_3C (Fig. 14(f)) and $(\bar{1}\bar{1}2)$ twin and $(0\bar{4}\bar{2})$ Fe_3C (Fig. 14(g)). Although the nature of the twinning is not understood, the present evidence for the existence of internal twinning in bainite is of significance that twinning actually can be a transformation mode or accommodation deformation mode in bainite.

As mentioned before the trace normals of the bainitic carbide fall in the region of $(112)_\alpha$ and $(335)_\alpha$. It is clearly seen that the cementite particles are situtated at an angle to the twin interface in Fig. 14. The carbide habit is obviously not (112) type since the twin plane has already been identified as (112) plane. The phenomenological theory of martensitic transformation was originally developed for the condition of $(112)_\alpha$

twin inhomogeneity. It seems quite clear that the bainite crystallography cannot be satisfactorily accounted for by martensitic theory. A similar point of view has also been pointed out before.[5] Furthermore, the current evidence shows that the unidirectional carbide morphology in lower bainite is not the result of cementite precipitation along twin boundaries. This is in disagreement with what has been discussed by Shackleton and Kelly.[15]

D. Summary of Principal Results

The most important results of this part of the investigation are summarized as follows:

(1) In addition to the characteristic lower bainitic carbide morphology, a long, fine carbide distribution, with particles arranged in rows parallel to the major growth axis of the plate was also found; the carbide was identified as cementite. These long carbides are part of the decomposition product of the entrapped austenite ($\gamma \rightarrow \alpha + Fe_3C$).

(2) Bainite grows from the austenite grain boundary and the interface between bainitic ferrite and austenite is usually planar.

(3) Carbides in the shape of kinks have been resolved. These could occur from a ledge growth mechanism.

(4) The ferrite and austenite in this alloy are related by the Kurdjumov-Sachs relationship.

(5) The bainitic carbide/ferrite orientation relationship deviates slightly from the relationship observed for tempered martensite.

(6) The habit plane of the bainitic carbide seems to be $(335)_\alpha$ instead of $(112)_\alpha$.

(7) Internal twinning has been resolved in lower bainite where carbides lie at an angle to the twin interface.

0 0 0 0 4 3 0 2 2 7 2

IV. DISCUSSION

A. Precipitation of Cementite in Lower Bainite

The cementite platelets were related to the bainitic ferrite by the Isaichev orientation relationship[29] rather than due to that of Bagaryatskii.[27] In order to understand this, it seems necessary to examine the possibility whether cementite precipitates in ferrite or in austenite.

In lower bainite, it has been generally believed that cementite precipitates from supersaturated ferrite which is formed by a shear type (martensite-like) mechanism from parent austenite.[1,6,33,34] Nevertheless, this formation sequence does not differ from that of the autotempering of martensite. The transformation nature of this process is also questionable. According to Pickering,[33] "Only when this precipitation (of carbides from supersaturated bainitic ferrite) has lowered the carbon content of the ferrite sufficiently, is the driving force restored to a level which allows the bainitic ferrite to grow. The new growth again produces supersaturated ferrite, and again carbide precipitation is required within the ferrite for the bainite to continue to grow." If there were sufficient driving force for the transformation of austenite to supersaturated ferrite to occur in the first place, it might be unreasonable to expect the carbide to precipitate from the supersaturated ferrite in order to proceed the growth process.[35] Moreover, the bainitic carbide has been observed to lie at an angle to the twin interfaces. The unidirectional morphology of bainitic carbide cannot be attributed to carbide precipitation on the internal twins; whereas in the tempered martensite such a carbide morphology can be expected from twin interface precipitation of

cementite particles. It has also been suggested that cementite precipitation might take place on stacking faults produced during martensitic transformation of supersaturated ferrite from austenite.[34] This is not convincing because stacking faults have never been observed in body centered cubic structures. In addition to this, the ferrite/cementite lattice relationship is that of Isaichev[29] instead of Bagaryatskii.[27] The Bagaryatskii orientation relationship would be attained if cementite were formed in ferrite as in the case of tempering of a martensite. Therefore, it seems unlikely that the bainitic carbide is formed either in ferrite or in contact with ferrite at the austenite/ferrite interface.

The second possibility is that the cementite particles precipitate within austenite. In fact the analysis shown in Fig. 13 demonstrated that the bainitic carbide is related to austenite by the Pitsch orientation relationship[31] suggesting that the cementite originates from austenite. However, this would not differ from that of the precipitation of proeutectoid cementite from austenite. Besides the unidirectional morphology of cementite cannot be accounted for is cementite precipitates in the bulk austenite.

Since it is almost certain that carbide nucleates on some particular crystallographic planes, an alternative is that the cementite is formed on the austenite side of the austenite/ferrite interface. As indicated by Andrews,[36] only small atomic rearrangements are necessary to produce the cementite structure from ferrite. The ferrite surface in austenite may thus serve as a favorable nucleation site for cementite because of the high similarity between the crystal lattice of the two structures.

0 0 0 0 4 3 0 2 2 7 3

Both ferrite/cementite and austenite/cementite orientation relationships should be concomitantly satisfied in this case. As pointed out in the stereogram analysis, Fig. 13, this lattice correspondence is in fact achieved.

B. Mechanism of Bainite Transformation

Despite the interest shown in the bainite reaction since it was first described in the 1930's there is still no universally accepted model for the mechanism of this mode of austenite decomposition.

Two principal mechanisms have been suggested to account for the characteristics of the reaction. The first was proposed by Davenport and Bain[1] and can be summarized as follows. Bainite forms initially as a carbon-supersaturated ferrite (which has the same chemical composition as the parent austenite) by a shear mechanism and carbides subsequently precipitate internally. This model was further developed by Zener[37] and subsequently supported by Ko and Cottrell[6] after observing the surface relief effect accompanying the formation of bainite. This model, which does not differ from that of autotempering of martensite, cannot explain satisfactorily the slow rate of growth of bainite. Besides, Cristian[38] has shown that surface relief only means that the interface is semicoherent and there is a lattice correspondence between bainitic ferrite and austenite. Surface tilts may not constitute sufficient evidence for a diffusionless transformation since Widmanstatten ferrite has also been observed to exhibit surface relief effects.[39]

The other model was proposed originally by Hultgren[40] and given as follows. The bainitic reaction consists of an initial nucleation and growth of carbide-free equilibrium ferrite, gradually enriching the surrounding austenite in carbon until a point is reached when particles of

Fe_3C form just ahead of the bainite grain. Hultgren believed that the ferrite grains grow relatively large because of the relatively high rate of diffusion of carbon and low rate of nucleation of carbide. The attractive feature of this model is that it explains the slow growth rate of bainite in terms of carbon diffusion away from α/γ interface. As further developed by Hillert[41] based on Zener's analysis,[37] it is now commonly called the Zener-Hillert model.

In the case of upper bainite, it has been shown that austenite becomes increasingly enriched in carbon content as the reaction proceeds.[7] Furthermore, crystallographic evidence has supported the fact that bainitic carbides nucleate in the austenite.[11] Therefore, the Hultgren model for the upper bainite reaction is generally accepted. Sheaves of parallel ferrite laths nucleate side by side, the entrapped austenite between the ferrite lath becomes progressively enriched in carbon and eventually transforms to elongated cementite particles.

In view of the structural, morphological and crystallographic similarities between tempered martensite of a high carbon steel and lower bainite, it[1,6,37,42] has been frequently assumed that the formation of lower bainite follows the Davenport and Bain mechanism. However, the kinetic data[43] suggest that the edge-wise growth of lower bainite proceeds by the Hultgren mechanism.

More recently, the growth mechanism of the ferritic component of bainite became the central controversey on the bainitic reaction. There appear to be two major schools of thought on this subject which are led notably by Hehemann and Aaronson respectively. Hehemann and co-workers[7,22] proposed that both upper and lower bainite form initially with substantial

supersaturation, by a shear mechanism. It was suggested that individual bainite plates grow substantially more rapidly than volume-diffusion-control allows. The bainite is assumed to grow by repeated nucleation of substructural units which rapidly attain a limited size similar to the case of sympathetic nucleation. This mechanism of growth ensures extensive supersaturation of bainitic ferrite with respect to carbon. The carbide precipitation plays only a secondary role in this shear mechanism.

The other growth model as proposed by Kinsman and Aaronson[26] is the diffusion-controlled mechanism. Here Widmanstatten ferrite, upper and lower bainite form a continuous series of reaction products, in which the rate of growth varies in a continuous fashion and is paced by partition of carbon to austenite. The bainites grow at rates of the order of, or less than, those allowed by volume diffusion-control. In this view, carbide precipitation plays an essential, rather than an ancilliary role. Based on the microstructural definition of bainite, the diffusion control model appears to be the more probable.

As mentioned before, the central issue of the controversy over the bainite reaction is mainly one of definition. It exists simply because the terminology that was used originally to designate a new transformation product in carbon steels has generally been used to describe a whole range of similar products in other alloys, moreover, often to imply a mechanism of formation.

For the past 40 years, tremendous efforts have been spent in trying to formulate a single transformation mechanism to account for all the observed phenomena simultaneously in the bainite transformation of all the alloy systems. So far no single model has been given that can explain

satisfactorily all the observed facts. This is not surprising. In solid-state transformations we know there is no one single theory which can explain all the characteristics of the martensitic transformation. Strictly speaking one can ask: is martensite formed by a truly diffusionless process? It is known that this depends on the system under discussion. It is a pure shear, diffusionless reaction in some alloy systems, e.g. high carbon alloys, but involves short-range diffusion in some other systems. Similarly, in a recent study it was found that short range ordering cannot be explained satisfactorily by either the microdomain model or the statistical model alone.[44] By the same token, although it is possible to explain the formation process of a particular kind of "bainite" in a specified system from physical and chemical informations, it is difficult to establish a general mechanism for all systems.

Among the two major formation mechanisms - the shear model and the diffusion-controlled model, it is the author's conclusion that a combination of both must operate during bainite transformations in steel. In a particular system, at high transformation temperature, the diffusion-controlled mechanism dominates while shear mechanism plays only a minor role. The shear mechanism becomes dominant at low transformation temperature but the reaction will not be accomplished without the contribution from diffusion. Thus, bainite formed at different temperatures in different systems can be explained if they were achieved by a combination but differing contributions from shear and diffusion, and this is exactly the case in many observations.

0 0 0 0 4 3 0 2 2 7 5

From the observations in this study, the formation of various morphologies of bainite is envisaged from a different viewpoint. The two main factors which dominate the morphologies of bainite are (1) the driving force which determines the formation mechanism of ferrite and (2) carbon diffusivity. The bainitic ferrite forms first during transformation, and the morphology of the ferrite is determined by the driving force. Precipitation of carbide subsequently takes place, which is dictated by the diffusity of carbon to conformed to the substructure of ferrite. The competitive process between ferrite growth and carbide nucleation gives rise to various morphologies of bainite, i.e. upper temperature formed bainite, lower temperature formed bainite and bainite of mixed structure. In other words, following the formation of bainitic ferrite (which contains less carbon than the parent austenite), the appearance of bainite is determined by the relative kinetics of carbide precipitation within the ferrite and of partitioning of carbon to the adjacent austenite. At high temperature, the carbon has a sufficiently rapid rate of diffusion in austenite to be able to diffuse away ahead of the moving α/γ interface before the carbide has a chance to precipitate inside the ferrite grains. As the ferrite laths grow together, the carbon content in the austenite entrapped between them is increased until it exceeds the solubility of carbon in austenite and the cementite precipitates directly from austenite. At lower temperature, the carbon diffuses so slowly that it can no longer maintain a complete partitioning between austenite and ferrite. The increase of the carbon

concentration in the austenite at the α/γ interface produces cementite at the interface.

As discussed before, the type of bainite formed is partially determined by the carbon diffusivity. The nucleation rates of carbide also play an important role in determining the kind of bainite formed. As observed in this study, silicon when used as an alloying element has a distinct influence on the morphology of bainite and this can be attributed to the role of silicon effect in modifying the rate of carbide precipitation. Thus carbide morphologies of typical high temperature bainite are observed in silicon steel when transformed at low temperature. The morphology of bainite is very much composition dependent and at similar transformation temperatures, different morphologies of bainite are observed in different steels.

0 0 0 0 4 3 0 2 2 7 6

V. CONCLUSIONS

(1) The cementite in bainite is related to ferrite with a specific variant of the Isaichev orientation relationship rather than due to that of Bagaryatskii.

(2) It appears that the bainitic carbide is formed in austenite at the ferrite/austenite interface.

(3) Internal twinning in bainitic ferrite has been resolved. The fact that the observed twins, whether accommodation or transformation, persisted after isothermal holding suggests that the unidirectional precipitation of carbides cannot be attributed to carbide nucleation on twins.

(4) In lower bainite, it has been shown that the uniform distribution of carbide is the outcome of cementite precipitation from austenite at the moving ferrite/austenite interface.

REFERENCES

1. E. S. Davenport and E. C. Bain, Trans AIME, 1930, vol. 90, p.117.
2. G. V. Smith and R. F. Mehl, Trans AIME, 1942, vol. 150, p.211.
3. M. D. Jepson and F. C. Thompson, JISI, 1949, vol. 162, p. 49.
4. A. B. Greninger and A. R. Troiano, Trans. AIME, 1940, vol. 140, p. 307.
5. J. S. Bowles and N. F. Kennon, J. Aust, Inst. Metals, 1960, vol. 5, p. 106.
6. T. Ko and S. A. Cottrell, JISI, 1952, vol. 172, p. 307.
7. R. H. Goodenow, S. J. Matas and R. F. Hehemann, Trans. AIME, 1963, vol. 227, p. 651.
8. G. R. Speich, Decomposition of Austenite by Diffusional Process, Interscience, New York, 1963, p. 353.
9. T. Ko, JISI, 1953, vol. 173, p. 16.
10. G. R. Speich and M. Cohen, Trans. AIME, 1960, vol. 218, p. 150.
11. D. N. Shackleton and P. M. Kelly, Acta Met., 1967, vol. 15, p. 979.
12. G. R. Srinivasan and C. M. Wayman, Acta Met., 1968, vol. 16, p. 621.
13. J. S. White and W. S. Owen, JISI, 1960, vol. 1951, p. 79.
14. J. S. White and W. S. Owen, JISI, 1961, vol. 196, p. 241.
15. D. N. Shackleton and P. M. Kelly, The Iron and Steel Institute, Special Report No. 93, 1965, p. 126.
16. S. K. Das, unpublished work, University of California, Berkeley.
17. R. F. Mehl and A. Duke, Phase Transformation in Solids, John Wiley & Sons, New York, 1951, p. 545.
18. Electron Microstructure of Bainite in Steel, Second Progress Report by Subcommittee XI of Committee E-4, ASTM Proc., 1952, vol. 52, p.543.

0 0 0 0 4 3 0 2 2 7 7

19. S. K. Das and G. Thomas, Trans. ASM, 1969, vol. 62, p. 659.

20. D. Huang and G. Thomas, Met. Trans., 1971, vol. 2, p. 1587.

21. J. Barford and W. S. Owen, JISI, 1961, vol. 197, p. 146.

22. J. M. Oblak and R. F. Hehemann, Transformation and Hardenability in Steels, Climax Molybdenum Co., Ann Arbor, 1967.

23. H. J. Aaronson, C. Laird and K. R. Kinsman, "Phase Transformations", ASM, 1968, p. 313.

24. K. R. Kinsman, E. Eichen and H. I. Aaronson, Met. Trans. 1971, vol. 2, p. 346.

25. R. F. Hehemann, K. R. Kinsman and H. I. Aaronson, Met. Trans., 1972, vol. 3, p. 1077.

26. K. R. Kinsman and H. I. Aaronson, Discussion to Oblak and Hehemann, Transformation and Hardenability in Steels, Climax Molybdenum, Ann Arbor, 1967, p. 33.

27. Yu A. Bagaryatskii, Doklady, Akademia Nauk SSSR, 1950, vol. 73, p. 1161.

28. P. M. Kelly and J. Nutting, Proc. Royal Socl, 1960, vol. A259, p. 45

29. I. V. Isaichev, Zhur. Tekhn, Fiziki, 1947, vol. 17, p. 835.

30. G. Kurdjumov and G. Sachs, Z. Physik, 1930, vol. 64, p. 325.

31. W. Pitsch, Arch. Eisenhutt Wess., 1963, vol. 34, pp. 381 and 641.

32. W. Pitsch, Acta Met., 1962, vol. 10, p. 897.

33. F. B. Pickering, Transformation and Hardenability in Steels, Climax Molybdenum, Ann Arbor, 1967, p. 109.

34. K. Shimizu, T. Ko and Z. Nishiyama, Trans. Japan Inst. of Metals, 1964, vol. 5, p. 225.

35. M. Cohen, Discussion to F. B. Pickering, Transformation and Hardenability in Steels, Climax Molybdenum, Ann Arbor, 1967, p. 131.

36. K. W. Andrews, Acta Met., 1963, vol. 11, p. 939.

37. C. Zener, Trans. AIME, 1946, vol. 167, p. 550.

38. J. W. Cristian, Decomposition of Austenite by Diffusional Process, Interscience, New York, 1962, p. 371.

39. A. P. Miodownik, J. Inst. Metals, 1954, vol. 83, p. 561, and "The Mechanism of Phase Transformations in Metals", Inst. of Metals, Monograph and Report Series, No. 18, 1956, p. 319.

40. A. Hultgren, Trans. ASM, 1947, vol. 39, p. 915.

41. M. Hillert, Jernkontorets Ann., 1957, vol. 141, p. 757.

42. J. C. Fisher, Thermodynamics in Physical Metallurgy, 1950, ASM, p. 201.

43. L. Kaufman, S. V. Radcliffe and M. Cohen, Decomposition of Austenite by Diffusional Process, Interscience, New York, 1962, p. 313.

44. S. K. Das and G. Thomas Proc. Int. Conf. "Order-Disorder Transformations", Edited by H. Warlimont, Springer-Verlag Berlin, 1974, p. 332.

0 0 0 0 4 3 0 2 2 7 8

FIGURE CAPTIONS

Fig. 1 Transmission electron micrograph of lower bainite in Fe/12 Ni/4 Co/.4 C alloy after transformation at 204°C for 140 hours. (a) Bright field image shows unidirectional carbide particles precipitated uniformly in the matrix, this is typical of lower bainite. (b) The carbides reverse contrast in the dark field image using (103) cementite reflection.

Fig. 2 (a) Transmission electron micrograph of the structure of lower bainite showing long striations of cementite in addition to the characteristic short bainitic carbides. (b) Both type of carbides reverse contrast in the dark field micrograph by imaging a (040) cementite spot.

Fig. 3 (a) Electron micrograph showing lower bainite grows from austenite grain boundary (marked by double arrow). Both long and short carbides are observed. The interface of the bainite at marked by single arrow is planar. (b) Selected area gives a $(100)_\alpha$ and $(111)_\alpha$ orientation which is typical of lath martensite.

Fig. 4 (a) Electron micrograph shows two grains of bainite with martensite forming in between. The bainite/martensite interface as indicated by arrows is straight. (b) Selected area electron diffraction pattern taken from the right hand sided grain of bainite showing a $[113]_\alpha$ orientation. (c) Dark field of (103) Fe_3C spot, indicated as C, shows the carbide clearly. (d) The contrast of the matrix is reversed by dark field imaging the $(\bar{1}10)_\alpha$ spot.

Fig. 5 (a) Electron micrograph of lower bainite in the Fe/Ni/Co/C alloy after transformation at 204°C for 900 hours showing another region

where Fe_3C can be seen lining up uniformly suggesting that the cementite precipitates behind the moving ferrite/austenite interface. (b) Dark field image of (103) Fe_3C reflection reverses the contrast of cementite.

Fig. 6 (a) Transmission electron micrograph showing another region of lower bainite formed in the Fe/Ni/Co/C alloy at 204°C for 900 hours. The carbides are in the shape of kinks suggesting the transformation mechanism to be ledge mechanism. Foil orientation is $[511]_\alpha$. (b) The corresponding crystallographic analysis.

Fig. 7 (a) Structure of lower bainite showing characteristic bainitic carbide and islands of ferrite formed from entrapped austenite. (b) The corresponding diffraction pattern and (c) the indexing. The matrix is in $[112]_\alpha$ orientation. (d) shows the dark field image of a $(\bar{2}00)$ spot of the ferrite island. (e) The contrast of the matrix is reversed by imaging $(\bar{1}10)_\alpha$ reflection. (f) a thin layer of cementite along the α island is detected by dark field imaging a (310) cementite reflection. (g) the bainitic carbide are clearly seen in a slightly tilted position and (f) the corresponding SAD.

Fig. 8 (a) Another area of the isothermally transformed specimen showing entrapped austenite as dark stringers. (b) The selected area diffraction pattern and (c) Indexed diffraction pattern showing that the Kurdjumov-Sachs orientation relationship holds between ferrite and austenite. Another orientation of ferrite is also indexed. (d) Dark field image reverses the contrast of austenite by using a (111) austenite reflection, (e) Blocky ferrite is clearly seen in the dark field image of $(110)_\alpha$ spot. (f) Dark field image of $\{110\}_\alpha\{111\}_\gamma$

reflection. (g) Bright field image of the same area with higher magnification.

Fig. 9 (a) Transmission electron micrograph showing the structure of lower bainite in Fe/12Ni/4Co/.4C steel after isothermally transformation at 204°C for 900 hours, (b) the selected area diffraction pattern, (c) the schematic representation showing the matrix orientation to be [331] and the cementite orientation to be $[0\bar{1}1]$. (d) Dark field image of a $(\bar{2}\bar{1}1)$ cementite reflection reverses the cementite contrast. (e) Stereographic projection corresponding to Fig. 7 showing the orientation relationship between bainitic ferrite and cementite.

Fig. 10 (a) Transmission electron micrograph showing another area of lower bainite. Typical bainitic carbides are seen in the matrix, (b) the corresponding selected diffraction pattern. (c) Indexed diffraction pattern indicating that ferrite and cementite are in $[120]_\alpha$ and $[1\bar{2}\bar{1}]Fe_3C$ orientation respectively. (d) Dark field image of cementite using a $(\bar{2}\bar{1}0)Fe_3C$ reflection. (e) Stereogram corresponding to Fig. 10. (c) The orientation relationship of tempered dislocated martensite is closely but not exactly followed between the bainitic carbide and ferrite.

Fig. 11 (a) Structure of typical lower bainite and (b) the electron diffraction pattern in Fe/12Ni/4Co/.4C alloy. (b) The corresponding stereogram showing the trace normal of cementite passes very close to (335) ferrite plane.

Fig. 12 Trace analysis of bainitic carbide particles showing the habit plane in the region of (112) to (335).

Fig. 13 Stereographic projection summerizing the orientation relationship between austenite, cementite and ferrite. Where K-S relationship, viz., $(011)_\alpha || (111)_\gamma$, $(11\bar{1})_\alpha || (10\bar{1})_\gamma$ and $(\bar{2}1\bar{1})_\alpha || (\bar{1}2\bar{1})_\gamma$ is obeyed between ferrite and austenite; Isaichev correspondence, viz., $(010)_c || (11\bar{1})_\alpha$ and $(103)_c || (011)_\alpha$ is observed between cementite and ferrite.

Fig. 14 (a) Lower bainite in Fe/Ni/Co/C alloy obtained by isothermal transformation at 204°C for 15 days showing carbides and internal twinning (delineated by double arrows). (b) The corresponding selected area diffraction pattern and its indexing. (c) Dark field image of a (021) cementite spot reverses the contrast of the carbide. The twins are in the background as indicated by double arrows. (d) Both the carbide and the twins reverse contrast by dark field imaging of a $(01\bar{1})$ twin spot and a (121) Fe_3C spot. (e), (f), and (g) are dark field micrograph using reflections of (221) Fe_3C, $(10\bar{1})$ twin + $(\bar{1}21)$ Fe_3C and $(\bar{1}\bar{1}2)$ twin + $(0\bar{4}\bar{2})$ Fe_3C respectively.

0 0 0 0 4 3 0 2 2 8 0

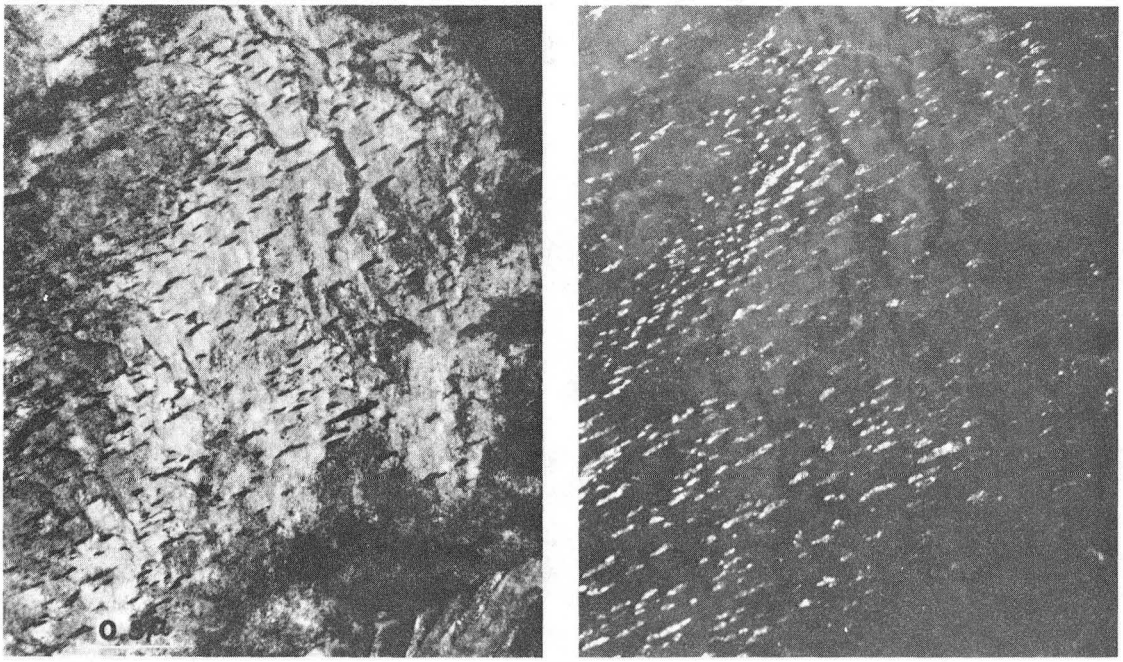

XBB 748-5793

Fig. 1 (a) (b)

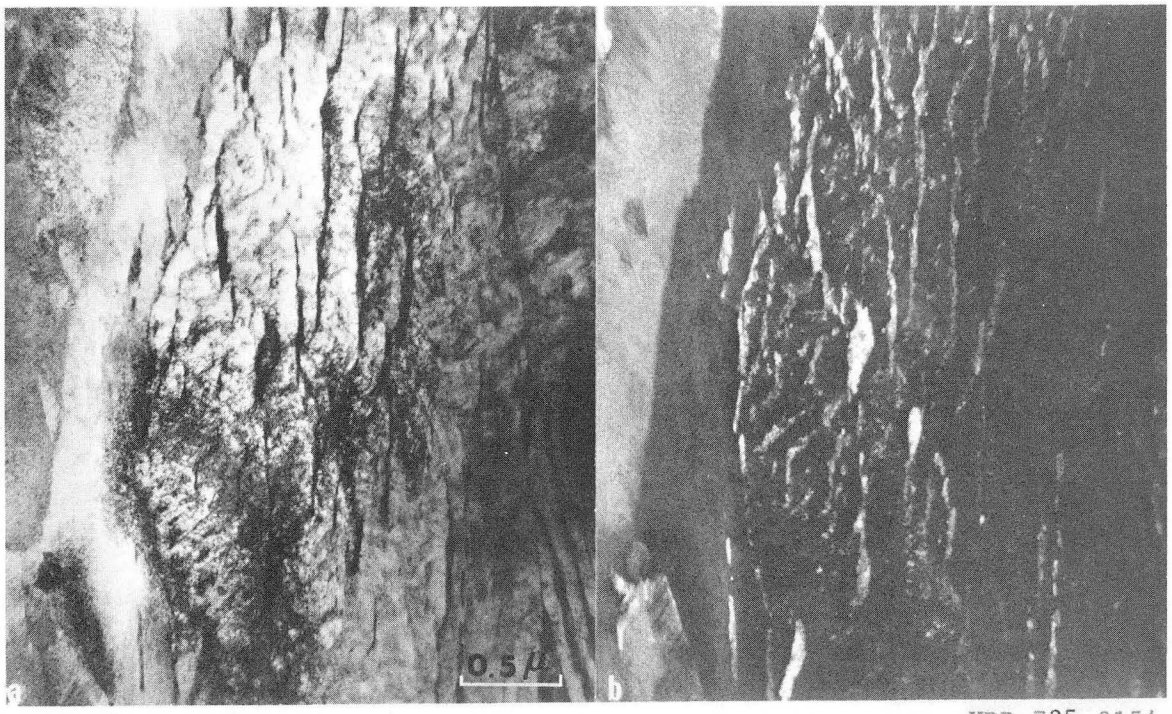

XBB 735-3154

Fig. 2

0 0 0 0 4 3 0 2 2 8 1

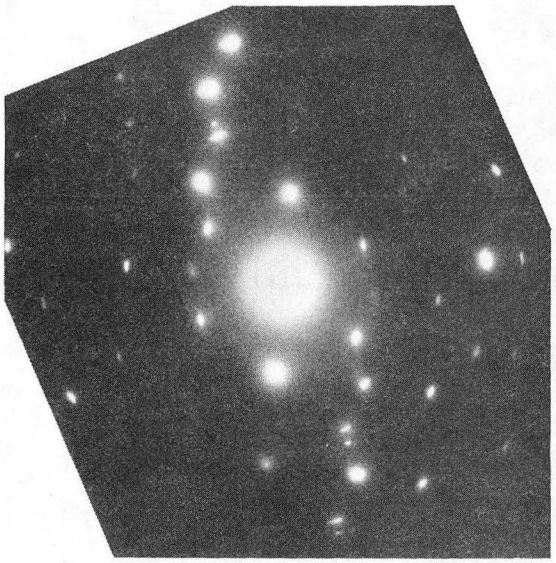

XBB 748-5429

Fig. 3 (a) (b)

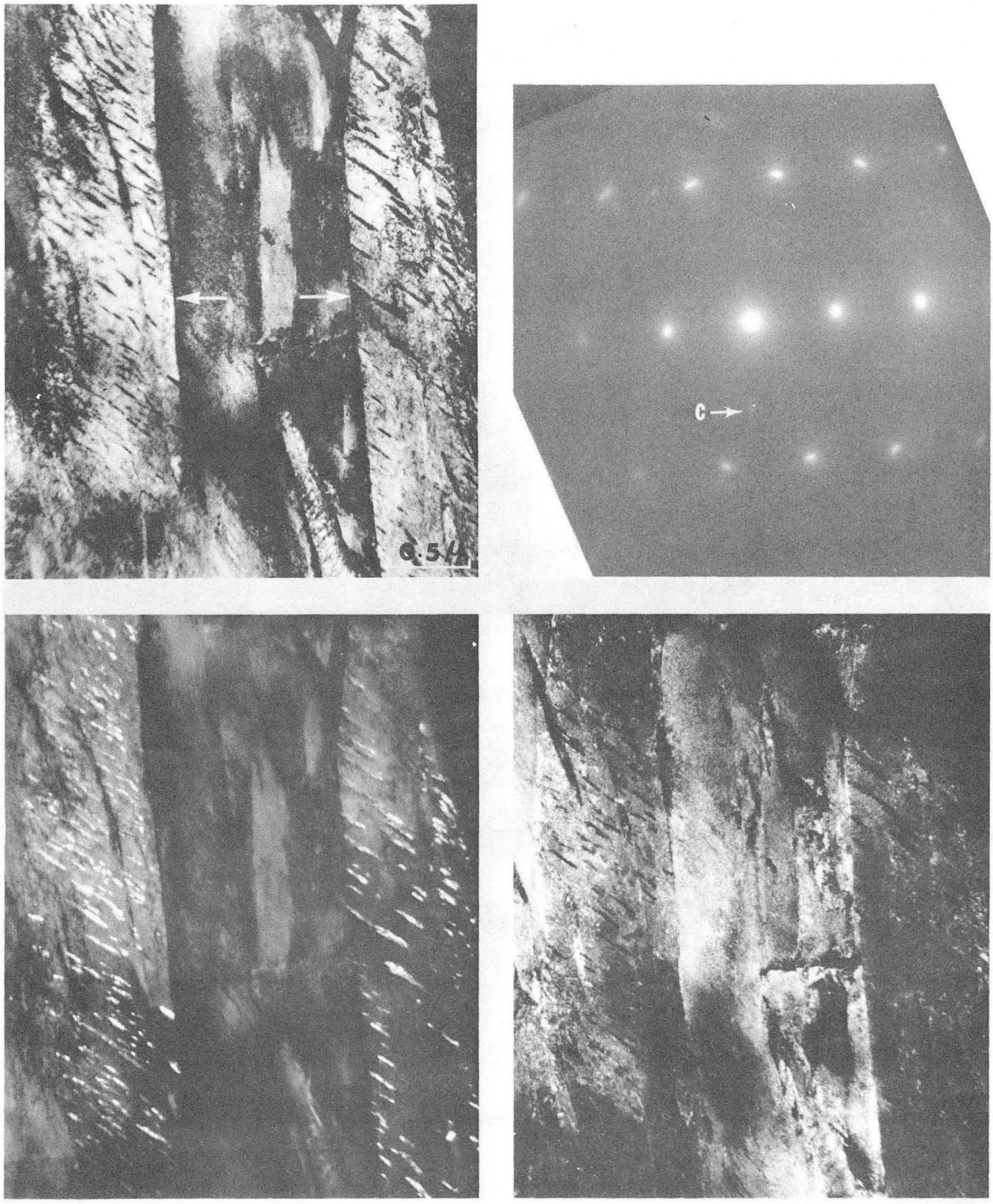

XBB 748-5428

(a) (b)

Fig. 4 (c) (d)

0 0 0 0 4 3 0 2 2 8 2

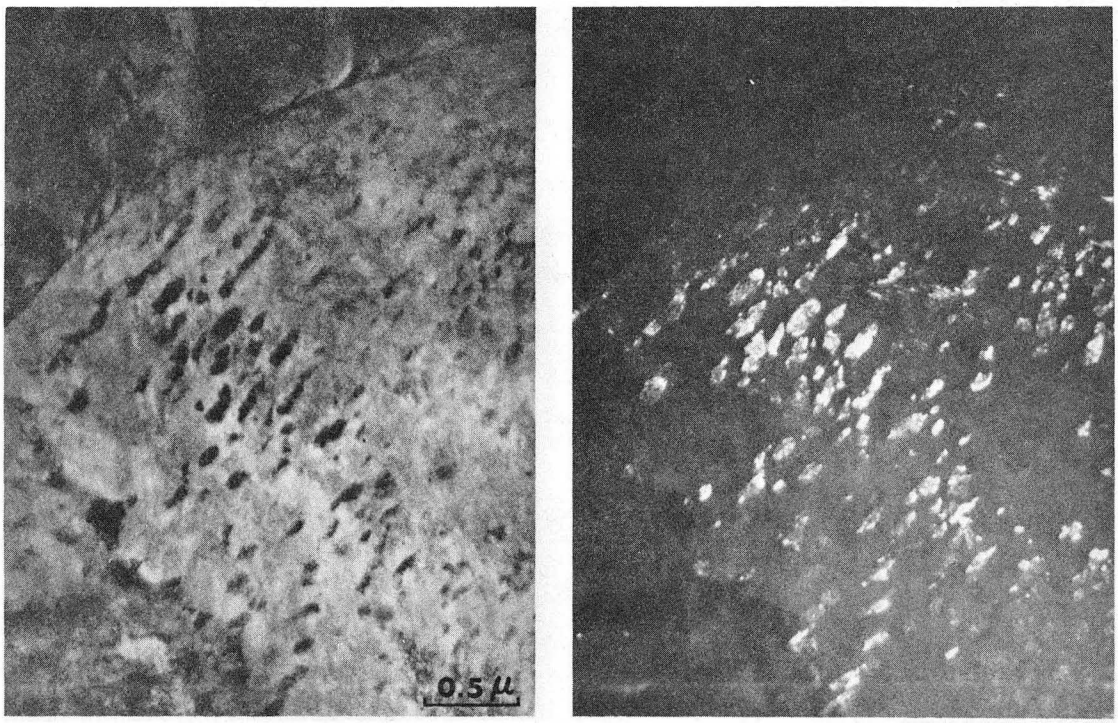

XBB 748-5792

Fig. 5 (a) (b)

XBB 749-6009

Fig. 6 (a)

0 0 0 0 4 3 0 2 2 8 3

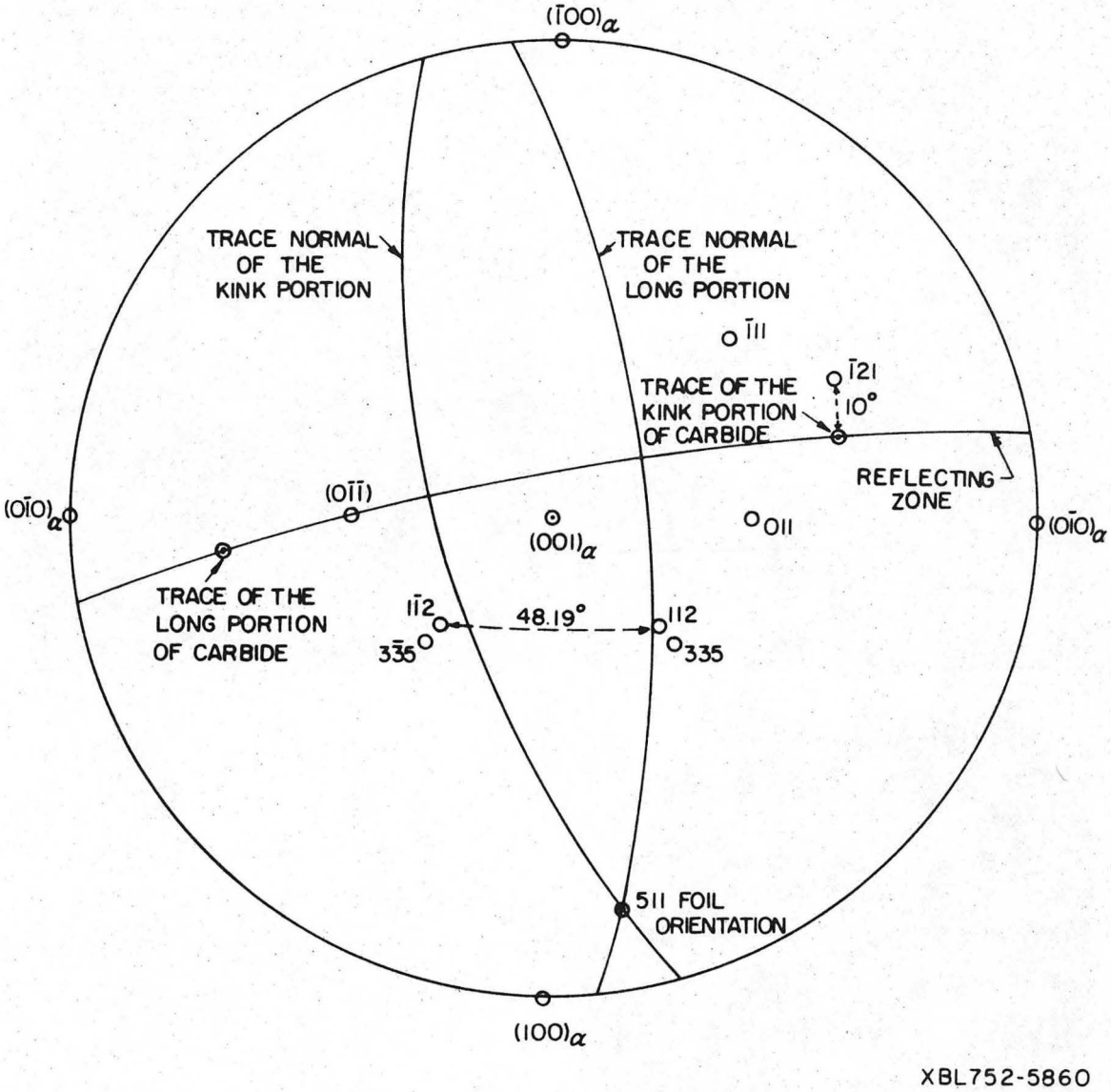

XBL752-5860

Fig. 6 (b)

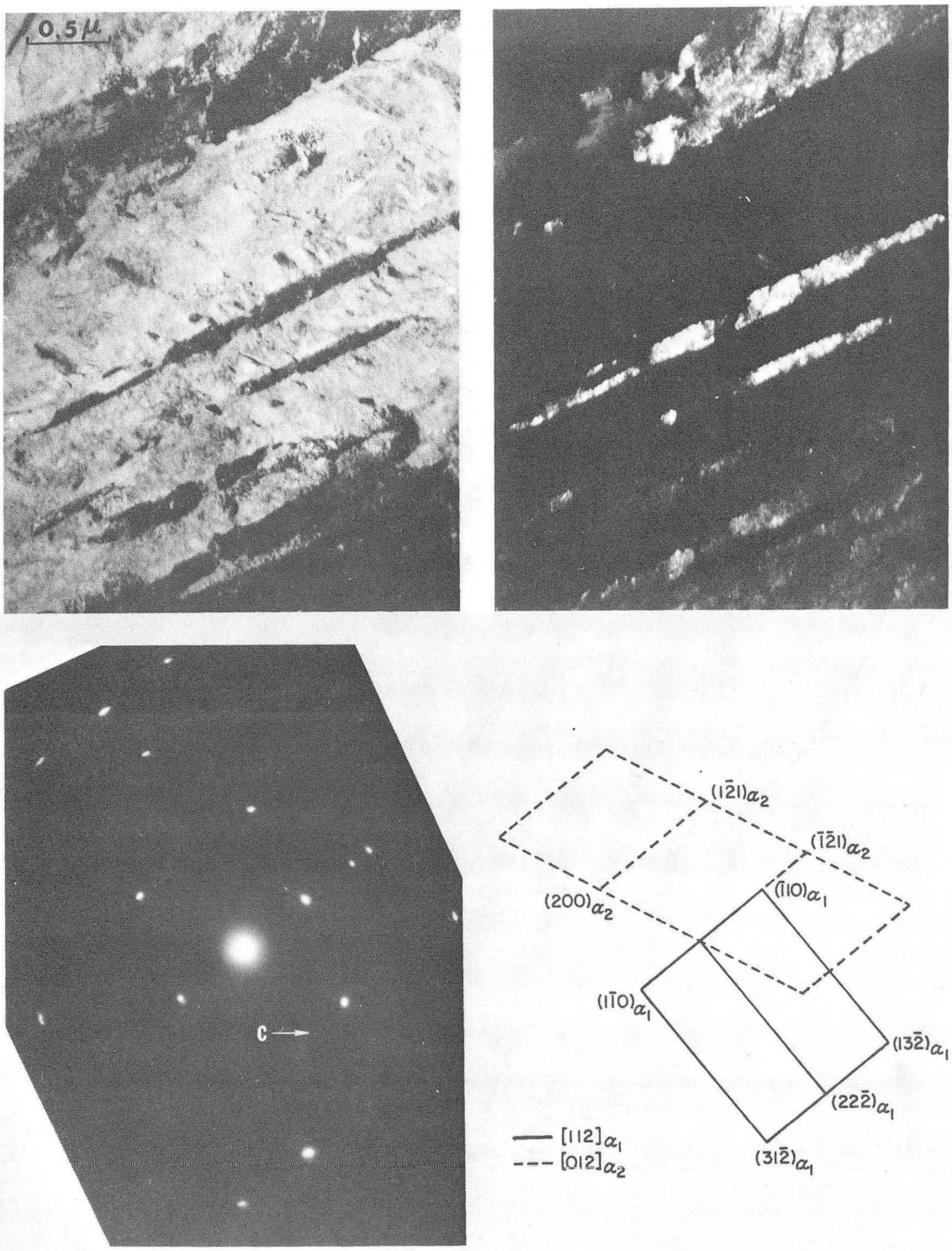

XBB 748-5425

(a)(d)

Fig. 7 (b)(c)

0 0 0 0 4 3 0 2 2 8 4

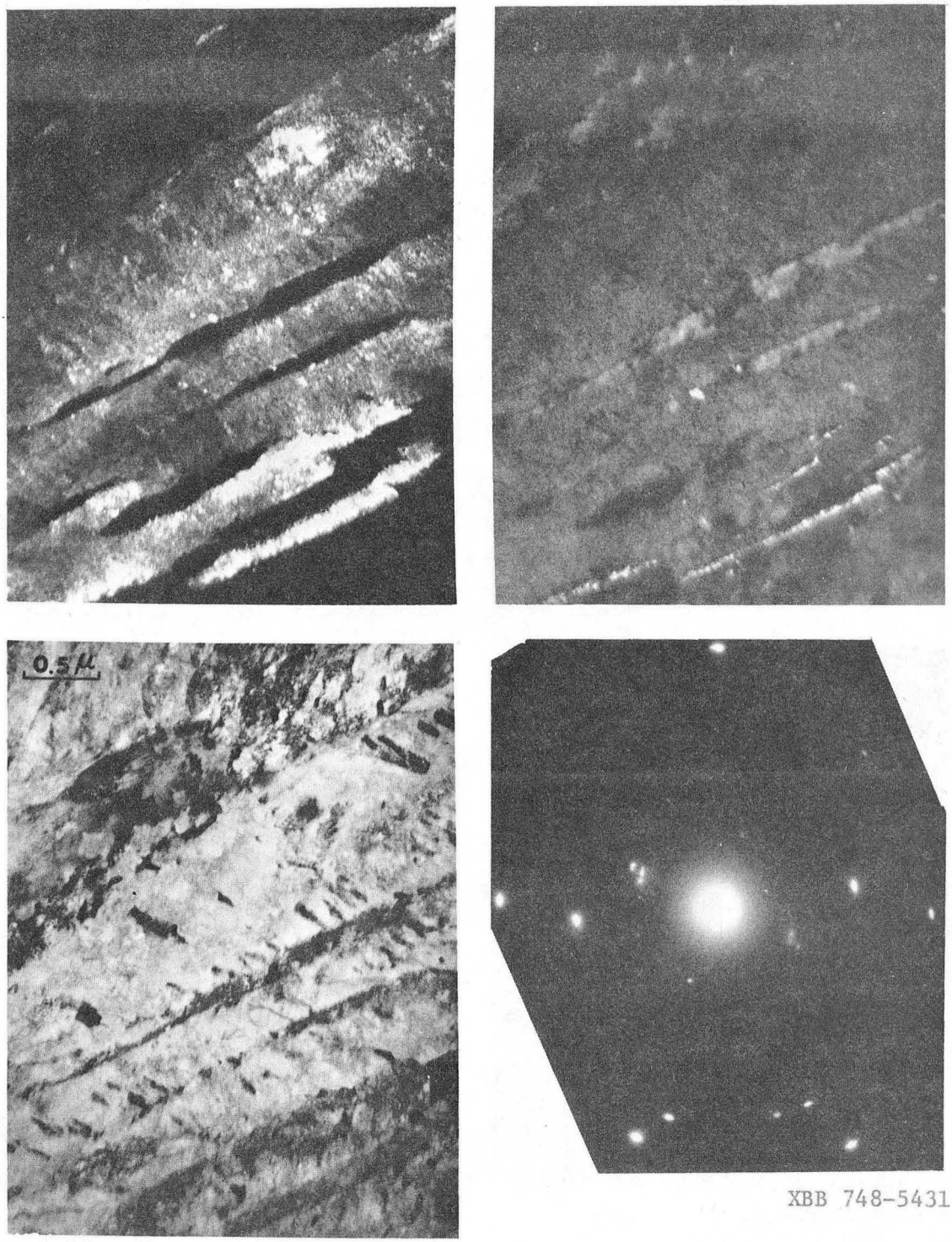

XBB 748-5431

(e)(f)
Fig. 7 (g)(h)

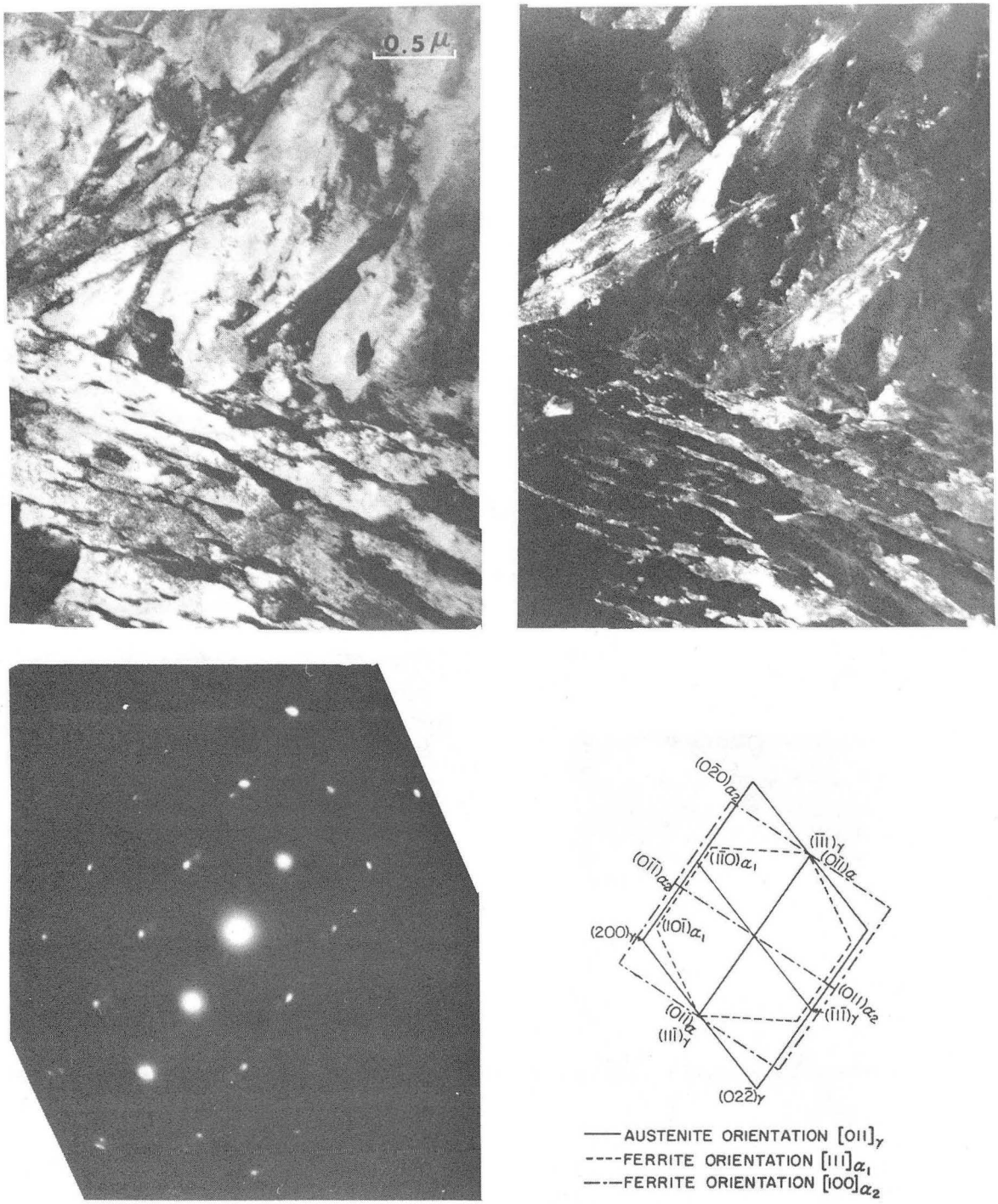

XBB 748-5427

(a)(d)

Fig. 8 (b)(c)

0 0 0 0 4 3 0 2 2 8 5

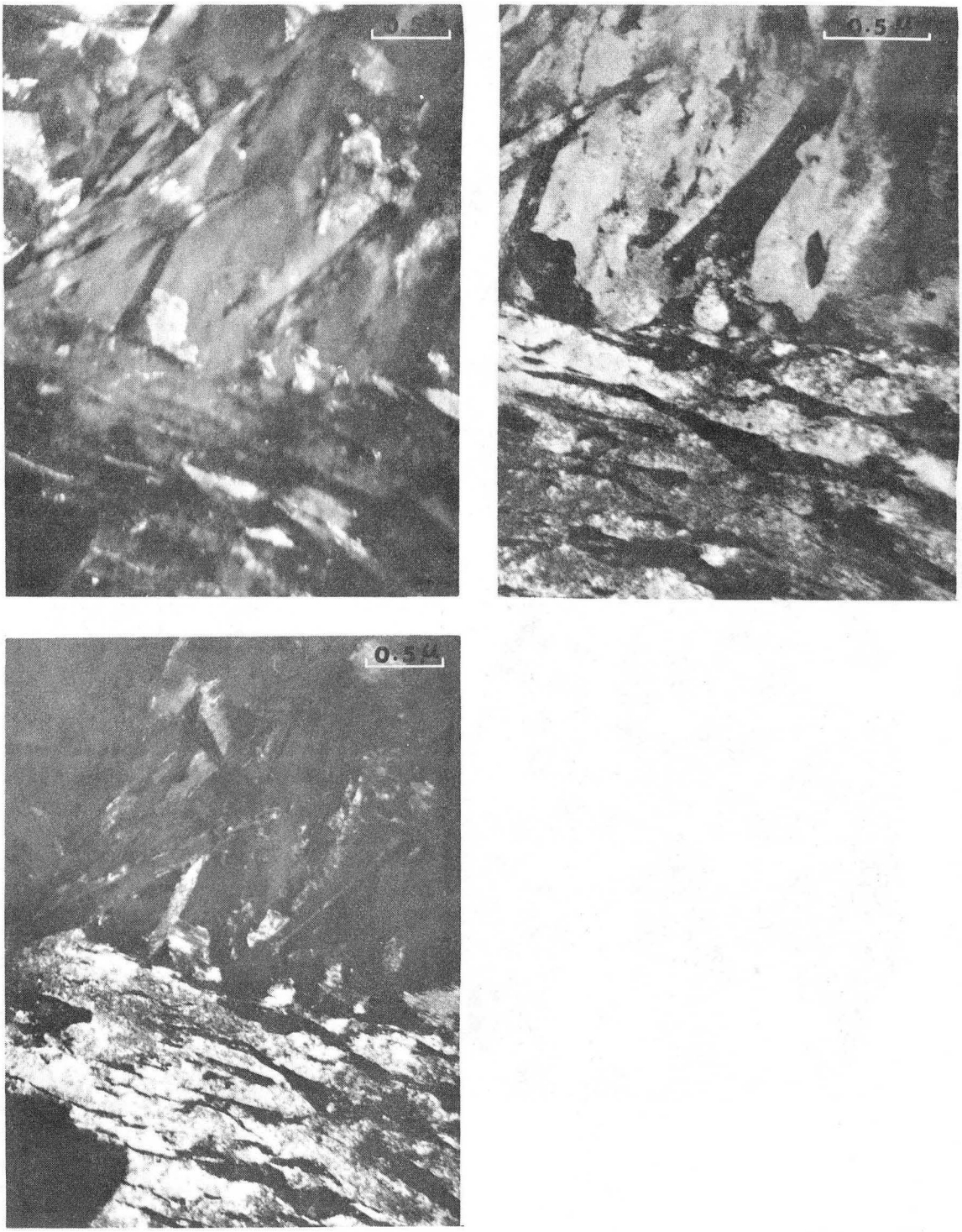

XBB 748-5430

(e)(g)

Fig. 8 (f)

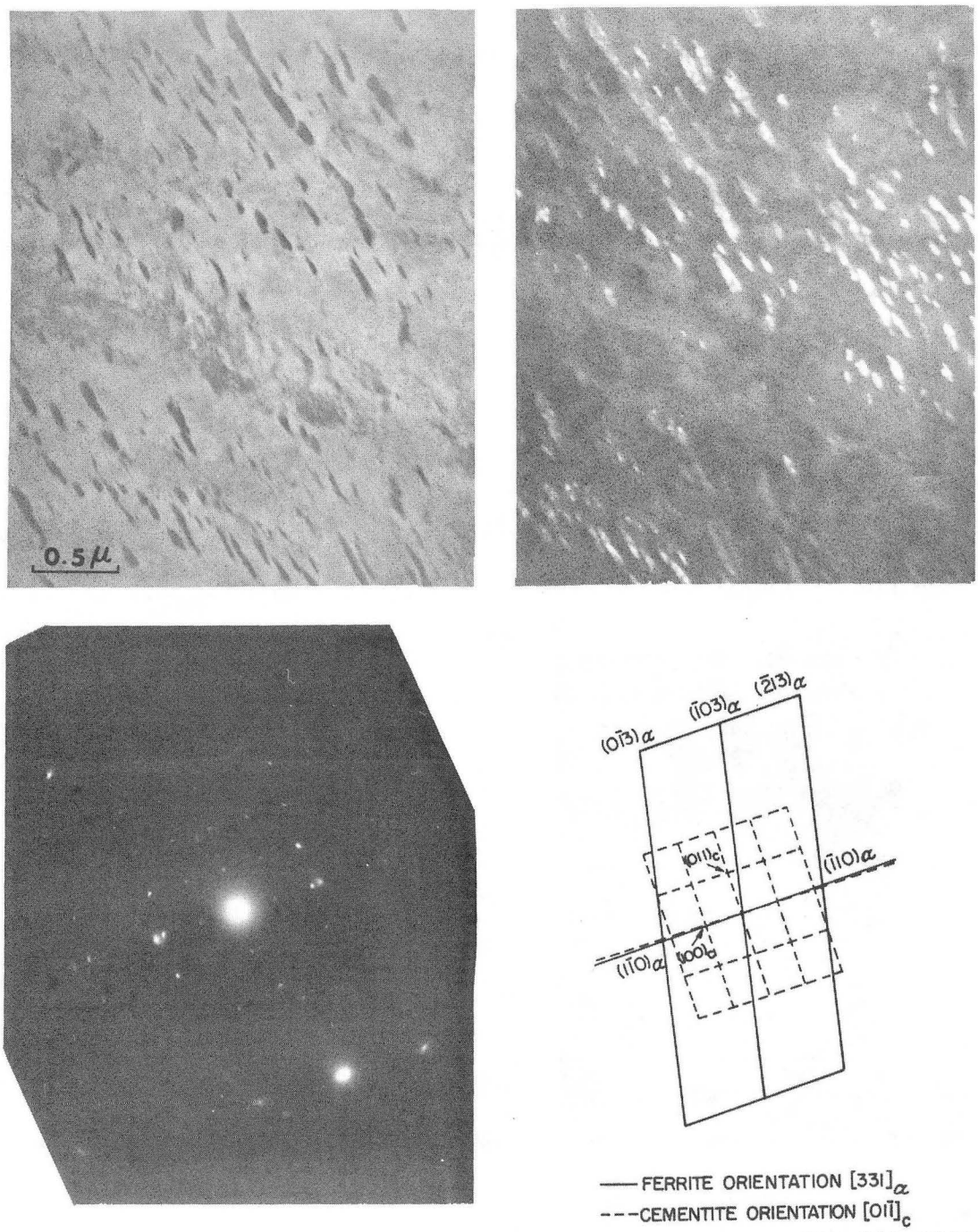

XBB 748-5795

(a)(d)

Fig. 9 (b)(c)

0 0 0 0 4 3 0 2 2 8 6

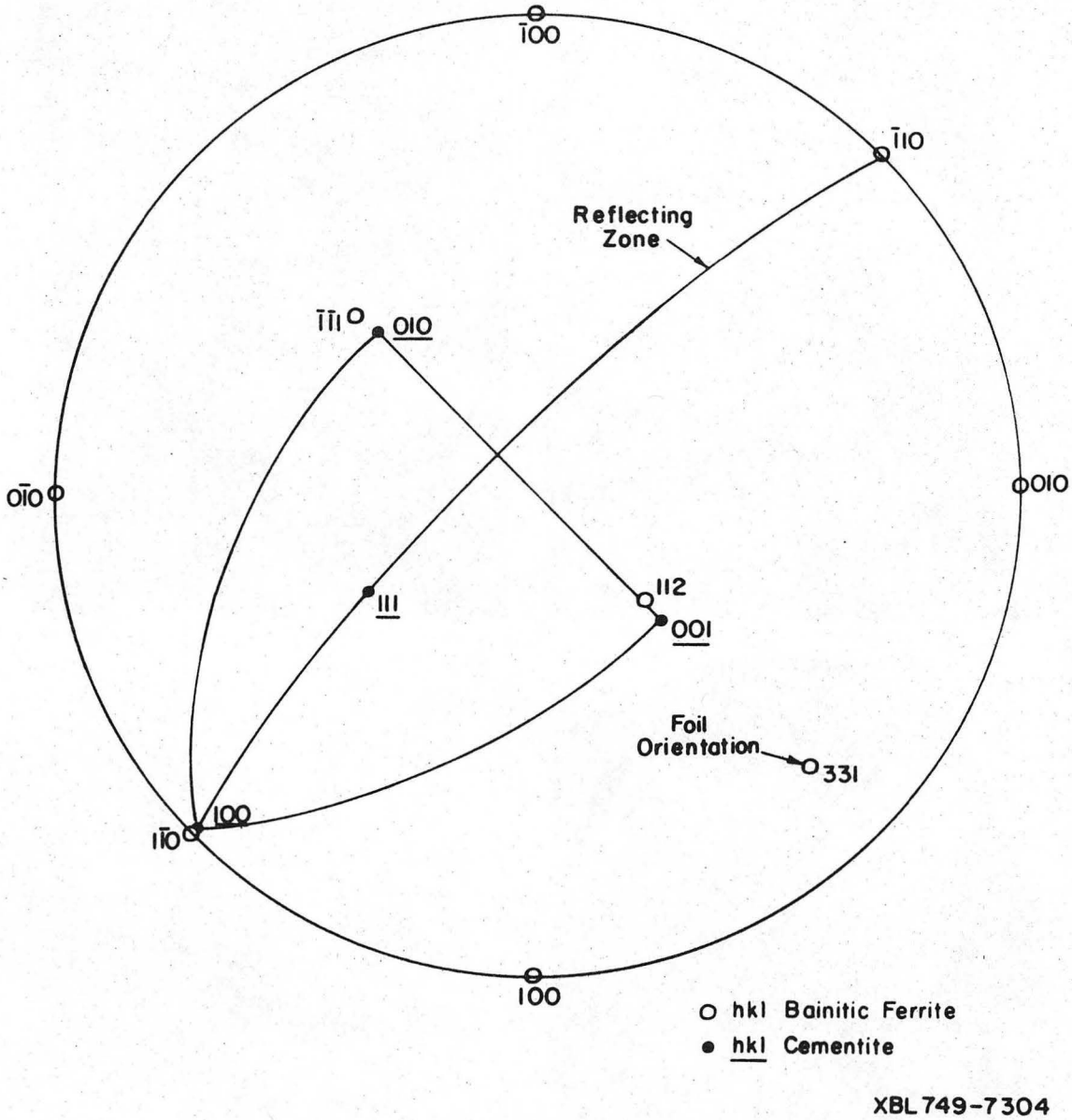

Fig. 9 (e)

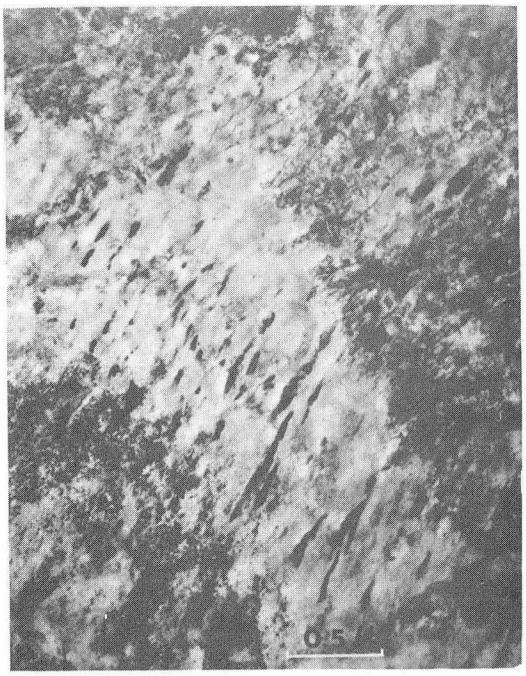

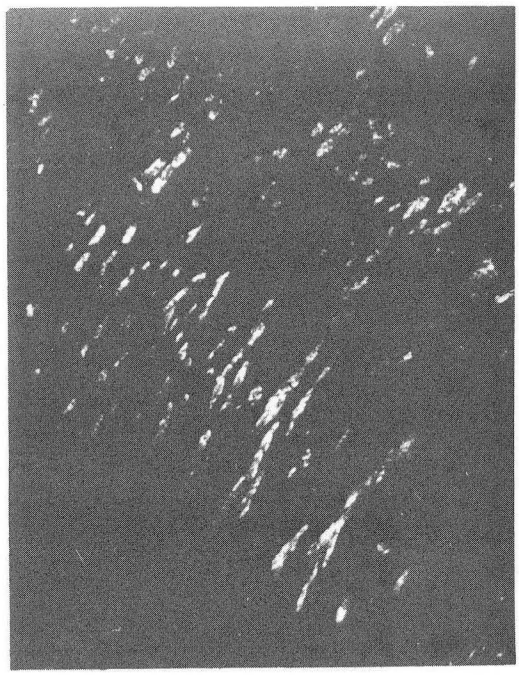

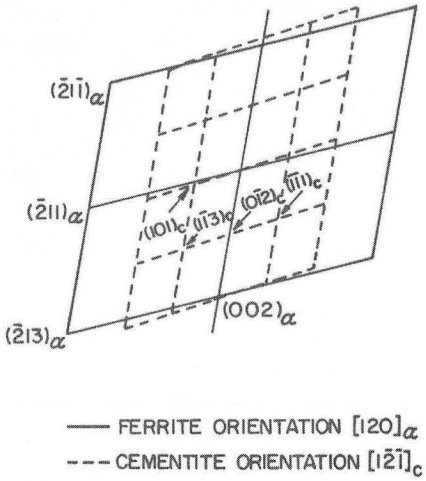

XBB 748-5794

(a)(d)

Fig. 10 (b)(c)

0 0 0 0 4 3 0 2 2 8 7

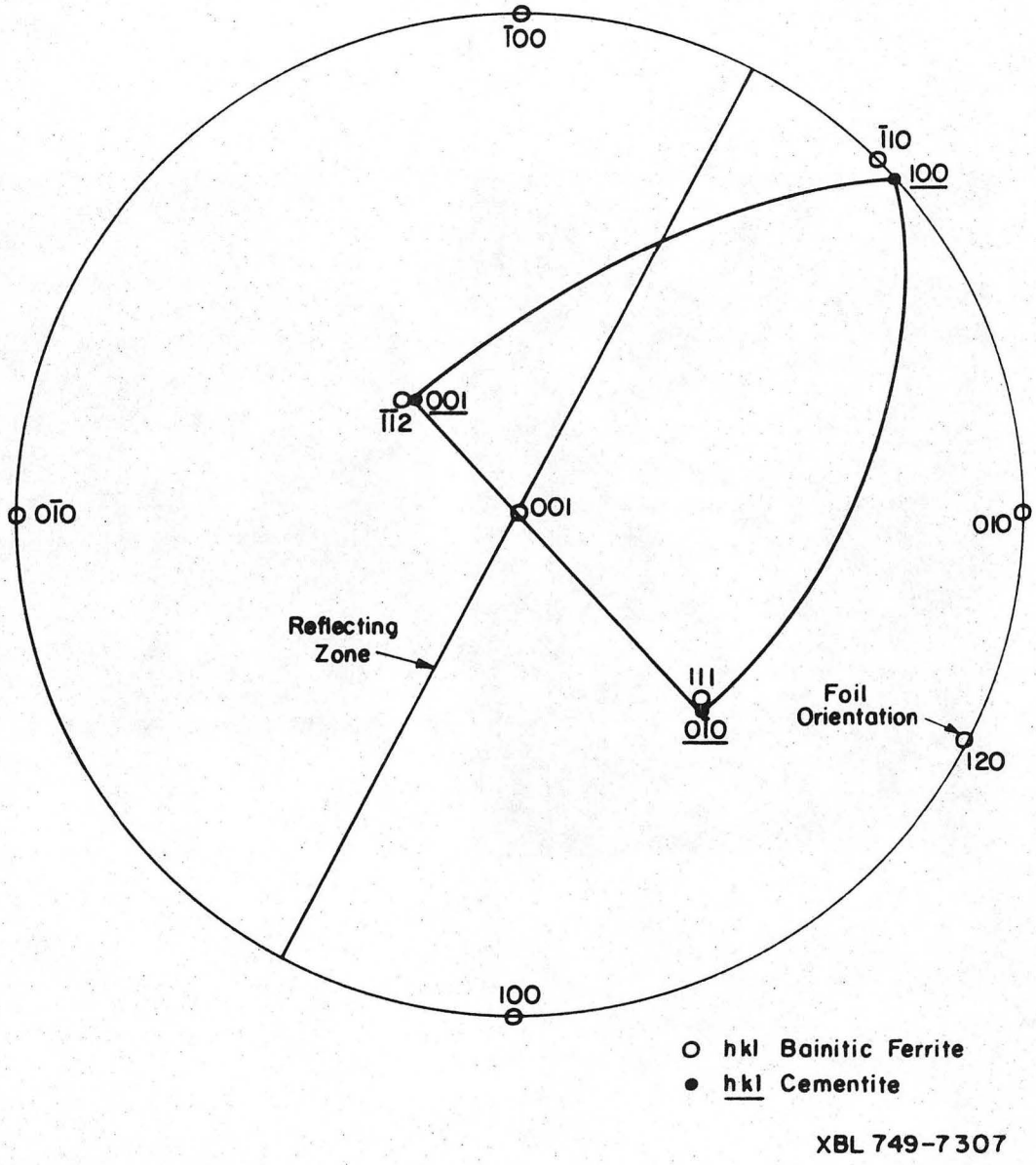

Fig. 10(e)

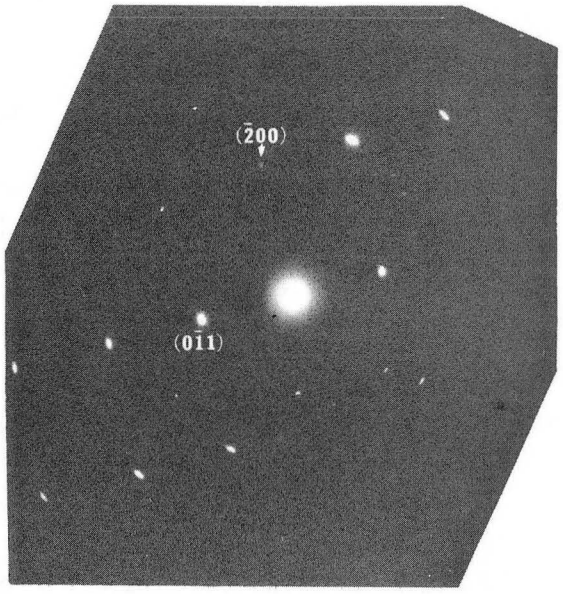

XBB 748-5790

Fig. 11 (a) (b)

0 0 0 0 4 3 0 2 2 8 8

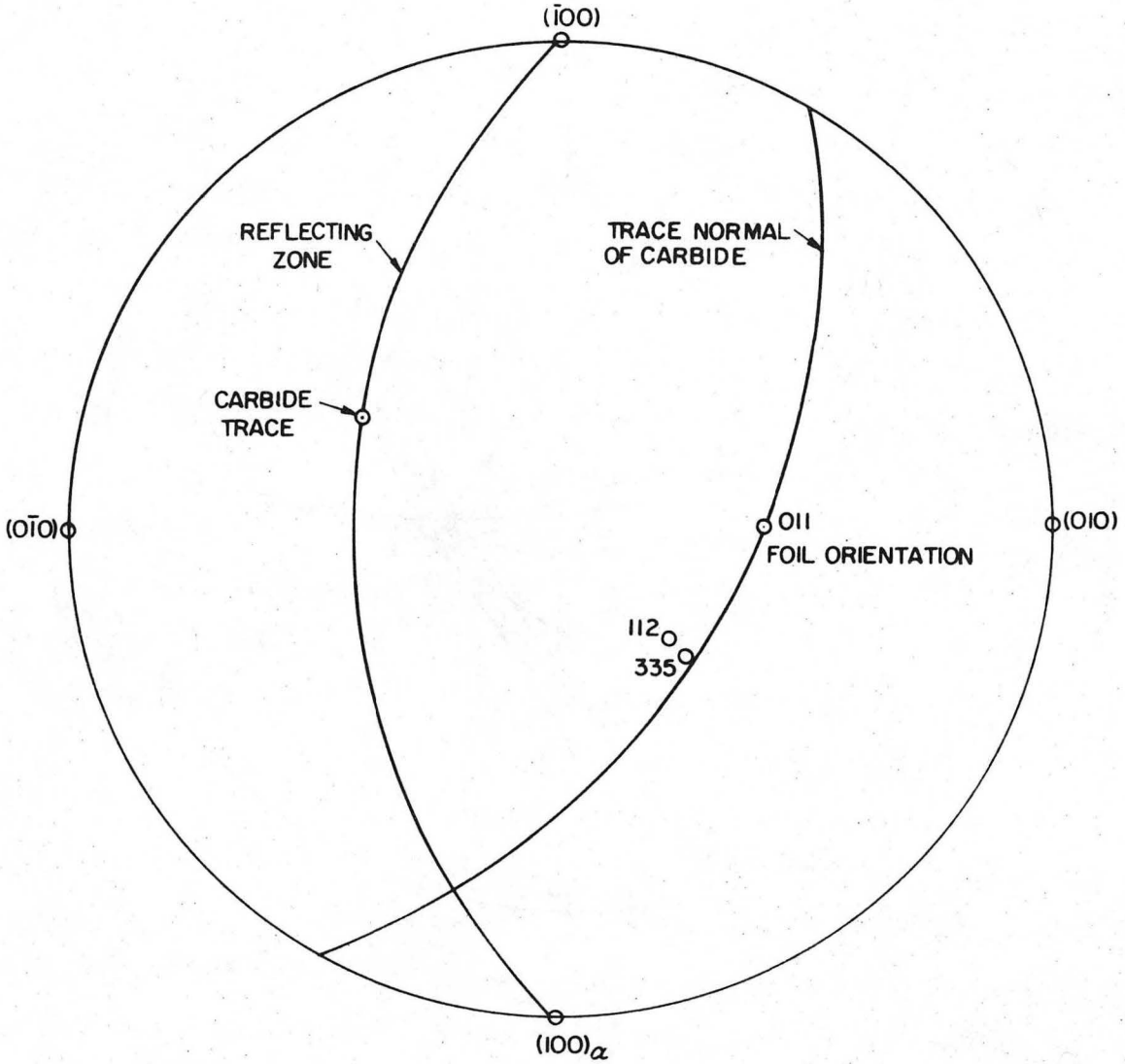

XBL 752-5861

Fig. 11 (c)

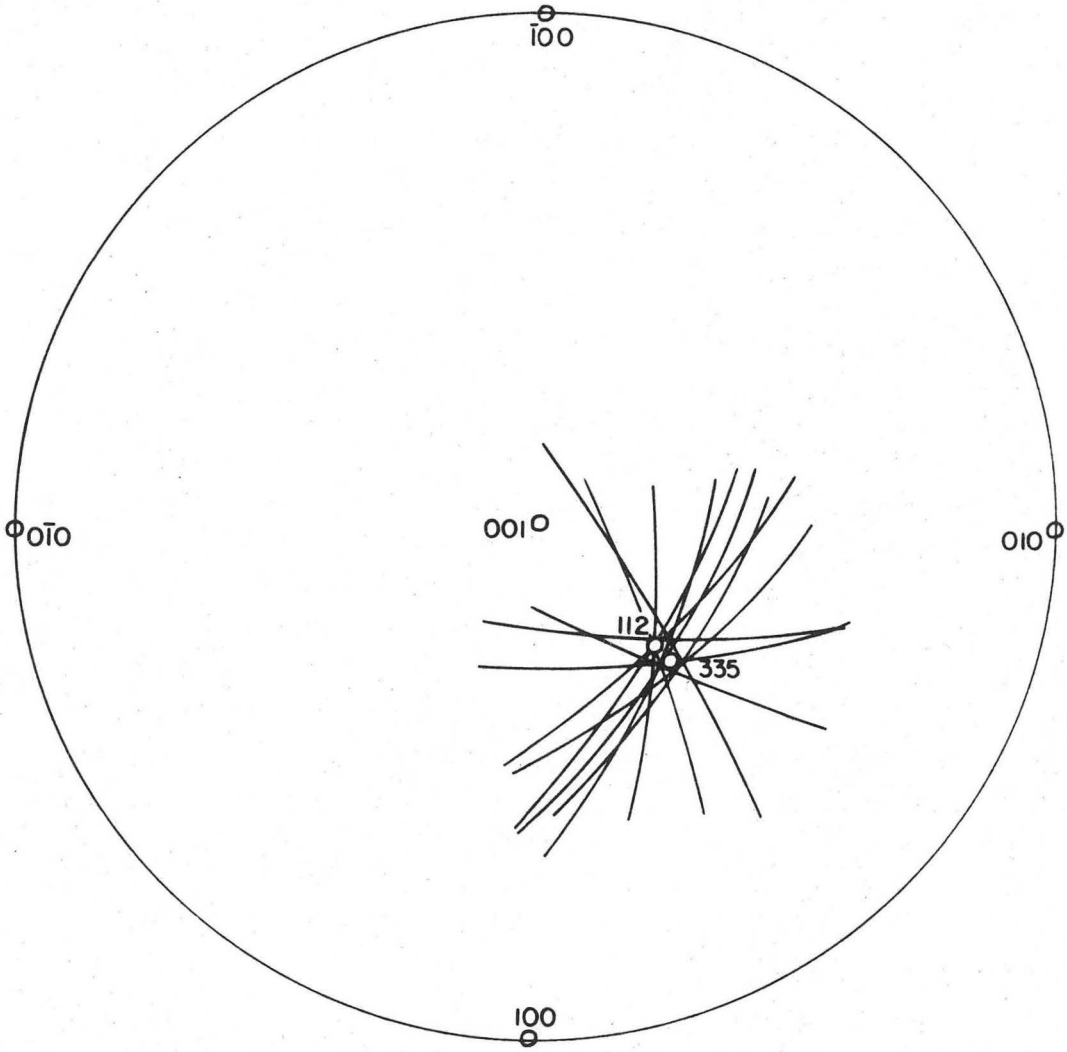

XBL 749-7306

Fig. 12

0 0 0 0 4 3 0 2 2 8 9

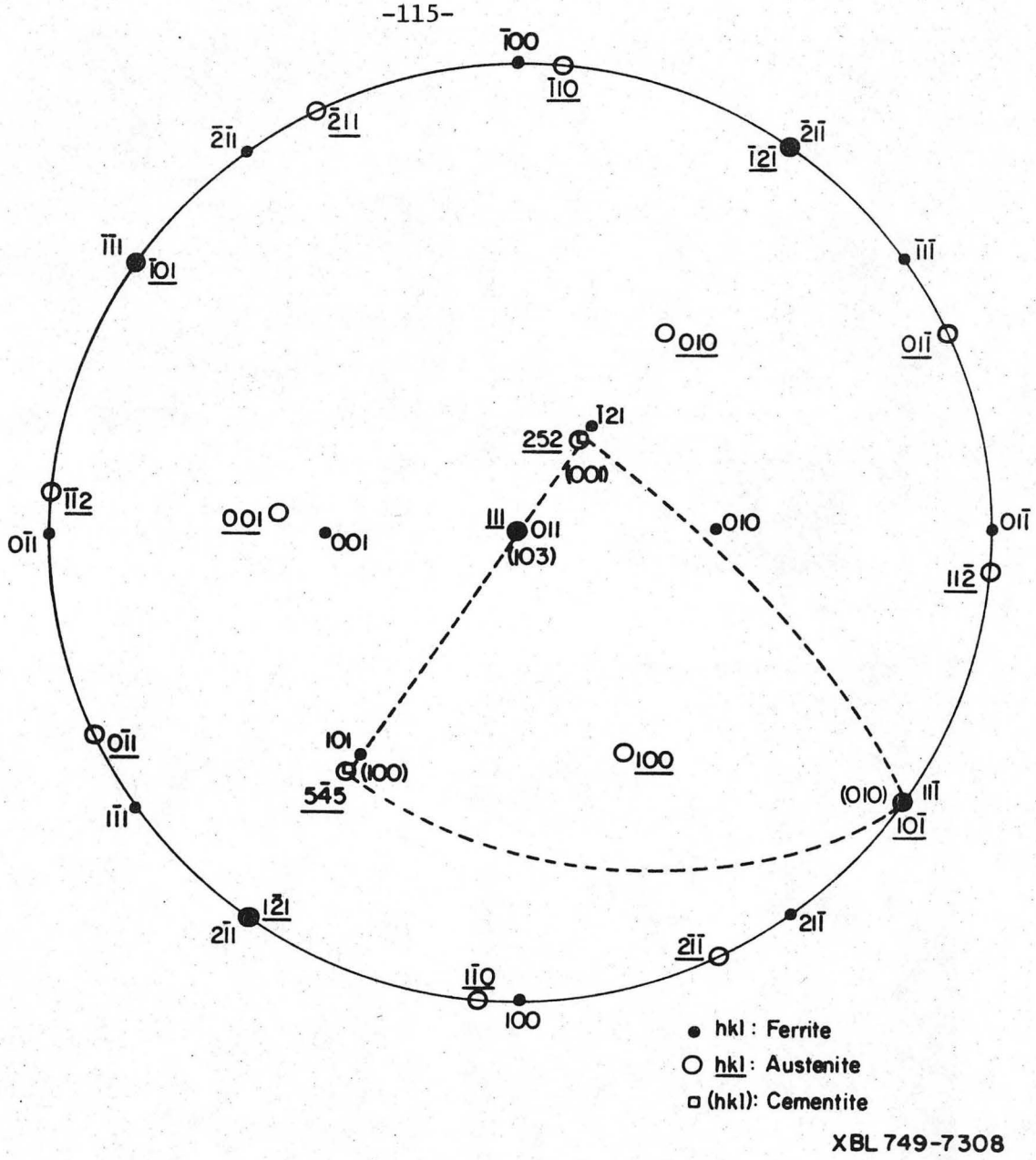

Fig. 13

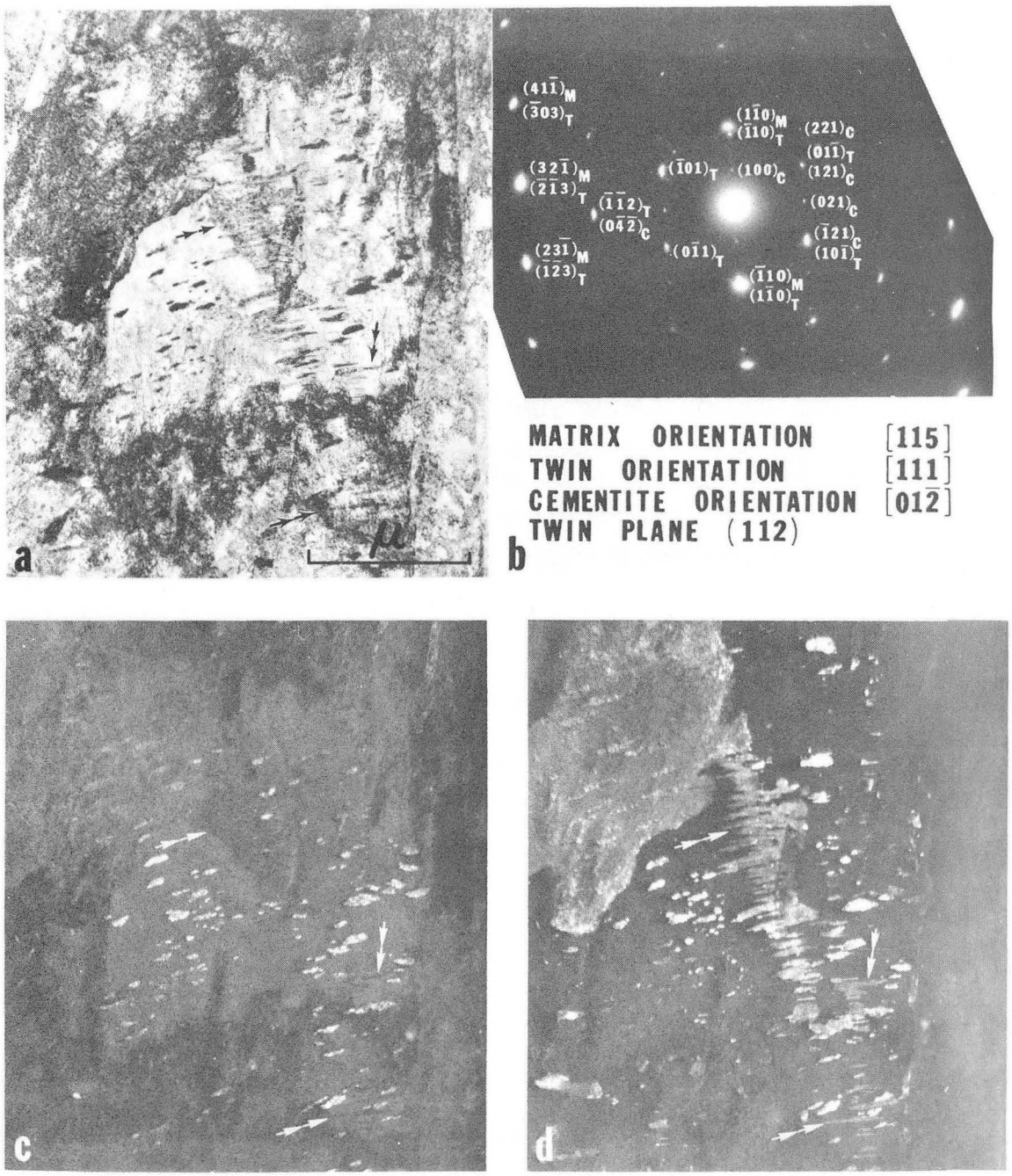

XBB 748-5426

Fig. 14

0 0 0 0 4 3 0 2 2 9 0

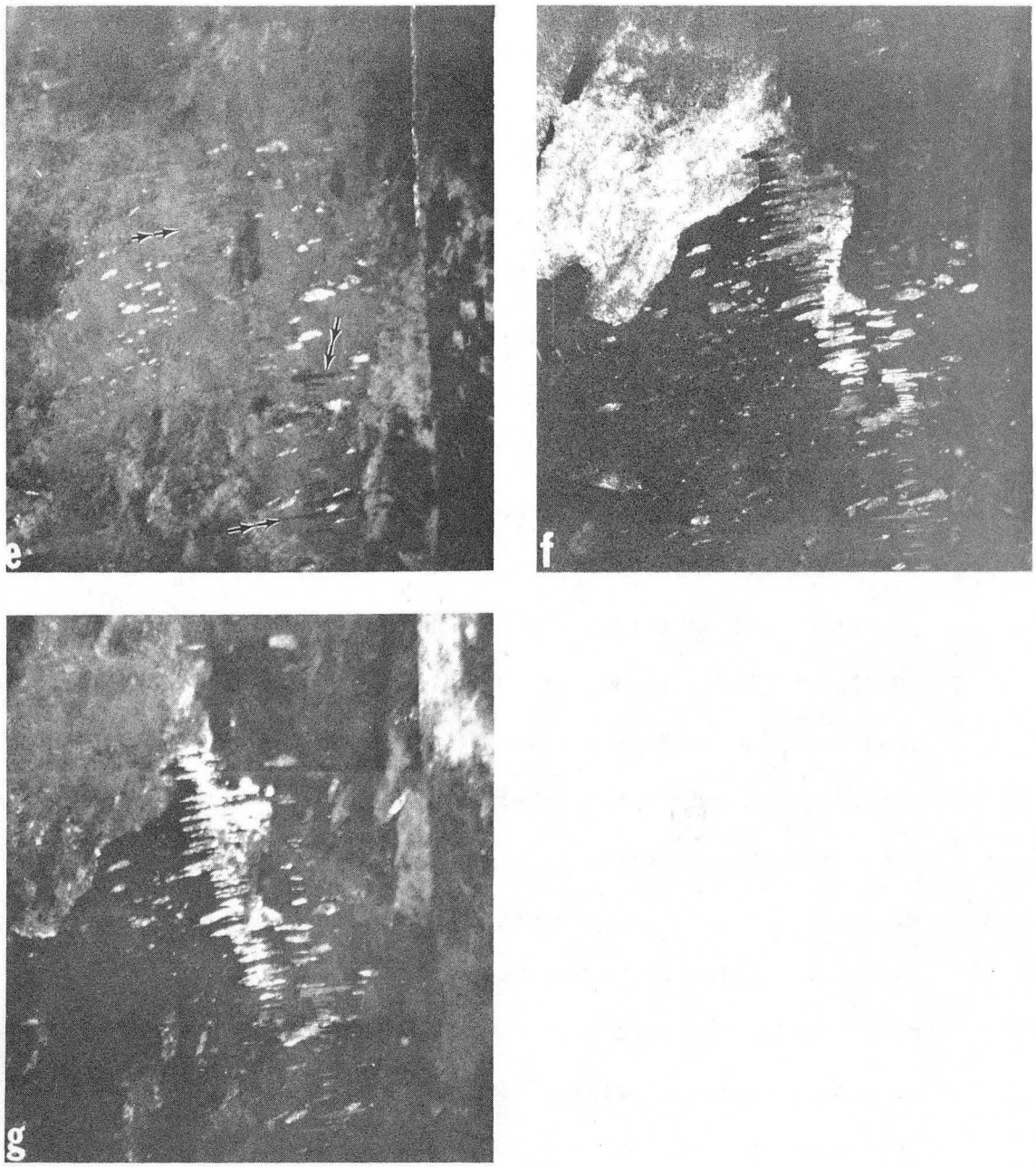

XBB 748-5432

Fig. 14 (Cont'd.)

GENERAL SUMMARY AND CONCLUSIONS

1) Bainite is an aggregate of ferrite and carbide, the microstructure may assume a variety of forms. Upper bainite and lower bainite should be differentiated microstructurally.

2) Epsilon carbide was unambiguously identified in lower bainite of a silicon containing steel. The orientation relationship between epsilon carbide and bainitic ferrite was found to follow that of Jack viz.,

$$(0001)_\varepsilon \parallel (011)_\alpha$$
$$(10\bar{1}0)_\varepsilon \parallel (2\bar{1}1)_\alpha$$
$$(\bar{1}2\bar{1}0)_\varepsilon \parallel (11\bar{1})_\alpha$$

3) The cementite observed in lower bainite was in the shape of small platelets and exhibited the Isaichev orientation relationship, viz., $(010)_C \parallel (1\bar{1}1)_\alpha, (103)_C \parallel (011)_\alpha$ with the bainite ferrite rather than that due to Bagaryatskii.

4) Instead of a well-established (112) habit plane, the habit plane of the cementite platelets in lower bainite was found to lie in a region of $(112)_\alpha$ to $(335)_\alpha$ which are 5° apart.

5) Evidence showing the existence of internal twinning in bainite has been found. The fact that the observed twins, whether accommodation or transformation, persist after isothermal holding suggests that the unidirectional precipitation of carbides cannot be attributed to carbide nucleation on the transformation twins.

0 0 0 0 4 3 0 2 2 9 1

6) The "auto-tempered" model of Pickering and the "rapid nucleation" model of Oblak and Heheman are not able to explain satisfactorily the unidirectional morphology of bainitic carbide but can explain the gross features of the dislocated structures in bainitic ferrite.

7) From morphological examinations and crystallographic analyses, it was concluded that bainitic cementite is formed in contact with austenite at the moving austenite/ferrite interface. This mode gives rise to the uniform distribution of carbides.

8) The major difference between upper and lower bainite is the carbide morphology instead of the formation mechanism. Both bainites involved carbide precipitation at the austenite/bainitic ferrite interface. In upper bainite the diffusion of carbon is sufficiently rapid to allow complete partition to occur between ferrite and austenite. The cementite precipitation occurs between bainitic ferrite laths when the enriched austenitic layer becomes supersaturated. During the formation of lower bainite, carbon diffusion is so restricted that carbon concentrations build up at the α/γ interface leading to the nucleation of uniformly distributed and well spaced cementite particles from austenite as the interface moves along.

ACKNOWLEDGEMENTS

The author is grateful to Professor G. Thomas for his guidance and encouragement throughout the course of this work. He would also like to express his gratitude to Professor V. F. Zackay and Professor F. Hauser for reviewing the manuscript. Special thanks are due to Dr. S. K. Das for many valuable discussions and contributions which made this thesis possible. He is also thankful to Professor H. I. Aaronson and the Republic Steel Corporation for supplying the alloys. The excellent technical assistance of Mrs. S. Ashley and Mrs. Gay Brazil is also very much appreciated.

This work was done under the auspices of the U. S. Energy Research and Development Administration through the Inorganic Materials Research Division of the Lawrence Berkeley Laboratory.

0 0 0 0 4 3 0 2 2 9 2

LEGAL NOTICE

This report was prepared as an account of work sponsored by the United States Government. Neither the United States nor the United States Energy Research and Development Administration, nor any of their employees, nor any of their contractors, subcontractors, or their employees, makes any warranty, express or implied, or assumes any legal liability or responsibility for the accuracy, completeness or usefulness of any information, apparatus, product or process disclosed, or represents that its use would not infringe privately owned rights.

TECHNICAL INFORMATION DIVISION
LAWRENCE BERKELEY LABORATORY
UNIVERSITY OF CALIFORNIA
BERKELEY, CALIFORNIA 94720